

INFORMATION TO USERS

This manuscript has been reproduced from the microfilm master. UMI films the text directly from the original or copy submitted. Thus, some thesis and dissertation copies are in typewriter face, while others may be from any type of computer printer.

The quality of this reproduction is dependent upon the quality of the copy submitted. Broken or indistinct print, colored or poor quality illustrations and photographs, print bleedthrough, substandard margins, and improper alignment can adversely affect reproduction.

In the unlikely event that the author did not send UMI a complete manuscript and there are missing pages, these will be noted. Also, if unauthorized copyright material had to be removed, a note will indicate the deletion.

Oversize materials (e.g., maps, drawings, charts) are reproduced by sectioning the original, beginning at the upper left-hand corner and continuing from left to right in equal sections with small overlaps. Each original is also photographed in one exposure and is included in reduced form at the back of the book.

Photographs included in the original manuscript have been reproduced xerographically in this copy. Higher quality 6" x 9" black and white photographic prints are available for any photographs or illustrations appearing in this copy for an additional charge. Contact UMI directly to order.

UMI

A Bell & Howell Information Company
300 North Zeeb Road, Ann Arbor MI 48106-1346 USA
313/761-4700 800/521-0600

DEVELOPMENT AND FLIGHT DEMONSTRATION OF A GPS RECEIVER FOR SPACE

A DISSERTATION SUBMITTED TO THE
DEPARTMENT OF AERONAUTICS AND ASTRONAUTICS
AND THE COMMITTEE ON GRADUATE STUDIES
OF STANFORD UNIVERSITY
IN PARTIAL FULFILLMENT OF THE REQUIREMENTS
FOR THE DEGREE OF
DOCTOR OF PHILOSOPHY

By
E. Glenn Lightsey
February 1997

UMI Number: 9723388

**Copyright 1997 by
Lightsey, Edgar Glenn**

All rights reserved.

**UMI Microform 9723388
Copyright 1997, by UMI Company. All rights reserved.**

**This microform edition is protected against unauthorized
copying under Title 17, United States Code.**

UMI
**300 North Zeeb Road
Ann Arbor, MI 48103**

© Copyright by Glenn Lightsey 1997
All Rights Reserved

I certify that I have read this dissertation and that in my opinion it is fully adequate, in scope and quality, as a dissertation for the degree of Doctor of Philosophy.



Professor Bradford W. Parkinson
(Principal Advisor)

I certify that I have read this dissertation and that in my opinion it is fully adequate, in scope and quality, as a dissertation for the degree of Doctor of Philosophy.



Dr. Clark E. Cohen

I certify that I have read this dissertation and that in my opinion it is fully adequate, in scope and quality, as a dissertation for the degree of Doctor of Philosophy.



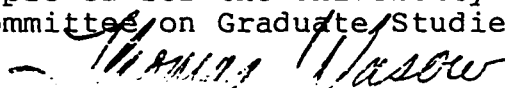
Prof. Jonathan P. How

I certify that I have read this dissertation and that in my opinion it is fully adequate, in scope and quality, as a dissertation for the degree of Doctor of Philosophy.



Prof. Stephen M. Rock

Approved for the University
Committee on Graduate Studies:



Abstract

Although the Global Positioning System (GPS) was principally designed for terrestrial applications, it offers significant benefits to spacecraft users as well. A single low cost GPS receiver can provide a host of critical spacecraft sensing functions, including orbit determination, attitude and attitude rate measurement, as well as precision timing. A spacecraft that employs this consolidation of information can obtain significant cost, power, mass, and reliability improvements over existing systems that offer comparable performance. In order to achieve this capability, however, GPS receiver algorithms designed for the terrestrial environment must be rewritten to function properly in space. The objective of this research is to discover and develop these necessary modifications to an existing terrestrial GPS receiver and demonstrate the new operational capability of this receiver through on-orbit experiments.

This dissertation documents several of the most important innovations that were accomplished to provide autonomous and reliable GPS receiver operation in space. For example, carrier phase integer resolution was enhanced for marginally observable measurements using a new singular value decomposition (SVD) algorithm. This approach shortens the initialization time needed to obtain real-time attitude solutions and improves the overall integrity of the solutions. The ability to perform attitude

determination on nonaligned antenna arrays was enabled by the characterization of a Right Handed Circular Polarization effect on the differential carrier phase measurements. Several other effects, such as antenna phase pattern modeling, on-orbit receiver calibration, nonaligned antenna arrays, and orbit propagation were also discussed in the context of the spacecraft measurement environment.

The new receiver capability is demonstrated through analysis of dynamic simulation and flight results from the RADCAL, REX II, and GANE spacecraft. Real-time on-orbit GPS-based attitude determination of better than 0.2 degrees rms is demonstrated using a 1.5 x 3 m antenna array the GANE experiment. Future applications and experiments are also described.

Acknowledgments

It has been a pleasure to perform research that has allowed me to work with a great diversity of groups and individuals. Their encouragement and assistance has made much of this work possible.

I greatly appreciate and value the guidance of my advisor, Professor Bradford W. Parkinson, whose legacy of accomplishments have made this work and so many others possible.

I would also like to acknowledge Dr. Clark E. Cohen, a pioneer of GPS attitude determination and other high accuracy applications, for his close counsel throughout the course of my work. His insight into physical phenomena and ability to anticipate potential applications are extraordinary.

I would like to thank my reading committee, including Professors Jonathan P. How and Stephen M. Rock, for their excellent and timely critique of this document; and Professor Gene F. Franklin, for chairing my oral defense. Their thoughtful comments and suggestions have improved the quality of this work.

NASA's Goddard Space Flight Center is acknowledged for being a great work environment before, during, and after the completion of this research. The willingness of so many individuals there to perform extra duties to allow me to bring this work to its conclusion is greatly appreciated. I especially wish to thank my supervisor, Mr. Frank H. Bauer, for his continued support and friendship. I greatly respect his dedication, integrity, and professionalism.

The assistance of Trimble Navigation, Ltd., in the form of consulting and access to capital resources, is deeply appreciated. Space Systems Loral is likewise commended for providing its assistance and hardware resources during the commission of this research. By cooperating with students such as myself, these companies have demonstrated their commitment to education as well as the future of GPS technology.

The United States Air Force, CTA Space Systems, and The Aerospace Corporation are gratefully acknowledged for providing flight opportunities and assistance on the RADCAL and REX II spacecraft. NASA's Goddard Space Flight Center, and Johnson Space Center, are also recognized for their GADACS, GANE, and other Space Shuttle experiments.

Most importantly, I wish to thank my wife Jeannie and son Connor, for not only supporting me but also tolerating me during this 5 year endeavor (I know that this was not always easy); and my father Harry, and mother Kathleen, who have always believed in me and brought the best out of me. This work is dedicated to them.

Table Of Contents

Chapter 1: Introduction	1
1.1. Overview.....	1
1.2. Motivation.....	2
1.2.1. Consolidation of Sensing Functions.....	2
1.2.2. Reliability	3
1.2.3. Autonomy	4
1.2.4. Reduced Operating Costs	4
1.3. Challenges of the Space Environment.....	6
1.3.1. High Velocity	6
1.3.2. Full Sky Pointing.....	7
1.3.3. Receiver Calibration.....	8
1.3.4. Severe Environment	9
1.4. Prototype GPS Receiver	9
1.5. History of GPS Space Experiments	11
1.6. Contributions and Outline.....	14
1.7. References.....	15
Chapter 2: Signal Acquisition.....	17
2.1. GPS Signal Description	18

2.2. Doppler / Code Correlation.....	20
2.3. Alternative Acquisition Methods.....	22
2.4. Orbit Propagation.....	24
2.4.1. Position Update from Orbit Elements	25
2.4.2. Orbit Update from Position	29
2.5. Comparison of Acquisition Performance.....	32
2.6. Bootstrap Acquisition	36
2.6.1. Initial Position Estimate.....	38
2.6.2. Refining the Initial Estimate.....	41
2.6.3. Simulation Results.....	42
2.7. Summary	44
2.8. References.....	45
Chapter 3: Attitude Determination	47
3.1. Sensor Metrics	48
3.2. Principles of Attitude Determination	50
3.2.1. Differential Phase Measurements	50
3.2.2. Perturbation Method of Attitude Determination	54
3.2.3. Double-Differenced Measurements.....	57
3.3. Spacecraft Attitude Determination Considerations.....	58
3.4. Cycle Ambiguity Resolution.....	63
3.4.1. Search and Motion Methods for Space.....	63
3.4.2. Quasi-Static Integer Resolution.....	65
3.4.3. Singular Value Decomposition Solution	70
3.5. Nonaligned Antennas.....	74
3.5.1. Roving Master Antenna.....	75
3.5.2. All in View Carrier Phase Measurements	77

3.5.3. Differential Phase Angle Correction	78
3.5.4. Signal Visibility Using Nonaligned Arrays.....	83
3.5.5. Orbit Visibility Study	85
3.6. Summary.....	90
3.7. References.....	90
Chapter 4: Receiver Calibration.....	93
4.1. Error Sources	94
4.1.1. Differential Carrier Phase Perturbation	95
4.1.2. Line of Sight Perturbation	101
4.1.3. Baseline Perturbation	102
4.1.4. Line Bias.....	105
4.1.5. Other Noise Sources	107
4.2. Relative Range Error Budget.....	107
4.3. Attitude Determination Accuracy	109
4.4. Self-Survey Calibration Methods	111
4.4.1. Principles of Receiver Self-Survey.....	111
4.4.2. Receiver to Body-Axis Alignment.....	113
4.4.3. Self-Survey Repeatability.....	113
4.4.4. Combining Self-Survey Results	115
4.5. Other Calibration Methods	117
4.5.1. Baseline Measurement Using Antenna Rotation.....	117
4.5.2. On-Orbit Line Bias Estimation.....	119
4.6. Summary.....	121
4.7. References.....	121
Chapter 5: Spaceflight Experiments	123
5.1. Attitude Determination: RADCAL.....	124

5.1.1. Satellite Description	124
5.1.2. Signal Acquisition and Navigation Performance	126
5.1.3. Attitude Analysis	128
5.1.4. Dynamic Equations.....	130
5.1.5. RADCAL Attitude Solutions.....	133
5.1.6. Assessment of GPS Attitude Accuracy	136
5.1.7. Failure Description of RADCAL Receivers.....	138
5.1.8. Summary of RADCAL Experiment	139
5.2. Attitude Control: REX II.....	140
5.2.1. Satellite Description	140
5.2.2. Dynamic Analysis.....	143
5.2.3. Magnetometer Solution Comparison.....	149
5.2.4. Control Sensor Performance.....	151
5.2.5. Summary of REX II Experiment	153
5.3. Integer Resolution: GANE.....	154
5.3.1. Experiment Description	154
5.3.2. Preliminary Results.....	156
5.3.3. Future Research	160
5.4. Summary	161
5.5. References.....	162
Chapter 6: Future Applications	165
6.1. Receiver Advances.....	166
6.1.1. Spaceborne Integrity Monitoring.....	166
6.1.2. Wide Area Augmentation System	167
6.1.3. Multipath Suppression.....	167
6.1.4. On-Orbit Self-Survey.....	168

6.1.5. Integrated Transponder	168
6.2. Planned Experiments	169
6.2.1. Autonomous Orbit Determination and Spacecraft Time Distribution	169
6.2.2. Sounding Rocket Applications	170
6.2.3. Coordinated Science Platforms and Formation Flight	171
6.2.4. Integrated Navigation and Attitude Systems	173
6.2.5. Attitude Determination of Spinning Spacecraft	173
6.3. Other Capabilities	174
6.3.1. Proximity Operations	174
6.3.2. GPS on High Altitude Satellites	175
6.3.3. Flexure Sensors/Control of Large Space Structures	176
6.3.4. Microsatellites	176
6.3.5. Transmit/Receive Autonomous Constellations	177
6.4. Summary	179
6.5. References	179
Chapter 7: Conclusion	181

List Of Tables

1.1. 0.1 degree 3-axis Attitude Determination system savings with GPS.....	3
1.2. Assumptions for Calculation of Total Mission Cost.....	5
1.3. Differential Carrier Phase Receivers Flown in Space.....	12
2.1. Transformation of \underline{n} from ECEF to Keplerian Reference Frame.....	41
2.2. Bootstrap Acquisition Simulation Results	43
3.1. Comparison of Terrestrial and Orbital GPS Attitude Determination.....	59
3.2. Navigation and attitude tracking availability.	87
4.1. Typical RMS Relative Range Error Budget.....	108
4.2. Self-survey Repeatability Test Results	114
5.1. Challenges of the RADCAL Analysis	140
5.2. Solution Availability vs. Pointing and Integer Resolution Method	158

List Of Figures

1.1. Total Mission Cost For 5 Year LEO Nadir Pointed Spacecraft.....	5
1.2. Maximum Doppler Shifts	7
1.3. GPS Antenna Pointing Vector on an Inertially Fixed Spacecraft	8
1.4. 6 Channel, 4 Antenna Multiplexing Receiver.....	10
1.5. TANS Vector Receiver With 4 Hemispherical Patch Antennas	11
2.1. GPS Signal Structure	18
2.2. Doppler Shift vs. Code Offset.....	21
2.3. Orbit Propagator Block Diagram	23
2.4. Relative Position and Velocity of GPS Transmitter and Observer	25
2.5. Orbit Elements and Reference Frames.....	26
2.6. Transformation Between Earth Fixed and Keplerian Reference Frame	28
2.7. GPS 'Hardware in the Loop' Simulation Block Diagram.....	33
2.8. Receiver On-Orbit Tracking Performance (Simulated)	34
2.9. Geometry for Bootstrap Acquisition	39
2.10. True Anomaly Estimation From Line of Sight Vector.....	41
3.1. Carrier Phase Interferometry Method of Attitude Determination	51
3.2. GPS Attitude Determination Information Flow Diagram	56

3.3. Three Different Pointing Profiles for Spacecraft.....	59
3.4. Three different antenna array geometries	60
3.5. Integer Resolution Performance for Earth Pointed Platform	73
3.6. Gravity Probe B Spacecraft with 4 Nonaligned GPS Patch Antennas	74
3.7. Roving Master Antenna Concept	76
3.8. Differential Phase Measurements from 4 Antennas.....	77
3.9. Spherical geometry accounting for RHCP phase contribution.....	79
3.10. Earth occultation and elevation angle	84
3.11. GPS signal availability for the inertially fixed example	87
3.12. GPS signal availability for the spinning example	87
4.1. Multipath Geometry	96
4.2. Experimental Measurement of Antenna Phase Pattern	98
4.3. Spherical Harmonic Fit to Measured Patch Antenna Phase Pattern	99
4.4. Receiver Calibration Parameters.....	102
4.5. “Line Bias” Thermal Drift.....	107
4.6. Attitude Error Budget.....	110
4.7. Variability of Self-Survey Parameters on Test Array.....	116
4.8. Phase Center Determination Using Antenna Rotation	118
4.9. Results of Experimental Determination of Antenna Phase Center	118
5.1. RADCAL Satellite	125
5.2. RADCAL Orbit Determined from GPS Position Fixes	127
5.3. RADCAL Orbit Elements	127
5.4. Carrier Phase Measurements from One GPS Satellite	129
5.5. Locally Level Reference Frame.....	130
5.6. Definition of Reference Frames for Equations of Motion	131

5.7. Nonlinear Simulation of RADCAL Dynamic Equations.....	134
5.8. RADCAL Attitude, Point and Extended Kalman Filtered Solutions.....	134
5.9. RADCAL Attitude Motion	135
5.10. Comparison of GPS and Magnetometer Solutions	137
5.11. REX II Spacecraft at Integration to Launch Vehicle.....	141
5.12. Deployed REX II Satellite.....	142
5.13. REX II 3-Axis Control Block Diagram.....	145
5.14. REX II Closed Loop Attitude Measurements, 24 Hours.....	147
5.15. Simulated REX II Attitude Without Hysteresis Rods	148
5.16. Simulated REX II Attitude With Hysteresis Rods	148
5.17. Residual of Magnetometer Derived and GPS Real-Time Solutions	150
5.18. REX II Attitude Dropouts As Functions of Latitude and Duration	152
5.19. GANE Hitchhiker Payload at Integration	155
5.20. GANE Attitude Solutions at ISS Orientation	157
6.1. SSTI-Lewis Spacecraft.....	170
6.2. Coordinated Navigation Between Two Spacecraft	172
6.3. GPS Signal Visibility at High Altitude	175
6.4. Microsatellite Concept with GPS Receiver	177
6.5. Distributed Interferometer Formation Concept.....	178

Chapter 1: Introduction

1.1. Overview

In one of his first policy addresses in April 1992, newly appointed Administrator Dan Goldin challenged the National Air and Space Agency (NASA) to build the next generation of spacecraft “safer, better, faster, and cheaper”.¹ His directive not only motivates new methods of designing, building, and testing spacecraft, but also invokes the use of new technology to achieve improved levels of performance and capability at reduced overall mission cost. Spacecraft designers are being increasingly driven to produce constellations of small, expendable spacecraft in Low Earth Orbit (LEO) to provide better coverage at lower total mission cost than the “big science” platforms of previous decades.

The Global Positioning System (GPS) is a strategic asset for achieving this vision. By providing an unprecedented number of critical spacecraft sensing functions— highly accurate time, position, velocity, attitude, and rate— in a single consolidated and robust device, it is now possible to consider smaller spacecraft performing more sophisticated operations at lower cost than the largest and most expensive satellites just a few years ago. Coupled with other developing technologies, such as electronic miniaturization, it is

easy to appreciate that the field of spacecraft design is at a new threshold, and GPS is an enabling technology that is leading the way.

This dissertation describes software modifications to an existing GPS ground receiver that are necessary to allow it operate in an efficient and robust manner in Earth orbit. A GPS receiver capable of navigation and attitude determination in space is desired at relatively low unit cost. The theoretical aspects of the receiver design are generalized for the higher velocity and greater range of attitude motion that are encountered in space. The practical importance of developing real systems that work is emphasized through *on-orbit demonstration of receiver performance* and analysis of flight data. Experimental flights of the prototype receiver validate the new receiver functionality and performance in space.

1.2. Motivation

There are several important benefits that may be achieved by successful implementation of a GPS receiver on a spacecraft. Some examples are given below.

1.2.1. Consolidation of Sensing Functions

A substantial amount of spacecraft hardware, interfaces, and ground support may be reduced or eliminated when replaced with a GPS system. The required GPS system hardware consists of no more than a few low-profile patch antennas, cables, and a solid-state receiver which is well suited for electronic miniaturization. Table 1.1 demonstrates that a reduction in mass, power, and cost by a factor of 3 to 5 is possible through the

Table 1.1. 0.1 degree 3-axis Attitude Determination system savings with GPS²

Component	Heritage System			GPS System		
	Mass (kg)	Power (W)	Cost (\$k)	Mass (kg)	Power (W)	Cost (\$k)
Digital Sun Sensor	2.0	2.8	300	-	-	-
Earth Sensor	7.2	14.0	300	-	-	-
Gyro	3.5	22.0	600	-	-	-
Magnetometer	1.0	1.7	90	1.0	1.7	90
Coarse Sun Sensors	0.2	0	50	0.2	0	50
GPS Receiver	-	-	-	2.2	4.5	200
Total	13.9 kg	40.5 W	\$1340k	3.4 kg	6.2 W	\$340k

replacement of traditional attitude sensors with GPS on a hypothetical LEO spacecraft with 0.1 degree accuracy pointing requirements. An additional windfall in design and testing costs is obtained from the reduction of hardware interfaces. Furthermore, these numbers do not include the substantial design and cost savings from the accurate time and navigation subsystem that GPS also provides.

1.2.2. Reliability

The reduction in spacecraft hardware that is possible by employing GPS provides improvements in overall vehicle reliability. Elimination of interfaces makes the design process simpler; and the reduction of the number of sensing devices means that a single, highly reliable system will replace a string of components which are all required to operate properly to guarantee mission success. There is also a smaller design penalty to

pay for component redundancy. This results in a more reliable spacecraft with a longer operating lifetime at lower total cost.

1.2.3. Autonomy

Utilization of GPS on spacecraft also provides unique capabilities that were previously not practical. With easily accessible navigation and velocity information, autonomous orbit control may be performed on the vehicle.³ Formation flight and autonomous maintenance of satellite constellations to within centimeters of precision are also possible.⁴ Spacecraft rendezvous and proximity flying may be performed by autonomous control systems.⁵ All of these capabilities may be achieved with minor, if any, modifications to the basic GPS sensing system required for navigation and attitude determination.

1.2.4. Reduced Operating Costs

By providing so many sensing functions and automatic control systems on the spacecraft, a new level of vehicle on-orbit autonomy is possible. Autonomous ground station scheduling and downlink may be performed without required operator assistance. In fact, the overall role of the operator is changed from one of active spacecraft maintenance to health and status monitoring and contingency action. This reduced need for active operations support and manpower can dramatically reduce the total mission cost. Figure 1.1 shows total mission cost for a typical LEO Earth-pointed payload over a 5 year life cycle. It is readily apparent that although the spacecraft can be made smaller, simpler, and less expensive with GPS, the more substantial savings is the estimated reduction in operations costs over the mission life achieved through greater vehicle autonomy. The

total mission cost can be halved by leveraging the capabilities of GPS, a savings of several millions of dollars in this example.

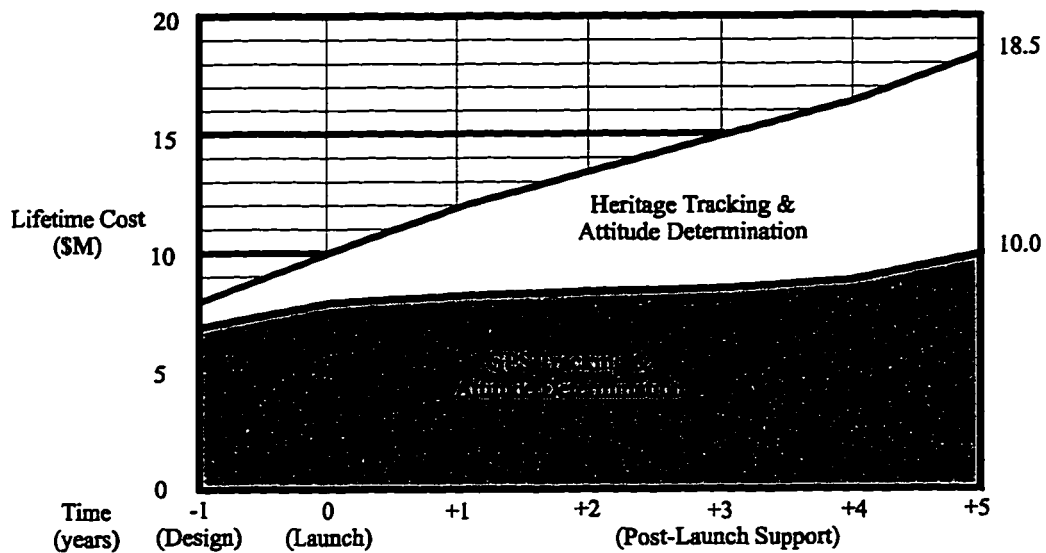


Figure 1.1. Total Mission Cost For 5 Year LEO Nadir Pointed Spacecraft

Table 1.2. Assumptions for Calculation of Total Mission Cost (Figure 1.1)⁶

Item	Cost Without GPS (\$M)	Cost With GPS (\$M)
Spacecraft Fabrication and Prelaunch Testing	10.0	8.0
Operations Cost per Year	1.5	0.2
Beginning and End of Life Operations Premium	0.5	0.5
Total Mission Cost	18.5	10.0

1.3. Challenges of the Space Environment

Unfortunately, simply installing a GPS receiver that has been designed for terrestrial applications does not provide acceptable performance in space. There are several differences between the space and ground environments that necessitate a designed-for-space GPS receiver. By accounting for these differences, a more general capability is obtained that may be used on the ground or in space. The most significant differences between terrestrial and space applications are briefly explained.

1.3.1. High Velocity

The orbital velocities of spacecraft are significantly higher than those encountered on the ground and create larger and more rapidly changing Doppler shifts in the GPS carrier signal. Figure 1.2 shows that for a GPS receiver in LEO, peak-to-peak Doppler excursions up to 100 kHz are possible, more than 10 times the typical Doppler variations observed from the ground. Furthermore, these excursions occur in 90 minutes as opposed to 12 hours, resulting in Doppler shift rates that are often more than 100 times higher than those seen in terrestrial applications.

These facts have fundamental implications for GPS receivers that are used in space. The carrier and code tracking loops must be properly redesigned to be able to track the higher Doppler rates. This modification is discussed by Cohen.⁷ The task of achieving a GPS signal lock without prior information is much more difficult because of the larger Doppler variations. And the receiver position will change significantly over time spans of a few minutes, meaning that GPS satellite visibility must be frequently re-evaluated.

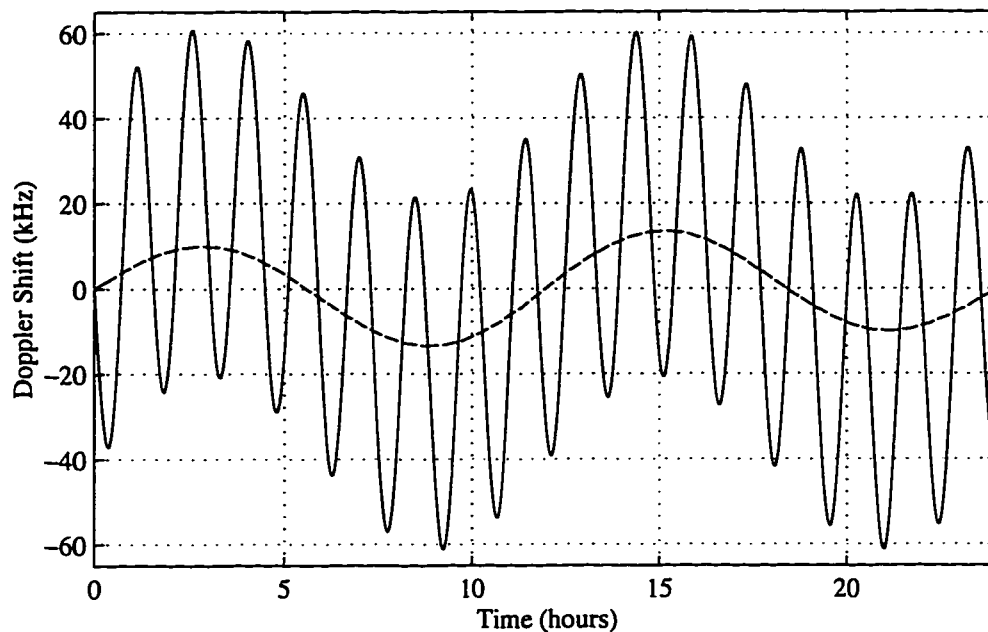


Figure 1.2. Maximum Doppler Shifts, Low Earth Orbit (—) vs. Terrestrial (- -) (Earth Occultation Omitted)

1.3.2. Full Sky Pointing

Experiment pointing requirements can result in widely varying vehicle orientations for spacecraft. Inertially pointed spacecraft will have a face of the vehicle that will rotate from "up" (zenith) to "down" (nadir) and back each orbit, as shown in Figure 1.3. This situation is very different from most ground applications, where one side of the vehicle generally points in the same direction during most of the operating time. The operational impact to a GPS receiver in space is that there will be significant outages of data if all of the hemispherical antennas are pointed in the same direction. In order to support continuous navigation and attitude solutions for an inertially pointed or spin stabilized spacecraft, a carrier phase measurement correction must be made for antennas that point in different directions (a design defined as a *nonaligned* antenna array in Chapter 3).

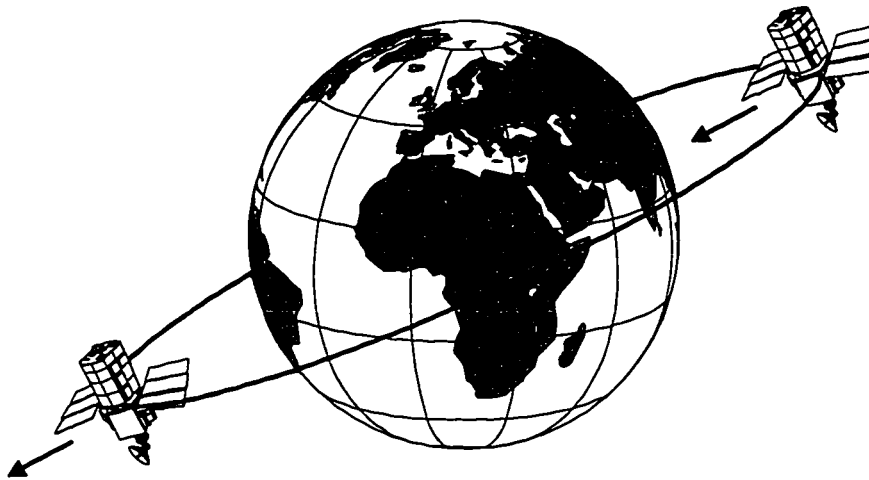


Figure 1.3. GPS Antenna Pointing Vector on an Inertially Fixed Spacecraft

1.3.3. Receiver Calibration

In order to make accurate carrier phase measurements between GPS antennas on a vehicle, several parameters must be calibrated *in situ*. These parameters are the distance between the antenna phase centers (the “baseline length”), and the electrical length from the antenna phase center to the point at which the measurement is made in the receiver (the “line bias”). They are traditionally estimated in advance using a “self-survey” procedure where the GPS system is placed in a static configuration on the ground and collects data over a period of several hours. The same hardware that will be used in the operating condition should be installed on the vehicle at the time of the self-survey.

This ground test is at best a difficult and expensive proposition to attempt during the spacecraft integration process. It is often not possible to assemble the spacecraft hardware in the flight configuration (with solar arrays deployed, for example) prior to launch or to leave the GPS hardware undisturbed once the self-survey has been

completed. As a result, alternate means of doing the calibration either before spacecraft integration or on-orbit are desired.

1.3.4. Severe Environment

The space environment is typically much more harsh for components and packaging than that encountered in ground applications. Temperature, vibration, and radiation are three major areas where electronic devices must be redesigned to survive greater extremes. As a result, many devices which were originally designed for ground use do not perform well for long periods of time (if at all) in space. It is possible to fly a ruggedized GPS aircraft receiver in space with some success for limited duration,⁸ but in order to achieve the levels of reliability that many science missions demand, the GPS receiver hardware must be repackaged for the space environment.

1.4. Prototype GPS Receiver

Except for the last issue (severe environment), most of the barriers to GPS operation in space are algorithmic. It is therefore possible to evolve a new GPS receiver suitable for space from an existing terrestrial GPS receiver, by redesigning and coding new algorithms in the receiver firmware. This is the approach adopted in this thesis to demonstrate the suitability of these algorithms on-orbit.

The GPS receiver that was reprogrammed for space operation was a Trimble Advanced Navigation Sensor (TANS) Vector, manufactured by Trimble Navigation, Ltd. This is a terrestrial receiver which was modified by Cohen in 1992 to enable attitude

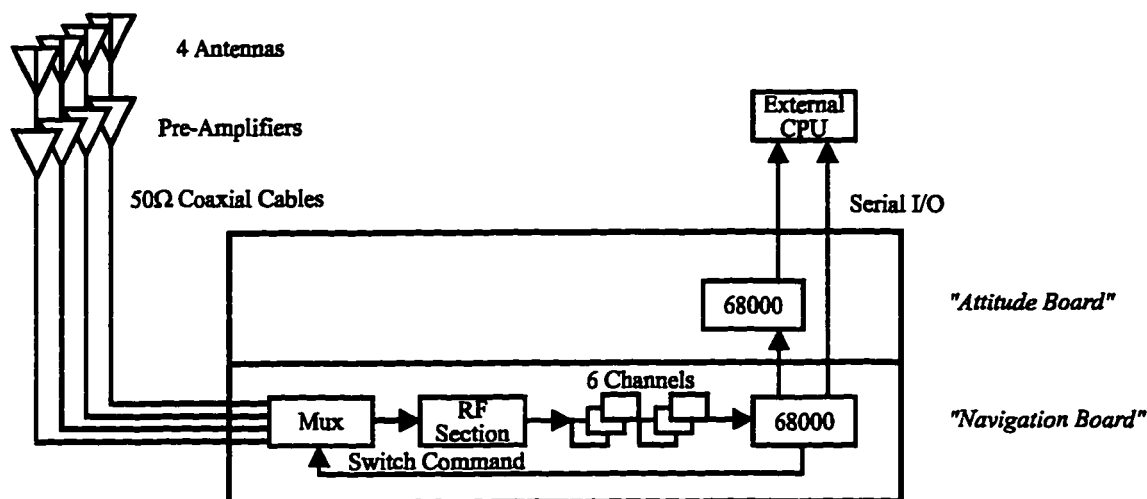


Figure 1.4. 6 Channel, 4 Antenna Multiplexing Receiver

determination.⁷ It is a low cost, 6-channel, single frequency receiver, which multiplexes across 4 antennas (shown in Figure 1.4). There are two Motorola 68000 processors which nominally support attitude and navigation update rates of a few cycles per second (these can be made more frequent by reducing other data output). The receiver unit weighs 2.2 kilograms, consumes 4.5 steady watts of power, and has dimensions of 5x8x2 inches (127x207x56 mm). A photograph of the TANS Vector receiver with 4 GPS patch antennas is shown in Figure 1.5.

The TANS Vector is a mass production receiver that is not environmentally qualified for space. It has been ruggedized for aviation applications, however, and shares many of the design characteristics (low size, mass, and power) that are also necessary for space. By generalizing the algorithms inside this receiver, it is possible to demonstrate the potential capabilities of *any properly qualified* GPS space receiver. The fact that it is at least minimally suited for space is evident by considering the receiver has been flown on many

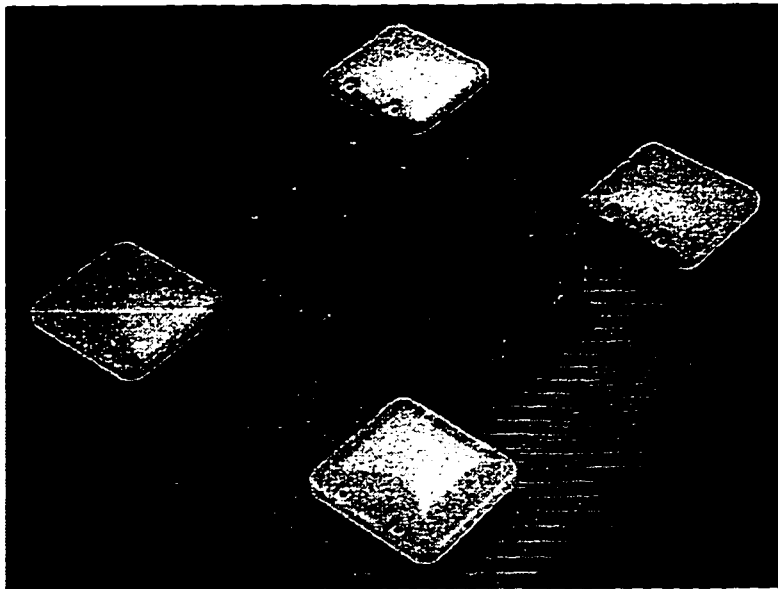


Figure 1.5. TANS Vector Receiver With 4 Hemispherical Patch Antennas

spacecraft with software developed in this thesis and has reliably provided years of service in every case. The Vector's low cost and availability therefore make it an ideal prototype receiver to demonstrate the acceptability of GPS space receiver algorithms as a flight experiment.

The issue of environmentally qualifying a receiver for space is not directly discussed in this thesis; it is assumed, however, that once the algorithms have been proven that any receiver with the appropriate capabilities could be repackaged for the space environment.

1.5. History of GPS Space Experiments

There have already been several experimental flights of GPS space receivers, and the number of flight opportunities is becoming more frequent all the time as spacecraft designers become aware of the potential benefits of the GPS service. The following is a

survey of some of the significant missions that have been flown to date. The Extreme Ultraviolet Explorer (EUVE) was one of the first civilian spacecraft to employ a GPS receiver, the Motorola Explorer, in 1992. This was a navigation-only receiver that did not provide attitude determination. The receiver had some initialization problems, and the original receiver firmware has been reprogrammed on-orbit.⁹

Since 1993, carrier phase tracking receivers which are capable of performing attitude determination have flown in space with software provided by this research. A timeline of these experiments is shown in Table 1.3. RADCAL, a radar calibration satellite sponsored by the US Air Force, was the first satellite to perform differential carrier phase measurements in June 1993. The GPS receiver was a TANS Quadrex, a predecessor to the real-time attitude determination TANS Vector. The carrier phase measurements taken by the Quadrex were post-processed for vehicle attitude determination. RADCAL is the first known successful attitude determination application of a GPS receiver in space.⁸ Crista-SPAS was a German Spartan payload that flew aboard the Space Shuttle in November 1994. This was the first real-time attitude determination using GPS on a spacecraft, using a TANS Vector receiver with space software provided by this research. In March 1996, the REX II satellite, another US Air Force satellite similar in many respects to RADCAL, flew a TANS Vector receiver and successfully performed real-time attitude determination and closed loop control using GPS.¹⁰ The first environmentally qualified-for-space, attitude determination GPS receiver, the Tensor, is planned to fly on the SSTI-Lewis pathfinder spacecraft provided by NASA in 1997. This receiver's core space capability is the same TANS Vector space software developed in this thesis.

Table 1.3. Differential Carrier Phase Receivers Flown in Space

Date	Mission	Receiver	Capability					
			Navigation			Attitude		
			1	2	3	4	5	6
4/93	STS-56	Quadrex	x			x		
<i>6/93</i>	<i>RADCAL</i>	<i>Quadrex</i>	<i>x</i>			<i>x</i>		
9/93	STS-51	Quadrex	x			x		
1/94	STS-61	Quadrex	x			x		
8/94	APEX	Quadrex	x			x		
11/94	Crista-SPAS	Vector	x			x	x	
3/95	Orbcomm	Vector	x			x		
1/96	GADACS	Vector	x			x	x	x
<i>3/96</i>	<i>REX II</i>	<i>Vector</i>	<i>x</i>			<i>x</i>	<i>x</i>	<i>x</i>
<i>5/96</i>	<i>GANÉ</i>	<i>Vector</i>	<i>x</i>			<i>x</i>	<i>x</i>	
1997	SSTI-Lewis	Tensor	x	x		x	x	
1997	SSTI-Clark	Vector	x			x	x	
1997	Globalstar	Tensor	x	x		x	x	
1998	Earth Observer-1	Tensor	x	x	x	x	x	
1999	Gravity Probe B	Tensor	x	x	x	x	x	

Navigation Capabilities:

- 1 - Standard Position Service
- 2 - Filtered Real Time Orbit Estimate
- 3 - Autonomous On-Orbit Stationkeeping Using GPS

Attitude Capabilities:

- 4 - Post Processed Attitude Determination
- 5 - Real Time Attitude Determination
- 6 - Attitude Determination and Control Using GPS

Highlighted missions have flight results presented in Chapter 5.

All of these listed GPS experiments since 1993 were made possible by the research in this thesis. The RADCAL, REX II, and GANE flight results will be discussed in detail later in this thesis to demonstrate the typical performance of the GPS attitude determination system.

1.6. Contributions and Outline

This thesis makes original contributions in the following areas:

On-Orbit Signal Acquisition

Acquisition and reacquisition of the GPS signal in space is accomplished in a rapid and efficient manner by the use of an orbit propagator. The orbit propagator is updated by receiver position fixes. When coarse knowledge of the orbit elements is available, a first position fix is reliably obtained with 5 minutes. When coarse position and an initial almanac are not available an original orbit bootstrap algorithm achieves a position fix within 30 minutes on a 6-channel receiver. [Chapter 2]

On-Orbit Attitude Determination

Attitude determination algorithms are generalized to handle nonaligned antenna arrays. This allows GPS attitude determination to be used on all types of LEO platforms, including inertially pointed and spin-stabilized spacecraft. Carrier phase cycle ambiguity resolution is accomplished using a new method for low observability conditions. The Quasi-static motion algorithm is implemented using a Singular Value Decomposition solution method. This enables rapid cycle resolution in space while retaining the desired high integrity of GPS attitude solutions. [Chapter 3]

Receiver Calibration

GPS carrier phase measurement error sources are investigated. The accuracy of receiver calibration using traditional self-surveys is investigated. The accuracy of antenna phase center and line bias calibration models are examined. Alternate means of estimating these quantities are discussed. An on-orbit line bias estimation algorithm is presented for autonomous receiver self-calibration. [Chapter 4]

Spaceflight Results

Data from the first flights to perform GPS carrier phase-based attitude determination (RADCAL) and control (REX II) are presented using the receiver developed in this dissertation. The attitude determination solution accuracy, real-time and post-processed, is assessed through data analysis and dynamic modeling. Attitude control results using GPS solutions are displayed. The Quasi-static motion cycle ambiguity resolution method is validated from an on-orbit flight experiment (GANE). A precise attitude reference is used on GANE to demonstrate real-time on-orbit attitude determination within 0.2 degrees rms per axis using a 1.5 x 3 m antenna array. [Chapter 5]

Future applications and capabilities of GPS space receivers are discussed in Chapter 6.

1.7. References

¹ D.S. Goldin, quoted in *Aviation Week and Space Technology*, May 4, 1992, p.86, vol. 136, no. 18.

² F.H. Bauer, "Technology For Small Spacecraft NASA Missions, Guidance and Control Technology," presentation package, July 1993.

³ P. Axelrad, *A Closed Loop GPS Based Orbit Trim System For Gravity Probe B*, Ph.D. Dissertation, Stanford University, Oct. 1990, SUDAAR No. 598.

⁴ J.C. Adams, A. Robertson, K. Zimmerman, J.P. How, "Technologies for Spacecraft Formation Flying," *Institute of Navigation (ION) GPS-96*, Kansas City, MO, Sept. 1996.

⁵ K.R. Zimmerman, R.H. Cannon, Jr., "GPS-Based Control for Space Vehicle Rendezvous," *ION GPS-94*, Salt Lake City, UT, Sept. 1994.

⁶ J.R. Wertz, W.J. Larson, eds., *Reducing Space Mission Cost*, Microcosm Press, 1996.

⁷ C.E. Cohen, *Attitude Determination Using GPS*, Ph.D. Dissertation, Stanford University, Dec. 1992.

⁸ C.E. Cohen, E.G. Lightsey, W.A. Feess, B.W. Parkinson, "Space Flight Tests of Attitude Determination Using GPS," *Intl. Journal of Satellite Communications*, Vol. 12, 1994.

⁹ E. Ketchum, R. Hart, "Attitude Determination of the Extreme Ultraviolet Explorer Satellite (EUVE) Using GPS," *Proceedings of the National Technical Meeting*, Institute of Navigation, 1995.

¹⁰ E.G. Lightsey, E. Ketchum, T.W. Flatley, J.L. Crassidis, D. Freesland, K. Reiss, D. Young, "Flight Results of GPS Based Attitude Control on the REX II Spacecraft," *ION GPS-96*, Kansas City, MO, Sept. 1996.

Chapter 2: Signal Acquisition

The most basic operation that a GPS receiver performs is the acquisition and tracking of a GPS signal. In fact, it is doubtful whether an electronics unit that fails to reliably provide this service should be called a ‘GPS receiver’ at all. However, most terrestrial receivers would experience difficulty acquiring GPS signals when operating at orbital velocities.

This chapter discusses modifications to the basic GPS receiver that enable it to acquire and reacquire GPS signals in space efficiently through the use of an internal orbit propagator. The equations of motion for the orbit propagator that allow the prediction of receiver position are fully detailed. The orbit propagator enables signal acquisition and reacquisition within seconds after an outage of navigation solutions. In a new method, the orbit propagator is updated automatically from position fixes, which keeps the orbit elements current and enhances the GPS receiver autonomy. The performance of the orbit propagator is demonstrated in hardware simulation and (later in Chapter 5) through flight experiments. A new “cold start” acquisition mode is also presented that allows a 6-channel receiver to acquire an initial position fix in a reasonable time of less than 30 minutes without an almanac.

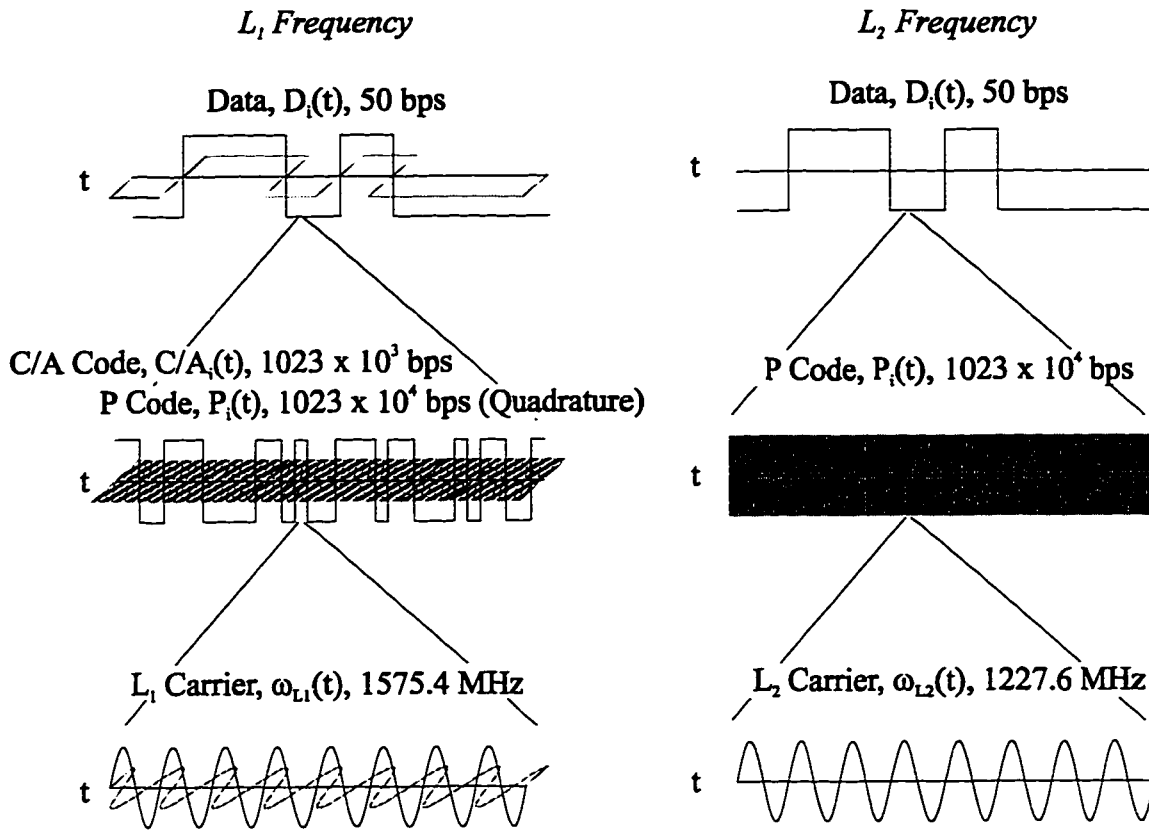


Figure 2.1. GPS Signal Structure

2.1. GPS Signal Description

There are many complete references on the detailed structure of the GPS signal (for example, Spilker¹). For the purposes of this discussion, only a very general knowledge of the signal components is required. The GPS signal is available at two L-band frequencies, known as L1 (1575.4 MHz) and L2 (1227.6 MHz). Each of these signals is composed of the basic carrier which is modulated by navigation data at the relatively slow rate of 50 bits per second (see Figure 2.1), and a precision 'P-code' signal at 10.23 Mbps (10^6 bits per second, also called chips per second) that may be encrypted. The L1 signal is additionally modulated in quadrature with the 'C/A-code' (coarse/acquisition) signal at 1.023 Mbps.

Mathematically, the transmitted L1 and L2 signals may be expressed:

$$S_{L1}(t) = C/A_i(t) D_i(t) \cos(\omega_{L1}t + \phi_1) + P_i(t) D_i(t) \sin(\omega_{L1}t + \phi_1) \quad (2-1)$$

$$S_{L2}(t) = P_i(t) D_i(t) \sin(\omega_{L2}t + \phi_2) \quad (2-2)$$

Each code signal (C/A and P) is a Gold code generated by means of a digital shift register which is unique to (and identifies) each GPS satellite. These codes are designed to have special cross-correlation properties which have almost no cross-correlation with one another or themselves (that is, autocorrelation). They are referred to as pseudo-random noise (PRN) signals, in reference to the observation that a pure white noise signal has no cross-correlation with another white noise signal or with itself, except at zero time shift where the autocorrelation function is equal to one. This cross-correlation property allows for multiple GPS signals to be transmitted at the same frequency with minimal interference. The autocorrelation property provides a sharp peak for measurement of the code offset inside the GPS receiver, which contains a replica of the expected incoming PRN signal for each GPS satellite.

The main differences between the C/A and P codes are the periodic length and bit rate ('chipping rate'). The C/A-code has a length of 1023 bits (chips) with a period of only 1 millisecond. The P-code has a much longer period of 200 days, broken into repeating one week segments, and a higher bit rate. It is therefore much easier to track the C/A portion of the signal, and this initial 'coarse' solution is used to assist the acquisition of the P-code in suitably equipped receivers (hence the name 'coarse/acquisition').

The data bits D_i are of course not periodic, although they do occur in periodic frames. The basic frame of data repeats every 30 seconds and contains, among other things, coarse position information about each GPS satellite. Since there are 24 GPS satellites, it

therefore takes 12.5 minutes from initial signal acquisition to scroll through a complete list of information about the GPS constellation (24 satellite frames plus one health frame). The lower data transmission rate (50 bps) is selected to eliminate interference with the PRN code tracking.

The main motivation for providing the GPS signals on two frequencies is to allow direct measurement of the ionospheric group delay. Considering, however, the cost of extra electronics required to track the L2 signal, the fact that the L2 P-code signal is usually encrypted, and the United States Government has not guaranteed the availability of the L2 signal, many of the so-called 'civilian' GPS receivers available today do not provide the capability to track the L2 signal, or even the P-code portion of the L1 signal. Nonetheless, with proper augmentation systems such as Differential GPS, Wide Area corrections, and carrier phase tracking, the single frequency C/A code civilian GPS receiver is a surprisingly capable and versatile device, in some cases even exceeding the accuracy standards of the dual frequency military receivers.

2.2. Doppler / Code Correlation

At its most basic level, the act of tracking a GPS signal consists of closing a code tracking loop about the C/A code that represents a particular GPS satellite. The received carrier signal is Doppler shifted by the relative motion between the GPS transmitter and the observer. Signal acquisition is obtained when a correlation peak is observed between the incoming signal and a replication of the *modulated carrier signal* generated inside the receiver. The correlation process may be therefore conveniently represented as a two-dimensional search, with code phase on the x-axis and Doppler shift on the y-axis,

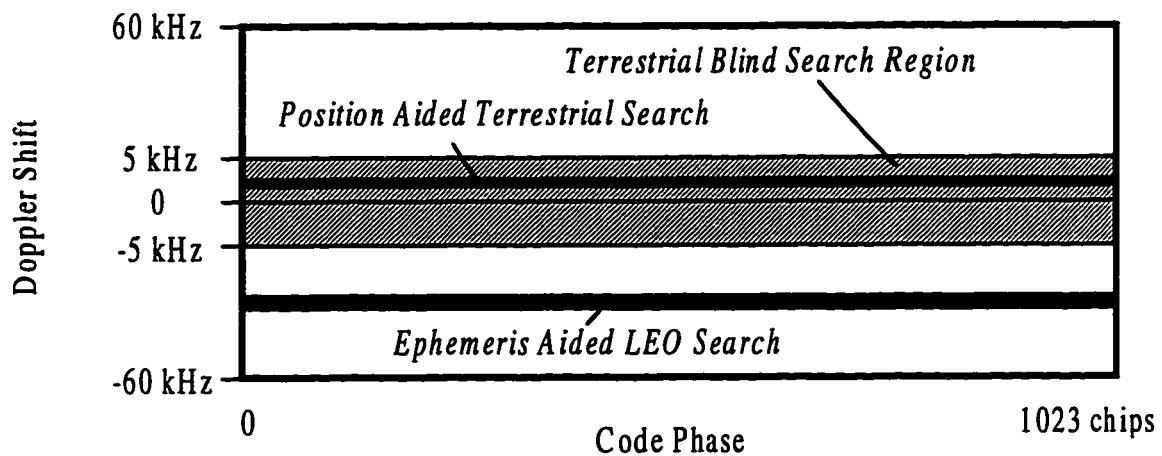


Figure 2.2. Doppler Shift vs. Code Offset

as shown in Figure 2.2. The speed with which a correlation peak can be found thus depends on the time required to make a horizontal sweep across the x-axis (about 2 seconds) and the minimum required y-axis step size to reliably detect a correlation peak (300 Hz).

The nature of the space receiver tracking problem is now apparent. The Doppler / Code correlation search space is more than 10 times larger than that for the terrestrial receiver. Whereas the entire search space can be reliably traversed in a few minutes for a single GPS satellite with a receiver on the Earth, it would take about 15 minutes to cover the greater range of Doppler shifts encountered at orbital velocities. For a 6-channel receiver in LEO with no prior information on its position or visible GPS satellites, there is a significant probability that a visible satellite might set before it could be acquired. Furthermore, as more satellites are acquired, fewer channels are available for searching, requiring even longer times to scroll through the set of remaining possible PRN codes. The result is that without prior information, it may take unacceptably long times to acquire the four GPS signals necessary for a position fix in the traditional 'blind search' methods associated with terrestrial receivers.

Another consideration for signal tracking in space is the greater speed of change of the Doppler shift. The code tracking loop bandwidth must be properly designed to perform during the greater accelerations that may occur during the launch ascent. Cohen adapted the TANS Vector tracking loops to include an acceleration term (3rd order) to improve that receiver's performance tracking space signals.²

2.3. Alternative Acquisition Methods

Clearly some form of position aiding is required to improve signal acquisition in space. The simplest approach is to command an initial position and velocity to the receiver together with an almanac of the GPS satellite locations to determine visible satellites and expected Doppler shifts. This method was used to initialize the TANS Vector receiver on the Crista-Spas spacecraft in 1994.³ The concept is attractive mainly because it requires no new modifications to the basic terrestrial receiver design. However, some drawbacks limit its overall practical value:

- requires initial position and velocity estimate provided from an external source
- rapid acquisition of four GPS signals is necessary before satellite position and velocity change significantly
- line of sight information to GPS satellites (required for attitude determination) is not updated
- reacquisition of signals is not obtained efficiently

The last point refers to a situation where a data outage occurs for an extended period of time (for example, the spacecraft GPS antenna rolls out of view of the GPS constellation

for one half of an orbit), and the previous position fix with dead reckoning is no longer adequate for reacquisition of the GPS signals.

A more general approach implemented by Cohen² would be to provide a set of spacecraft ephemeris parameters that would be used to propagate the position estimate as the spacecraft advances through its orbit. In this case the reacquisition problem is handled very efficiently, since the orbit position is periodically updated. This algorithm was first successfully employed on the RADCAL spacecraft.⁴ The only significant drawbacks to that implementation are that 1) an initial set of orbit elements are required from an external source, and 2) an error in the initial set would persist, because position fixes are not used to update the commanded element set.

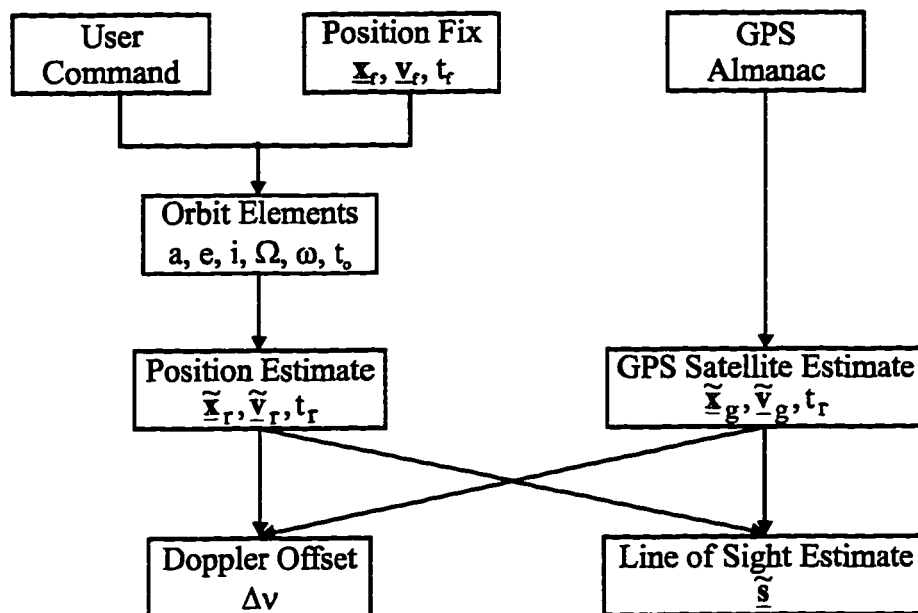


Figure 2.3. Orbit Propagator Block Diagram

In this work, the basic algorithm has been enhanced by allowing updates from the position fixes themselves to correct any errors in the element set, and updating GPS satellite line of sight information, which enables GPS attitude solutions to be performed even if a current position fix is not available. A block diagram demonstrating the flow of information is shown in Figure 2.3. A bootstrap acquisition capability has also been added, where only limited knowledge of the orbit elements is required to proceed to a position fix in a reasonable time.

2.4. Orbit Propagation

If position and velocity estimates are available for both the transmitter (GPS satellite) and the observer, then the predicted Doppler offset $\Delta\nu$ is approximately linear with the relative velocity u between the transmitter and the observer projected along the line of sight:

$$\nu' = \nu \left(\frac{1 - u/c}{\sqrt{1 - (u/c)^2}} \right) = \nu \left(1 - (u/c) + \frac{1}{2}(u/c)^2 - \dots \right) \quad (2-3)$$

$$\Delta\nu = (\nu' - \nu) \approx -u \nu / c, \quad u \ll c \quad (2-4)$$

where ν is the transmitted frequency, ν' is the received frequency, c is the speed of light, and u is defined from the following initial estimates of position and velocity (see Figure 2.4):

$$\underline{\mathbf{r}}_d = \underline{\mathbf{r}}_t - \underline{\mathbf{r}}_o \quad (2-5)$$

$$\underline{\mathbf{u}}_d = \underline{\mathbf{u}}_t - \underline{\mathbf{u}}_o \quad (2-6)$$

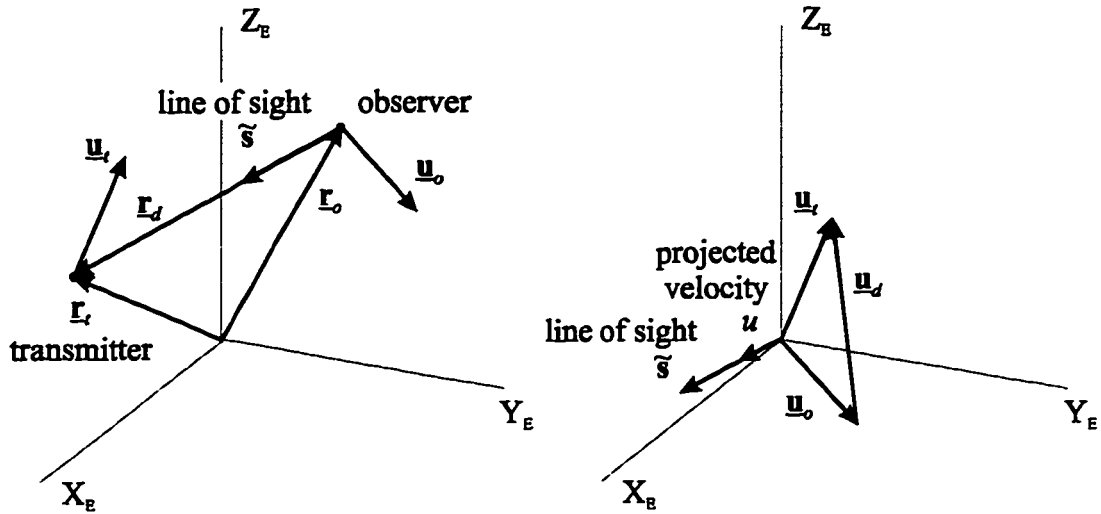


Figure 2.4. Relative Position and Velocity of GPS Transmitter and Observer

$$u = \frac{\underline{r}_d \cdot \underline{u}_d}{|\underline{r}_d|} \quad (2-7)$$

The position and velocity estimate for the GPS satellite (transmitter) is available from curve fit coefficients that are provided in the GPS data message; this procedure is documented as part of the standard GPS interface.⁵ The purpose of the orbit propagator is to produce a position and velocity estimate for the observer from orbit elements.

2.4.1. Position Update from Orbit Elements

Since the Doppler shift is not sensitive to small variations in position and velocity, GPS signal acquisition may be readily performed without complicated orbit models. In the interests of simplicity and computation speed, the following Keplerian six-element orbit set is employed, as shown in Figure 2.5, with standard J_2 Earth oblateness corrections:

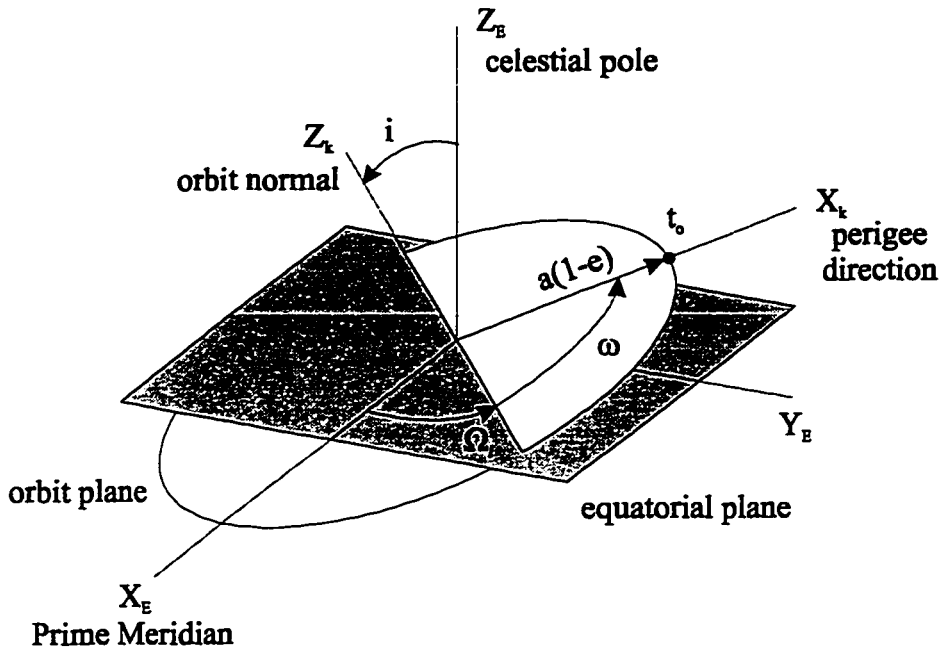


Figure 2.5. Orbit Elements and Reference Frames

- a , semi-major axis
- e , eccentricity
- i , inclination
- Ω_l , *longitude* of ascending node
- ω , argument of perigee
- t_0 , epoch time (perigee passage)

Five of the six elements are the well known classical elements that are fully defined in many references such as Bate⁶ and Battin.⁷ The remaining element, Ω_l , is an Earth-referenced term and should not be confused with the *right ascension* of the ascending node, which is a stellar-referenced term. An Earth-referenced expression for the ascending node is convenient for computing the position in an Earth-Centered/Earth-Fixed (ECEF) reference frame, since it accounts for the hour angle of the Earth. The typical procedure for computing Ω_l is to compute the right ascension Ω_0 using classical methods and then correct for the right ascension of Greenwich at the epoch time, Ω_G , as follows (from Wertz⁸). Given the following definitions:

$$\begin{aligned}
t_o &= \text{epoch time expressed in days of current year} = d_o + h_o \\
d_o &= \text{epoch day of current year, } 0 \leq d_o \leq 365 \text{ (integer)} \\
h_o &= \text{fractional day at epoch time, } 0 \leq h_o < 1 \\
\eta_o &= 360 \cdot h_o = \text{Earth hour angle at epoch time (degrees)} \\
d_J &= d_o \text{ expressed as Julian day (= 0 at noon, January 0, 1990)} \\
d_C &= d_J / 36525 = d_o \text{ expressed as Julian Centuries}
\end{aligned}$$

then

$$\Omega_G = 99.6910 + 36000.7689 d_C + .0004 d_C^2 + \eta_o \quad (2-8)$$

Equation 2-8 is simply a second order curve fit to the Earth's rotation in degrees since the beginning of the latest Julian century (which happens to begin at noon on the first day of the century). Using the *rem* operator as the traditional remainder function (not strictly required for Equation 2-9 to be correct):

$$\Omega_{l,t_o} = \text{rem}(\Omega_o - \Omega_G, 360) \quad (2-9)$$

The oblateness effect of the Earth is then expressed:⁸

$$\frac{d\Omega_o}{dt} = -\frac{3}{2} J_2 \sqrt{\mu} R_e^2 a^{-7/2} (1-e^2)^{-2} \cos(i) \quad (2-10)$$

$$\frac{d\omega}{dt} = \frac{3}{2} J_2 \sqrt{\mu} R_e^2 a^{-7/2} (1-e^2)^{-2} \left(2 - \frac{5}{2} \sin^2(i) \right) \quad (2-11)$$

$$n = \frac{dM}{dt} = \frac{\sqrt{\mu}}{a^3} \left\{ \frac{3}{2} J_2 \left(\frac{R_e}{a} \right)^2 (1-e^2)^{-3/2} \left(1 - \frac{3}{2} \sin^2(i) \right) \right\} \quad (2-12)$$

with the standard nomenclature: μ is the Earth's gravitational constant, R_e is the radius of the Earth, and n is the orbit mean motion. Drag and other disturbance forces are neglected.

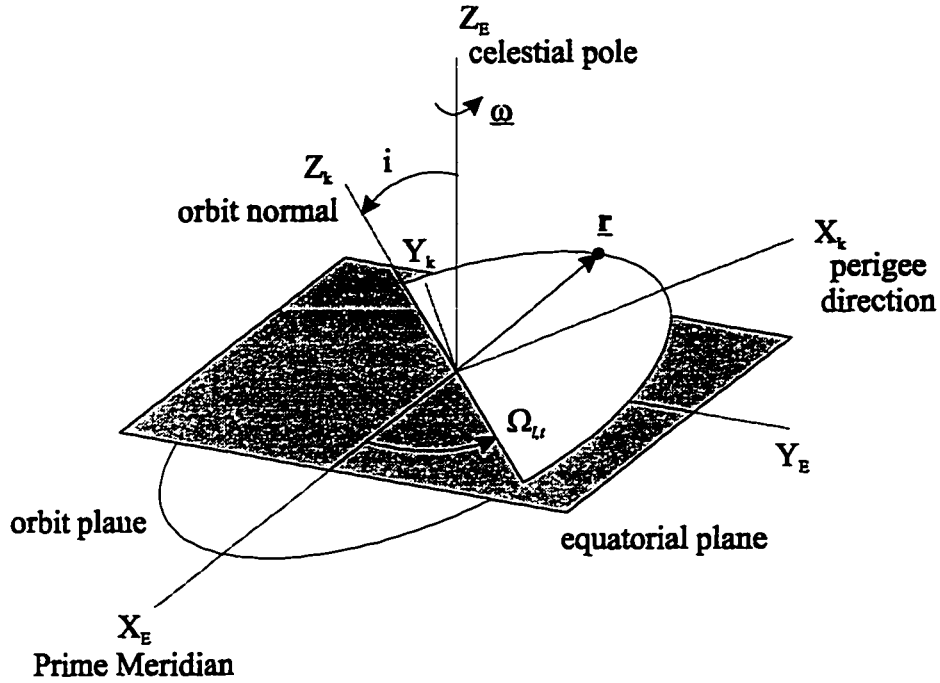


Figure 2.6. Transformation Between Earth Fixed Reference Frame and Keplerian Reference Frame (Orbit Plane)

Once the Keplerian position is obtained in the orbit plane by the standard process, it is transformed to the Earth-Centered/Earth-Fixed (ECEF) WGS-84 reference frame. The precession of the longitude of the ascending node is first updated since epoch time:

$$\Omega_{l,t} = \Omega_{l,t_o} + \left(\frac{d\Omega_o}{dt} - \frac{d\Omega_l}{dt} \right) (t - t_o) \quad (2-13)$$

$d\Omega_l/dt$ is the angular velocity of the Earth, approximately $7.292e-5$ radians/second. The ECEF position is now defined as in Figure 2.6:

$$[\mathbf{r}]_E = \begin{bmatrix} \cos(\Omega_{l,t}) & -\cos(i)\sin(\Omega_{l,t}) \\ \sin(\Omega_{l,t}) & \cos(i)\cos(\Omega_{l,t}) \\ 0 & \sin(i) \end{bmatrix} [\mathbf{r}]_k \quad (2-14)$$

$[\mathbf{r}]_E$ is the $[3 \times 1]$ position vector of the receiver in WGS-84 coordinates, and $[\mathbf{r}]_k$ is the $[2 \times 1]$ Keplerian position of the satellite in the orbit plane (also a function of time).

With the angular rate of the Earth represented as a $[3 \times 1]$ vector, $[\underline{\omega}]_E$, the Coriolis rule may be employed to find the WGS-84 representation of the satellite velocity:

$$[\underline{\omega}]_E = \begin{bmatrix} 0 & 0 & \frac{d\Omega_t}{dt} \end{bmatrix}^T \quad (2-15)$$

$$[\mathbf{v}]_E = \begin{bmatrix} \cos(\Omega_{t,r}) & -\cos(i)\sin(\Omega_{t,r}) \\ \sin(\Omega_{t,r}) & \cos(i)\cos(\Omega_{t,r}) \\ 0 & \sin(i) \end{bmatrix} [\mathbf{v}]_k - [\underline{\omega}]_E \times [\mathbf{r}]_E \quad (2-16)$$

The acceleration may be also found by reapplication of the Coriolis rule, if required.

2.4.2. Orbit Update from Position

It is highly advantageous to provide updates to the user's orbit elements from the position fixes computed by the receiver. This enables any errors in the initially commanded orbit element set to be corrected, since it is usually a coarse estimate based on ground tracking. More importantly, fresh position fixes allow the orbit elements to be adjusted for unmodeled disturbances such as atmospheric drag. Without updates, an initial orbit element set might become grossly inaccurate in a matter of days, depending on the disturbance environment. Position fixes provide a natural method for keeping the orbit elements accurate without requiring complicated modeling or ground intervention. An original method of obtaining orbit elements from GPS position fixes is now derived.

Apply the Coriolis rule to obtain the inertial velocity from the position fix (expressed in ECEF coordinates):

$$[\underline{\mathbf{v}}]_I = [\underline{\mathbf{v}}]_E + [\underline{\boldsymbol{\omega}}]_E \times [\underline{\mathbf{r}}]_E \quad (2-17)$$

The orbit angular momentum and eccentricity may then be obtained:

$$\underline{\mathbf{h}} = [\underline{\mathbf{r}}]_I \times [\underline{\mathbf{v}}]_I \quad (2-18)$$

$$\underline{\mathbf{e}} = \frac{(\underline{\mathbf{v}}_I \times \underline{\mathbf{h}})}{\mu} - \frac{[\underline{\mathbf{r}}]_E}{|[\underline{\mathbf{r}}]_E|} \quad (2-19)$$

where $\underline{\mathbf{e}}$ is the [3x1] eccentricity vector whose magnitude equals the value of the eccentricity scalar e . The semi-major axis, inclination, and longitude of the ascending node are given by:

$$a = \frac{\underline{\mathbf{h}}^T \underline{\mathbf{h}}}{\mu (1 - e^2)} \quad (2-20)$$

$$i = \arccos(h_z / |\underline{\mathbf{h}}|) \quad (2-21)$$

$$\Omega_{l,t_o} = \text{atan2}(h_x, -h_y) \quad (2-22)$$

with h_x , h_y , and h_z the various components of the angular momentum vector $\underline{\mathbf{h}}$. Note that the *longitude* of the ascending node is obtained rather than the *right ascension* of the ascending node in Eq. (2-22). This result is valid because the angular momentum is already expressed in the ECEF reference frame. For elliptical orbits (the special case of a circular orbit is discussed below), the argument of perigee and true anomaly are then determined as:

$$\omega = \text{acos} \left(\frac{e_y \cdot h_x - e_x \cdot h_y}{e \sqrt{h_x^2 + h_y^2}} \right) \quad (2-23)$$

$$\theta = \text{sgn}(\underline{\mathbf{r}} \cdot \underline{\mathbf{v}}) \text{acos} \left(\frac{\underline{\mathbf{e}} \cdot \underline{\mathbf{r}}}{|\underline{\mathbf{e}}| |\underline{\mathbf{r}}|} \right) \quad (2-24)$$

As before, e_x, e_y, e_z , and r_x, r_y, r_z are components of the vectors $\underline{\mathbf{e}}$ and $\underline{\mathbf{r}}$ with magnitudes e and r . The eccentric anomaly is derived from the following relation:

$$\psi = [\text{sgn}(-\theta) + 1]\pi + \text{sgn}(\theta) \text{acos} \left[\frac{e + \cos(\theta)}{1 + e \cos(\theta)} \right] \quad (2-25)$$

The time elapsed since perigee passage, and epoch time are then:

$$\delta t = \frac{(\psi - e \sin(\psi))}{\sqrt{\mu/a^3}} \quad (2-26)$$

$$t_o = t - \delta t \quad (2-27)$$

Finally, the longitude of the ascending node at epoch time is obtained:

$$\Omega_l = \Omega_{l,t_o} + \frac{d\Omega_l}{dt} \delta t \quad (2-28)$$

This derivation completes the update of the orbit element set from the GPS position fix information.

The derivation assumes non-equatorial, elliptical orbits. For the case of these special orbits, numerical precision and rounding error will always produce slightly eccentric,

non-equatorial orbits. If a circular and/or equatorial orbit is commanded to the receiver, some convention must be defined to determine the epoch time and argument of perigee. Any convention may be used as long as it is internally consistent, such as defining $\omega = 0$ at the ascending equatorial crossing. A test is performed on the magnitudes of e , h_x , and h_y to prevent Equations 2-23 and 2-24 from being used near singularity.

It should be noted that the J_2 Earth oblateness effect is not used in the update of the orbit elements, although it is used in the propagation of the orbit elements for a position estimate. The update algorithm for the orbit elements always uses the most recent perigee passage for the epoch time; therefore, any unmodeled disturbances (such as J_2) have acted on the satellite for one orbit at most. During the orbit propagation, however, there is no guarantee that the epoch time is close to the current time and so the J_2 effect must be included.

In most LEO cases, atmospheric drag will be the largest unmodeled disturbance, and will principally determine the longest propagation times that can be tolerated and still produce satisfactory signal acquisition. The magnitude of this term of course depends on the vehicle and orbit characteristics. Due to the fact that reasonably large errors in the position estimate (on the order of a few hundred kilometers) can still lead to successful signal acquisition, it is believed that the orbit propagator could span a time interval of at least several days before an update is required.

2.5. Comparison of Acquisition Performance

A GPS constellation simulator was used to assess the performance of the various methods of receiver initialization discussed in Sections 2.3 and 2.4. This simulator (shown in

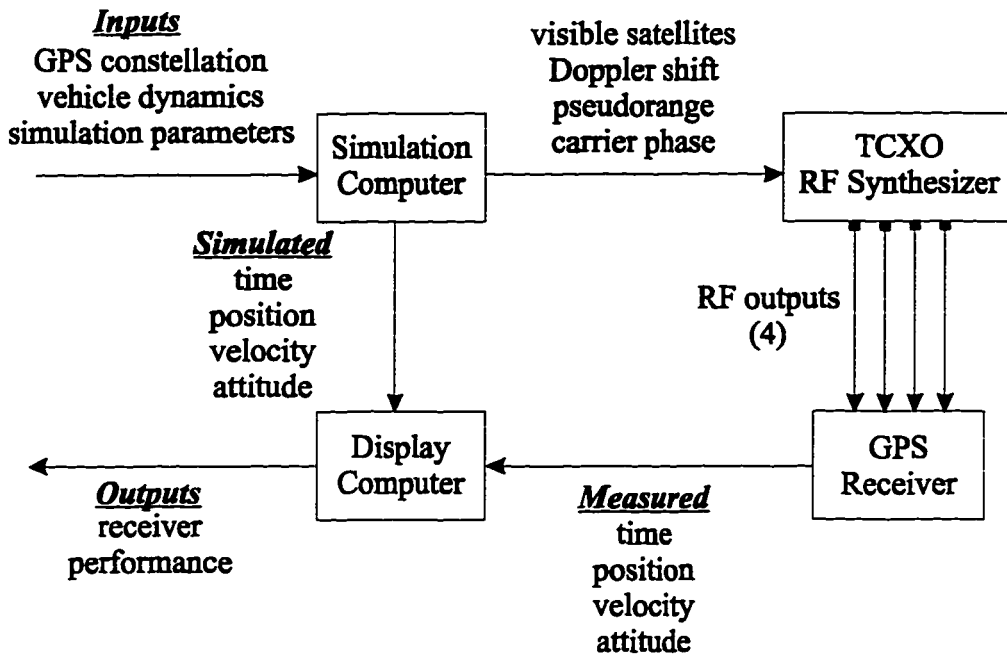


Figure 2.7. GPS 'Hardware in the Loop' Simulation Block Diagram

Figure 2.7) is a commercially available tool that takes user provided information about the GPS constellation and the vehicle characteristics (for example, four hemispherical antennas on a rotating spacecraft in LEO) to compute the visible GPS signals and the proper Doppler shifts for the prescribed motion. These signals are then generated in hardware and provided directly to the GPS receiver hardware. The receiver hardware is therefore directly tested in real-time using simulated GPS signals for the desired motion. Using this test setup, a nadir pointed vehicle was simulated in a common LEO orbit (29 degrees inclination, 280 km altitude) to demonstrate on-orbit signal acquisition performance.

Results that have been shown by simulation to be typical of practically all LEO orbits are shown in Figure 2.8. In the case of a 'terrestrial blind search,' an unmodified terrestrial algorithm, isolated GPS satellites are acquired in an essentially random fashion. The time

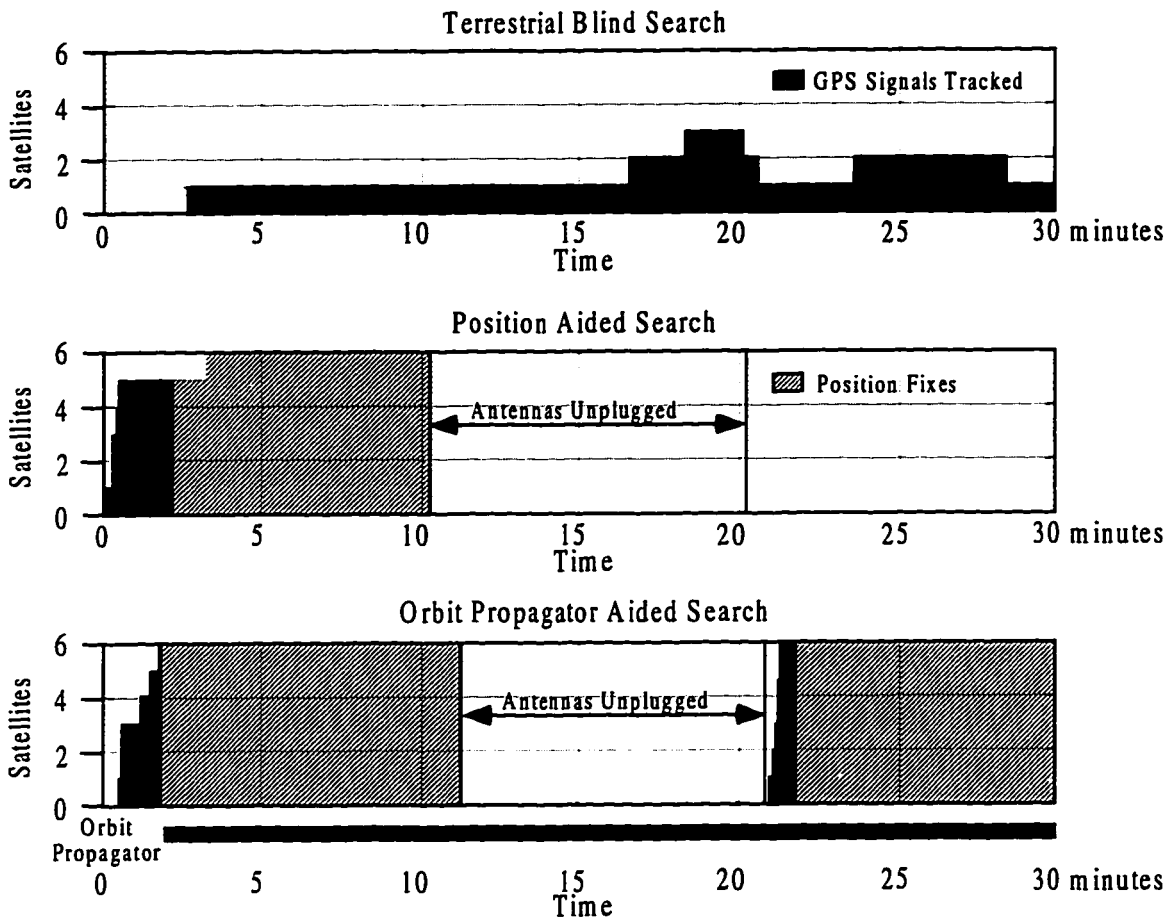


Figure 2.8. Receiver On-Orbit Tracking Performance (Simulated)

to a first fix depends on the likelihood that four satellites can be tracked before the first one sets. This task is made more difficult by the fact that as more satellites are tracked, fewer channels are available to search for the remaining satellites. Although it is fairly likely to lock onto one or two signals, it is a question of probability to get the necessary four signals for a position fix using a 6-channel GPS receiver.

For receivers with significantly more channels (9 or more, for example), the penalty of a blind search is less severe. However, additional channels cost power and size, which are

at a premium for spacecraft, and so the value of an efficient signal acquisition algorithm is still significant.

The position aided search technique refers to the case where an accurate position estimate is commanded to the receiver at power on. Presumably, the accurate position information comes from ground tracking or perhaps another nearby vehicle. An almanac of the GPS satellite positions is also stored within the receiver. In this case, initial signal acquisition occurs rapidly, and within 3 minutes from turn on the receiver is computing position fixes. The reacquisition problem is demonstrated when the antennas are unplugged from the receiver 10 minutes into the simulation, and reconnected 10 minutes later. In reality this effect might be caused by the satellite executing a maneuver, perhaps upon entry to a safe hold orientation. The receiver propagates its position using dead reckoning information from its last position fix, and contains a position estimate that is significantly in error after only 10 minutes. In this case the receiver is substantially “lost” and does not find any new satellites. To reacquire the GPS constellation, a new, accurate position must be provided from an external source.

The final case shows acquisition and reacquisition using the receiver orbit propagator. A position error of 50 km that was contained in the initial commanded orbit elements was corrected from the first position fix update of the orbit elements. In this example reacquisition occurs within 3 minutes of return to visibility of the GPS constellation. This method of using the receiver orbit propagator is clearly the most convenient and robust one for receiver signal acquisition in space.

2.6. Bootstrap Acquisition

The orbit propagator assumes that orbit information is available for the spacecraft in LEO orbit and that this information can be provided somehow (for example from ground command) to the GPS receiver at power on. In most cases this is a reasonable expectation for a satellite with a communications link that is being tracked from the ground. However, for the purposes of enhancing spacecraft *autonomy and recovery from contingency situations* it is important to be able to relax the requirement of having detailed position information about the spacecraft in order to initialize the receiver. It is desirable to have the capability to proceed from limited information about the vehicle's orbit and the GPS constellation to a full GPS position fix within a reasonable amount of time, typically less than 30 minutes. This method of using limited or no prior information is referred to as bootstrap acquisition of the GPS signals.

In the design of a bootstrap algorithm, there are many possible approaches to consider. If the receiver has enough channels, simply scrolling through all the possible satellite codes will eventually acquire enough signals to obtain a position fix. As mentioned previously, however, the electronics needed for extra channels consumes power and volume that must be minimized for spacecraft. Alternatively, information from the first signals acquired could be used to eventually produce a position estimate which would update the satellite search procedure. While this technique is attractive in an theoretical sense, all six orbit elements must be estimated from nonlinear equations of motion. The most important characteristics of a successful bootstrap algorithm— speed and simplicity— are likely to suffer because of the complexity of this estimation problem.

In fact, even in the case of initial power on after launch (the most demanding application of bootstrap acquisition), much information is already known about the spacecraft. Assuming that the launch vehicle has done its job and placed the vehicle somewhere near the target orbit, reasonable estimates of three of the six orbit elements exist (semi-major axis, inclination, and eccentricity). These estimates are adequate for GPS signal acquisition to within the delivery tolerance of modern launch vehicles (several hundred kilometers in semi-major axis, a few degrees in inclination, and a few percent in eccentricity). The remaining three parameters are functions of spacecraft launch and deployment time: argument of perigee, longitude of the ascending node, and epoch time. A simpler bootstrap acquisition algorithm takes advantage of the information that is known prior to launch (these elements may be stored in the receiver firmware). It estimates only the remaining parameters that are functions of launch and deployment time. This algorithm assumes that the semi-major axis, inclination, and eccentricity, are known at least coarsely; in the event of very large errors, time limit logic should transition the receiver into a random search (or await a ground command).

Using the principles derived earlier in this chapter, it is possible to proceed from receiver lock onto a *single* GPS satellite, acquired from random search, to a full position fix within a matter of minutes. It may be surprising to learn that the longest step of the entire process is the accumulation of a complete almanac of the GPS satellite positions, which takes 12.5 minutes of continuous signal tracking. In an unlucky case, a recently acquired satellite might set before the necessary time has elapsed (normally 12.5 minutes), and the receiver must wait until another GPS signal is acquired. The information required to develop the receiver position estimate—current time, GPS broadcast ephemeris, and Doppler shift—is all available within 30 seconds of initial signal acquisition. The orbit information that is assumed to be approximately known in advance is semi-major axis, inclination, and eccentricity. If a reasonably accurate GPS almanac is also available

(perhaps stored within the receiver), a position fix may be achieved within 10 minutes of initial signal acquisition using this bootstrap method.

2.6.1. Initial Position Estimate

The receiver will have the current time and GPS broadcast ephemeris for the satellite being tracked within 30 seconds of signal acquisition. Current time may then be used to update two of the remaining orbit elements. An initial value of the argument of perigee must be defined at some prior time or specified at launch time. This value may then be updated with the current time using Equation 2-11. The right ascension of the ascending node is computed from current time and the longitude of the ascending node is derived from Equations 2-8 and 2-9.

The only remaining orbit element that is required to specify the receiver position is the epoch time of perigee passage. The current time and the broadcast ephemeris allow the GPS satellite position to be determined as described in the GPS Interface Control Document.⁵ The line of sight (unit) vector from the receiver to the GPS satellite, as shown in Figure 2.4, is then:

$$\hat{\underline{s}} = \frac{\underline{r}_d}{|\underline{r}_d|} = \frac{\underline{r}_t - \underline{r}_o}{|\underline{r}_t - \underline{r}_o|} \quad (2 - 29)$$

where \underline{r}_d is the difference between the transmitter (the GPS satellite), \underline{r}_t , and the observer (the receiver), \underline{r}_o . When the distance from the origin (i.e., the Earth's center) to the transmitter is much greater than the distance to the observer, as it is in the case of a spacecraft in LEO orbit, the line of sight vector may be approximated as just the unit vector directed from the origin to the transmitter, $\hat{\underline{s}}$.

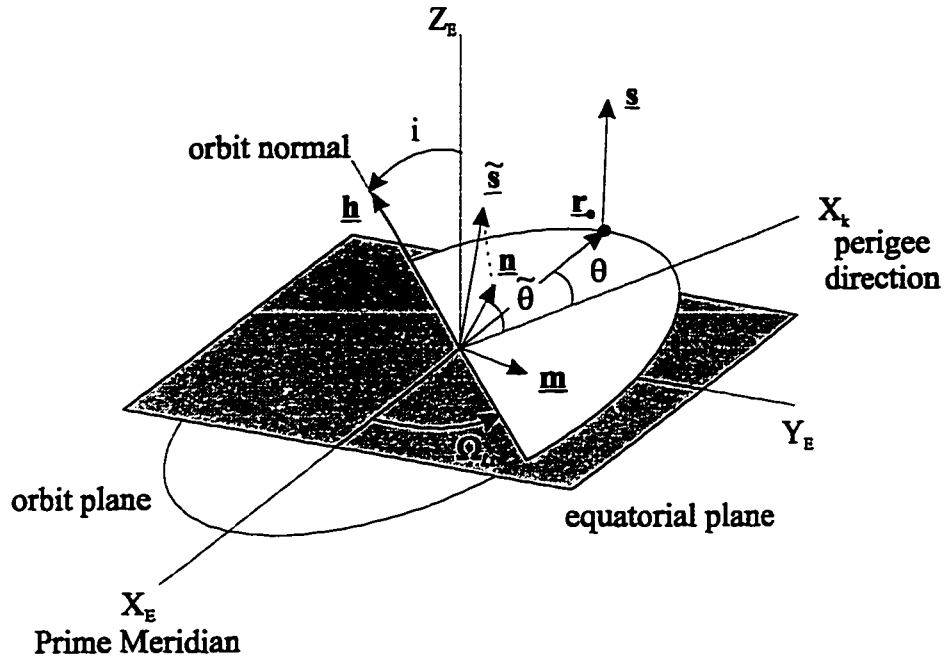


Figure 2.9. Geometry for Bootstrap Acquisition

$$|\varphi_i| \approx \frac{r_i}{|r_i|} \quad (2-30)$$

The true anomaly, θ , and thus epoch time, may then be estimated by projecting the line of sight estimate into the orbit plane as follows. First, define the unit angular momentum vector that points in the direction of the orbit normal (and defines the orbit plane):

$$\hat{\underline{\mathbf{h}}} = \begin{bmatrix} \sin(i)\sin(\Omega_{l,t}) \\ -\sin(i)\cos(\Omega_{l,t}) \\ \cos(i) \end{bmatrix} \quad (2-31)$$

Define a temporary vector that is orthogonal to both $\underline{\hat{s}}$ and $\underline{\hat{h}}$ (and therefore lies in the orbit plane):

$$\mathbf{m} = \hat{\mathbf{s}} \times \hat{\mathbf{h}} \quad (2-32)$$

$$\hat{\underline{m}} = \frac{\underline{m}}{|\underline{m}|} \quad (2-33)$$

The magnitude $|\underline{m}|$ is an important quantity because it measures the observability of the position estimate from the line of sight estimate (see Figure 2.9). In order for this method to work well, $|\underline{m}|$ should be large, typically greater than 0.3. If $|\underline{m}|$ is small, it means that the orbit plane is not favorably aligned to the line of sight estimate and the position estimate should be bypassed until a new GPS signal is acquired (usually within a few minutes). If $|\underline{m}|$ is of sufficient magnitude, the next step is to compute the projection of the line of sight estimate in the orbit plane, \underline{n} :

$$[\underline{n}]_E = \hat{\underline{h}} \times \hat{\underline{m}} \quad (2-34)$$

$$[\hat{\underline{n}}]_E = \frac{[\underline{n}]_E}{|\underline{n}|} \quad (2-35)$$

The subscript ‘E’ has been included as a reminder that this vector is expressed in the Earth fixed reference frame. By basic geometry, and using numerical values that are well defined, the components of the vector \underline{n} may be expressed in the Keplerian reference frame (orbit plane) ‘K’ as described in Table 2.1 (n_x and n_y are the x and y components of \underline{n}). Then:

$$[\hat{\underline{n}}]_k = \frac{[\underline{n}]_k}{|\underline{n}|} \quad (2-36)$$

The true anomaly is then estimated as (Figure 2.10):

$$\tilde{\theta} = \text{atan2}(\hat{n}_{y,k}, \hat{n}_{x,k}) \quad (2-37)$$

Epoch time may now be computed from Equations 2-25 through 2-27.

Table 2.1. Transformation of \underline{n} from ECEF to Keplerian Reference Frame

Values of $i, \Omega_{l,t}$	$ \cos(\Omega_{l,t}) \geq \sqrt{2}/2$	$ \sin(\Omega_{l,t}) > \sqrt{2}/2$
$ \cos(i) \geq \sqrt{2}/2$	$\begin{bmatrix} n_{x,k} \\ n_{y,k} \end{bmatrix} = \begin{bmatrix} \cos(\Omega_{l,t}) & \sin(\Omega_{l,t}) \\ -\sin(\Omega_{l,t})/\cos(i) & \cos(\Omega_{l,t})/\cos(i) \end{bmatrix} \begin{bmatrix} n_{x,e} \\ n_{y,e} \end{bmatrix}$	
$ \sin(i) > \sqrt{2}/2$	$n_{y,k} = n_{z,e}/\sin(i)$ $n_{x,k} = \frac{n_{x,e} + (\cos(i)\sin(\Omega_{l,t})n_{y,k})}{\cos(\Omega_{l,t})}$	$n_{y,k} = n_{z,e}/\sin(i)$ $n_{x,k} = \frac{n_{y,e} - (\cos(i)\cos(\Omega_{l,t})n_{y,k})}{\sin(\Omega_{l,t})}$

The orbit estimate is now complete, and current position and velocity may be estimated by the procedure outlined in Section 2.4.1. The whole procedure can be efficiently executed on a microprocessor.

2.6.2. Refining the Initial Estimate

The position estimate obtained above may be perfectly acceptable for the purposes of bootstrap signal acquisition. But there may also be cases where the estimated line of sight vector, while generally pointed in the right direction, is not totally suitable by itself for orbit estimation. There is another piece of readily available information, however, which may be used to refine the estimate to improve its accuracy. This information is the

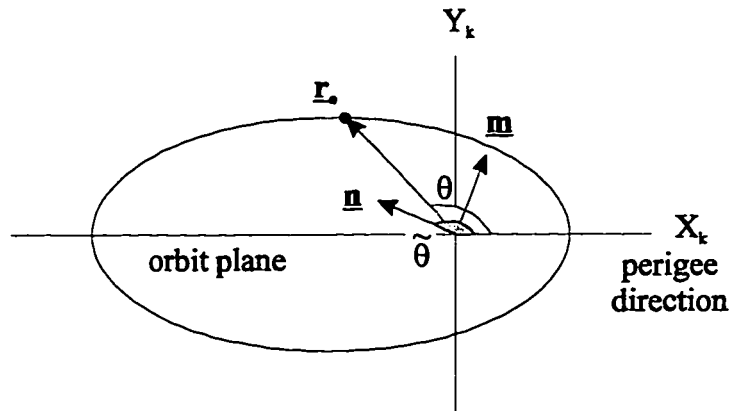


Figure 2.10. True Anomaly Estimation From Line of Sight Vector

Doppler shift in the received signal, ν_x , which may be compared to the expected Doppler shift from the position estimate, ν_o , and the predicted Doppler shift $1/12^{\text{th}}$ of an orbit later (this number has been chosen heuristically), to compute a linear correction to the true anomaly:

$$\tilde{\theta}_1 = \tilde{\theta}_0 + \frac{2\pi}{12} \left(\frac{\nu_x - \nu_0}{\nu_1 - \nu_0} \right) \quad (2-38)$$

The Doppler shift variation is actually sinusoidal with true anomaly, but the linear approximation works well over short periods of time, particularly in the region near zero Doppler shift where most GPS signals are acquired.

This procedure may be iterated if desired to obtain successive position estimates. If no new signals are acquired after a preset time of searching with the current estimate (perhaps 3 minutes), it is abandoned and the next GPS signal that is acquired is used to provide a new estimate.

2.6.3. Simulation Results

This algorithm was simulated in software to demonstrate its effectiveness on a 6-channel GPS receiver in a polar, 800 km orbit. The simulation duration was slightly over 2 orbits (about 3 hours). A GPS almanac was used to simulate GPS satellite positions and signal Doppler shifts. When a signal passed through 0 Doppler shift, it was assumed to be acquired by a blind search tracking algorithm. Equations 2-30 through 2-37 were then applied to compute a set of estimated orbit elements.

For the first study, the receiver was assumed to have a GPS almanac loaded into memory. The highest elevation satellites and their predicted Doppler shifts were then calculated from the estimated receiver position and assigned to the 5 remaining receiver channels. A successful position fix was declared if 4 or more receiver channels were assigned to visible satellites within 500 Hz of the correct Doppler shift for at least 30 seconds. The results are presented in Table 2.2. The algorithm was found to be very effective: 100% of all simulated cases successfully acquired a position fix. The mean time to first position fix was slightly longer than 6 minutes.

In the second case, the receiver was assumed to have no prior almanac information. The first signal therefore had to stay in lock for at least 13 minutes to complete an almanac load before employing Equations 2-30 through 2-37. Even in this case, a position fix was successfully obtained 68.2% of the time. In approximately 1 out of 3 cases, the first GPS satellite would set before the 13 minute time period had elapsed. When successful, the mean time to first fix was almost 20 minutes. Accounting for failed attempts, the

Table 2.2. Bootstrap Acquisition Simulation Results

Mean time to first signal acquisition	277 seconds
Maximum time to first signal acquisition	795 seconds
$\tilde{\theta}$ error, rms	4.85 degrees
Position fix acquisition, with almanac	100 % (22 out of 22 cases)
Mean time to first fix, with almanac	367 seconds
Position fix acquisition, no almanac	68.2 % (15 out of 22 cases)
Mean time to first fix, no almanac	1684 seconds

mean time to first fix was slightly over 28 minutes. This value is believed to be conservative because it does not account for partial almanac loads that occurred during the first failed almanac load attempt.

This simulation study is not intended to provide complete results for bootstrap acquisition performance under all possible conditions. For example, only one orbit case has been considered during a 3 hour time span. Even so, these results validate the basic concepts presented in this section. A hardware simulation using an implementation of this algorithm on a GPS receiver is the next logical step to demonstrate bootstrap performance under more realistic conditions.

2.7. Summary

In this chapter, the utility of the orbit propagator for acquiring and reacquiring GPS signals has been demonstrated. The equations that update the receiver position from a set of orbit elements using current time are presented, and conversely, update the orbit elements from a receiver position fix. In this manner, the orbit elements are automatically self-adjusted to maintain accuracy over time. When there is no initial position estimate or orbit element set, a “cold start” or bootstrap acquisition sequence can be used that takes limited information about the current orbit and acquires the signals necessary for a position fix within 15 minutes. Using these tools, a GPS receiver can quickly and efficiently acquire the signals needed for navigation and attitude determination in nearly all spacecraft applications.

2.8. References

¹ J.J. Spilker, Jr., "GPS Signal Structure and Performance Characteristics," *Reprint of Global Positioning Papers Published in Navigation*, Institute of Navigation, vol. 1, 1980.

² C.E. Cohen, *Attitude Determination Using GPS*, Ph.D. Dissertation, Stanford University, Dec. 1992.

³ J.K. Brock, et al, "GPS Attitude Determination and Navigation Flight Experiment," *Institute of Navigation (ION) GPS-95*, Palm Springs, CA, Sept. 1995.

⁴ C.E. Cohen, E.G. Lightsey, W.A. Feess, B.W. Parkinson, "Space Flight Tests of Attitude Determination Using GPS," *Intl. Journal of Satellite Communications*, Vol. 12, 1994.

⁵ Headquarters, USAF Space and Missile Systems Organization, *Systems Specification for the NAVSTAR Global Positioning System*, Sept. 1997.

⁶ R.R. Bate, D.D. Mueller, J.E. White, *Fundamentals of Astrodynamics*, Dover Publications, Inc., 1971.

⁷ R.H. Battin, *Astronautical Guidance*, McGraw-Hill, Inc., 1964.

⁸ J.R. Wertz, ed., *Spacecraft Attitude Determination and Control*, D. Reidel Co., 1978.

Chapter 3: Attitude Determination

Attitude determination of a platform or vehicle using carrier signals is not traditionally considered a standard GPS measurement, but it greatly enhances the overall utility of the sensing device. All of the information required for spacecraft attitude control, autonomous orbit control, and precision timing is now available in a single package at reasonable mass, power, and cost. It is this consolidation of sensory resources that makes the GPS receiver a powerful component for many LEO space applications.

The concept of attitude determination using GPS carrier phase interferometry was first demonstrated by Greenspan, et al, in 1982.¹ After several initial demonstrations on platforms, ships, and aircraft during the 1980s (see Kruczynski² and van Graas³), the first commercial terrestrial receivers capable of performing 3-axis GPS carrier phase-based attitude determination were marketed in the early 1990s. Cohen made several algorithmic improvements to the state of the art and demonstrated the accuracy of the attitude determination system through aircraft experiments in 1992.⁴

In this Chapter, the GPS attitude determination capability is fully extended to spacecraft. The theoretical foundation is established for robust attitude determination on most dynamic platforms, regardless of the vehicle pointing profile. A new set of attitude

determination algorithms is developed specifically for the spacecraft dynamic environment.

The Quasi-static motion algorithm for cycle ambiguity resolution, originally proposed by Cohen⁴, is implemented on a GPS receiver for the first time. Several new enhancements enable the algorithm to work very efficiently when the number of available measurements is limited and the observability is low. In a new technique, the Singular Value Decomposition is used to automate the measurement collection and produce a correct solution under widely varying dynamic conditions. The Quasi-static motion algorithm is successfully demonstrated on-orbit in Chapter 5.

GPS carrier phase-based attitude determination is generalized to nonaligned antenna arrays for the first time through the calculation of a previously unquantified Right Handed Circularly Polarized (RHCP) effect on the differential phase measurement. This enhancement greatly extends the capability of GPS attitude determination for different spacecraft pointing profiles. An orbit visibility study validates that navigation and attitude determination are possible 100% of the time in most LEO orbits using a 6-antenna, 12 channel GPS receiver, even for inertially fixed and spinning spacecraft.

3.1. Sensor Metrics

There are many ways to evaluate the capability of a device. Each metric should answer a fundamental question about the behavior of the device that is of particular interest to the potential user. For spacecraft, several of the most important metrics are listed as follows:

- *Integrity* - Is the data as reported by the device guaranteed to be accurate within some acceptably small probability of error?
- *Availability* and *continuity* - Are measurements regularly available without significant interruptions in service?
- *Autonomy* - How much human intervention is required to configure and operate the device?
- *Versatility* - In how many different types of applications will the device perform satisfactorily?
- *Reliability* - Is the probability of hardware failure within the operating environmental conditions acceptably small?
- *Performance* - Is the measurement of sufficient accuracy; and is the mass, power, and cost of the device acceptable?

Performance is listed last, but in many cases, it is the only parameter that is used to differentiate between alternative devices and technologies. All of these considerations are important, however, to assess the total value of the design to any particular application.

As the interest in spaceborne GPS attitude determination systems increases, it is important to appreciate the metrics that determine the suitability of different algorithms for this application. A set of attitude determination algorithms is sought that provides high measurement integrity, availability, and continuity, with substantial autonomy and versatility for many spacecraft applications, at acceptable performance and reliability. Because reliability is a hardware standard in the present context, it will not be directly addressed in this chapter. Although many different algorithms are available, these sensor metrics provide the basis for evaluating the suitability of each method.

3.2. Principles of Attitude Determination

The principles of attitude determination using GPS carrier phase interferometry are well documented in the literature.^{4,5} This section presents a brief review of the most fundamental concepts and discusses the relevance of two different measurement techniques for the spacecraft attitude determination problem.

3.2.1. Differential Phase Measurements

Probably the most widely used method of GPS attitude determination is illustrated in Figure 3.1. Two antennas are separated by a known fixed distance, $[\underline{\mathbf{b}}]_B$ (also referred to as the antenna *baseline* vector), expressed in a body referenced coordinate frame 'B'. L_1 carrier wave signals (wavelength $\lambda \cong 19$ cm) originate from a GPS satellite along a known line of sight $[\underline{\mathbf{s}}]_E$, expressed as a unit vector in an external reference frame 'E'. The known line of sight implies that the GPS satellite and receiver position are at least approximately known. Because the GPS satellite is so far away, the carrier wavefronts are essentially planar.

The range projection of the antenna baseline onto the line of sight vector may be expressed as:

$$\Delta r = \underline{\mathbf{s}}^T \underline{\mathbf{b}} \quad (3-1)$$

Δr can be expressed in any units of distance, such as meters, but is more conveniently represented in wavelengths (λ) for this derivation. Recognizing that one carrier phase wavefront is indistinguishable from the next, the true range projection can be expressed in terms of an *ideal* differential carrier phase measurement:

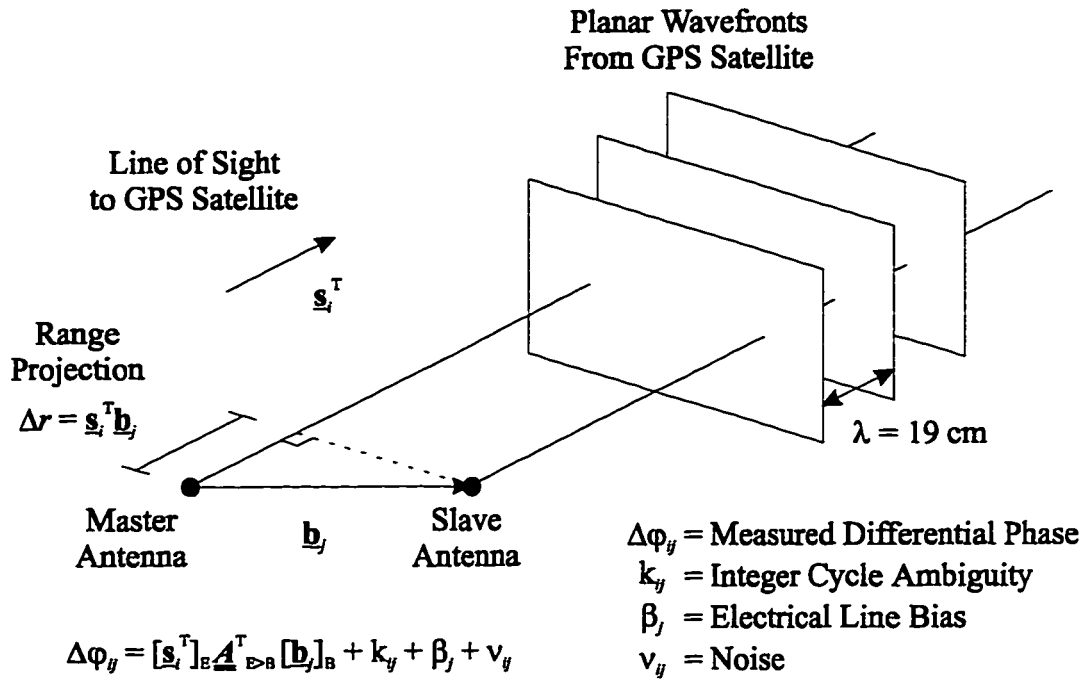


Figure 3.1. Carrier Phase Interferometry Method of Attitude Determination

$$\Delta r = \underline{s}^T \underline{b} = \Delta\phi - k \quad (3-2)$$

where $\Delta\phi$ is the differential carrier phase measurement (a fractional number between 0 and 1 wavelength) and k is a *differential* integer that accounts for the integer number of wavelengths in the distance Δr . For example, if $\Delta r < 19 \text{ cm}$, $k = 0$ regardless of the orientation of \underline{b} . The minus sign on k results from construction in Figure 3.1.

It should be noted that $\Delta\phi$ can in general go outside the bounds of one wavelength due to phase wraparound. The integer k is adjusted only at discrete times (such as the first attitude computation), and during other times it is treated as a constant. $\Delta\phi$ may therefore contain an integer component as well, after the carrier phase measurement has gone through more than one rotation of 2π ; it is nonetheless termed the ‘fractional’ carrier phase measurement to distinguish it from the integer term k .

Since the baseline vector \underline{b} is known in the vehicle body reference frame, and the GPS signal line of sight \underline{s} is known in the external reference frame, the attitude of the body frame may be expressed with respect to an ideal differential carrier phase measurement as:

$$\Delta r = \underline{s}^T \underline{b} = \left[\underline{s}^T \right]_E \underline{A}_{E \rightarrow B}^T [\underline{b}]_B = \Delta \phi - k \quad (3-3)$$

where $\underline{A}_{E \rightarrow B}$ represents the 3x3 direction cosine transformation matrix from the external reference to the body reference. If the differential integers (“cycle ambiguities”) are known, this represents a nonlinear equation that can be solved to obtain the attitude of the antenna platform in the external reference frame. $\underline{A}_{E \rightarrow B}$ has three independent unknowns, meaning that this equation may be theoretically solved if there are as few as three differential phase measurements; for example from three antennas and two GPS signals, provided these measurements span a three dimensional space (for example, two GPS signals along the same line of sight would *not* span a three dimensional space).

Equation 3-3 is modified to account for *real* measurements by including two additional terms:

$$\left[\underline{s}^T \right]_E \underline{A}_{E \rightarrow B}^T [\underline{b}]_B = \Delta \phi - k - \beta - v \quad (3-4)$$

β is a known calibration constant which is a function of the receiver hardware and the antenna pair in question. It is called the line bias, and represents the electrical line length from the antenna phase center through the cable to the measurement point inside the receiver. In this difference equation, the term line bias actually refers to the *differential* bias; i.e., the line bias of the slave antenna electrical path minus the master antenna electrical path. This quantity is a function of the GPS antenna/receiver hardware and can

be determined in advance and saved using a calibration technique.⁴ The assumption that this term is an unchanging function of receiver hardware alone shall be investigated in Chapter 4.

The remaining term, v , is an additive measurement noise term. It includes all noise effects such as multipath, carrier tracking noise, bias drifts, and others. Once again, what is actually measured in this case is a *differential* noise between the slave and master antenna; only non-common mode noise sources remain after the differencing operation. Clock offset, for example, is not a differential noise source, since it is common to each antenna. The noise term v has time correlated properties that in some cases may be modeled or calibrated, but in this analysis these effects are treated as measurement error.

Equation 3-4 is the fundamental GPS differential carrier phase measurement equation. It may be expanded to account for all GPS satellites being tracked (i), across all antenna baselines (j), to accommodate all measurements made during one sample interval:

$$\Delta\phi_{ij} = \left[\underline{s}_i^T \right]_{\text{E}} \underline{\mathbf{A}}_{\text{E} \rightarrow \text{B}}^T \left[\underline{\mathbf{b}}_j \right]_{\text{B}} + k_{ij} + \beta_j + v_{ij} \quad (3-5)$$

The equation is rearranged so that the fractional carrier phase measurement appears on the left and all other terms are separated on the right. With enough measurements, it is possible to solve for the cycle ambiguities, k_{ij} , and the direction cosine matrix $\underline{\mathbf{A}}_{\text{E} \rightarrow \text{B}}$. Although, as previously noted, the attitude may be theoretically determined from as few as three ideal (i.e., noiseless) differential carrier phase measurements, more measurements are required in practice to account for the presence of the measurement noise.

3.2.2. Perturbation Method of Attitude Determination

Once the cycle ambiguities k_{ij} are known (a new method for determining these is presented in Section 3.4), they may be removed from the problem, and if $\underline{A}_{E>B}$ is approximately known as $(\underline{A}_{E>B})_0$, a perturbation equation may be developed as follows:

$$(\Delta\varphi_{ij})_0 = [\underline{s}_i^T]_E (\underline{A}_{E>B}^T)_0 [\underline{b}_j]_B + k_{ij} + \beta_j \quad (3-6)$$

$$\delta\varphi_{ij} = \Delta\varphi_{ij} - (\Delta\varphi_{ij})_0 = [\underline{s}_i^T]_E \underline{A}_{E>B}^T [\underline{b}_j]_B - [\underline{s}_i^T]_E (\underline{A}_{E>B}^T)_0 [\underline{b}_j]_B + v_{ij} \quad (3-7)$$

For sufficiently small perturbations, the attitude matrix $\underline{A}_{E>B}$ may be linearized for small rotations about the body axes:

$$\underline{A}_{E>B} = (\underline{A}_{E>B})_0 \cdot (\underline{I} + \underline{\Theta}^\times) \quad (3-8)$$

$$\underline{\Theta}^\times = \begin{bmatrix} 0 & -\delta\theta_z & \delta\theta_{yz} \\ \delta\theta_z & 0 & -\delta\theta_x \\ -\delta\theta_{yz} & \delta\theta_x & 0 \end{bmatrix} \quad (3-9)$$

Then

$$\begin{aligned} \delta\varphi_{ij} &= [\underline{s}_i^T]_E (\underline{A}_{E>B}^T)_0 \underline{\Theta}^\times [\underline{b}_j]_B + v_{ij} = -[\underline{s}_i^T]_E (\underline{A}_{E>B}^T)_0 \underline{B}_j^\times \underline{\delta\theta} + v_{ij} \\ &= \underline{h}_{ij} \underline{\delta\theta} + v_{ij} \end{aligned} \quad (3-10)$$

$$\underline{B}_j^\times = \begin{bmatrix} 0 & -b_{jz} & b_{jy} \\ b_{jz} & 0 & -b_{jx} \\ -b_{jy} & b_{jx} & 0 \end{bmatrix}, \quad [\underline{b}_j]_B = \begin{bmatrix} b_{jx} \\ b_{jy} \\ b_{jz} \end{bmatrix}, \quad \underline{\delta\theta} = \begin{bmatrix} \delta\theta_x \\ \delta\theta_y \\ \delta\theta_z \end{bmatrix} \quad (3-11)$$

Equation 3-10 represents a linearized sensitivity equation between the measured differential carrier phase and the perturbation to the initial attitude guess. \underline{h}_{ij} is a 1x3 row vector that may be thought of as a set of linearized sensitivity coefficients for every measurement equation. For a given sample, all ‘valid’ differential phase measurements (i.e., those for which the cycle ambiguities are known) are stacked into a single linearized vector equation:

$$\underline{\underline{H}} = \begin{bmatrix} \underline{h}_{11} \\ \vdots \\ \underline{h}_{mn} \end{bmatrix} \quad (3-12)$$

$$\underline{\delta\phi} = \underline{\underline{H}} \underline{\delta\theta} + \underline{v} \quad (3-13)$$

This equation presents an overdetermined linear system with additive noise whose solution may be obtained by minimizing the residual in the least squares sense (or according to any other appropriate performance index). The solution, $\underline{\delta\theta}$, is a 3x1 vector correction of small rotations to the direction cosine matrix $(\underline{A}_{E \rightarrow B})_0$ as defined by Equation 3-8. The solution may be obtained iteratively using the previous epoch solution as an initial guess.

The flow of information for differential, carrier phase-based attitude determination is now summarized in Figure 3.2. Many types of measurements are combined in different ways to produce the ultimate output product, real-time attitude solutions. Prior to real-time operation, calibration measurements are taken to determine the antenna line biases and baseline vectors in the body reference frame. This information is then saved for later use. During the real-time operation, the receiver position estimate is obtained from a position fix, if available, or an orbit propagator solution in the manner discussed in Chapter 2.

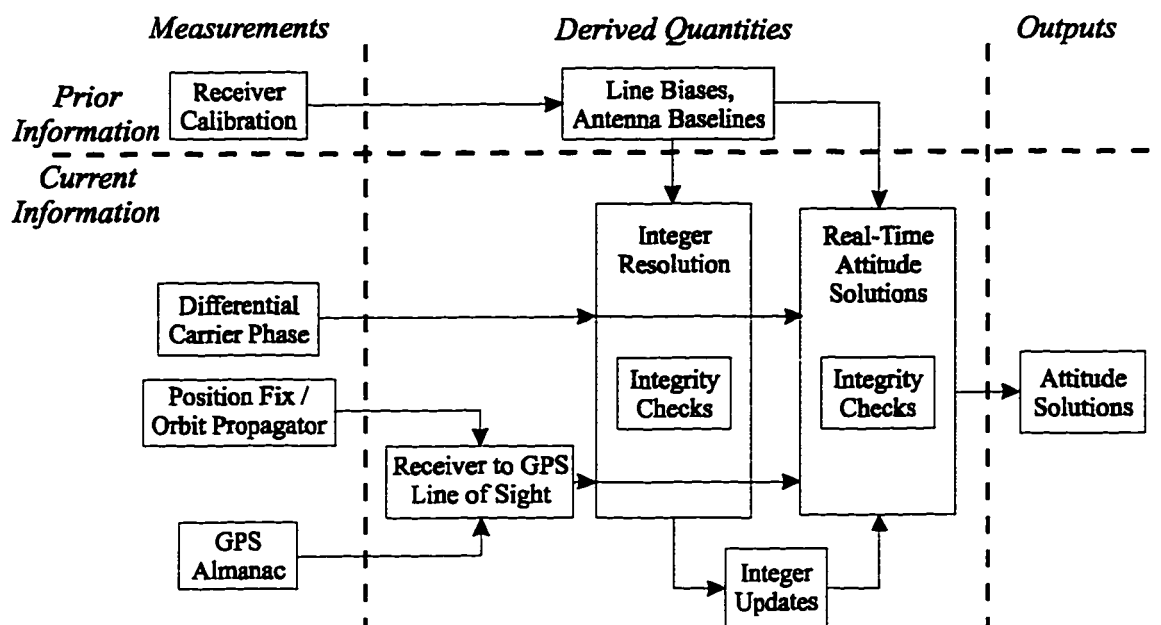


Figure 3.2. GPS Attitude Determination Information Flow Diagram

The GPS satellite position is computed from the broadcast GPS ephemeris and combined with the receiver position to produce the signal line of sight vector, $[\underline{s}]_E$. This information is collected along with differential carrier phase measurements which are used to resolve the carrier cycle ambiguities. The integer resolution procedure is solved once (per the method to be discussed in Section 3.4), and then removed from the attitude determination problem as in Equations 3-6 and 3-7. Once the integers are obtained, these values are periodically updated as new measurements are added and real-time attitude solutions are computed in the method of Equations 3-7 to 3-13. As long as the sample rate is relatively fast compared to the vehicle dynamics, the previous sample may serve as an initial guess to the next solution. Integrity checks are readily available in the form of the solution residual, and other parameters, during both the bootstrap integer resolution and the real-time attitude solution processes.

3.2.3. Double-Difference Measurements

Equations 3-6 and 3-7 assume that the line bias terms β_j are known in advance and may be subtracted from the available measurements. In fact, these parameters may not be constants nor well known in advance. These issues will be discussed more fully in Chapter 4. One idea that has been proposed to bypass the need to know the line bias term is to *double-difference* the carrier phase measurements along the same baseline vector:⁶

$$\nabla\Delta\phi_{12j} = \left[(\underline{s}_1 - \underline{s}_2)^T \right]_{\text{E}} \underline{\underline{A}}_{\text{E} \rightarrow \text{B}}^T \left[\underline{b}_j \right]_{\text{B}} + (k_{1j} - k_{2j}) + (v_{1j} - v_{2j}) \quad (3-14)$$

This formulation circumvents the problem of calibrating and/or modeling β_j at the cost of a decrease in the number of available total measurements, which are reduced by the double differencing operation. The double-difference measurements are also more noisy than in the single-difference case. The algorithm works well when the number of visible GPS satellites in common to two antennas is large, as is the case when the antenna array is aligned (i.e., all antennas point in the same direction) and zenith pointed. As will be shortly discussed, however, a single highly versatile algorithm that supports all types of LEO pointing profiles requires generalization to a nonaligned antenna array. In the case of a nonaligned array, the number of GPS signals that are common to two or more antennas may be greatly reduced. In this case, the measurement of Equation 3-14 is of less value than for an aligned array. However, the nonaligned attitude determination algorithm could be augmented with information provided by any available double difference measurements.

3.3. Spacecraft Attitude Determination Considerations

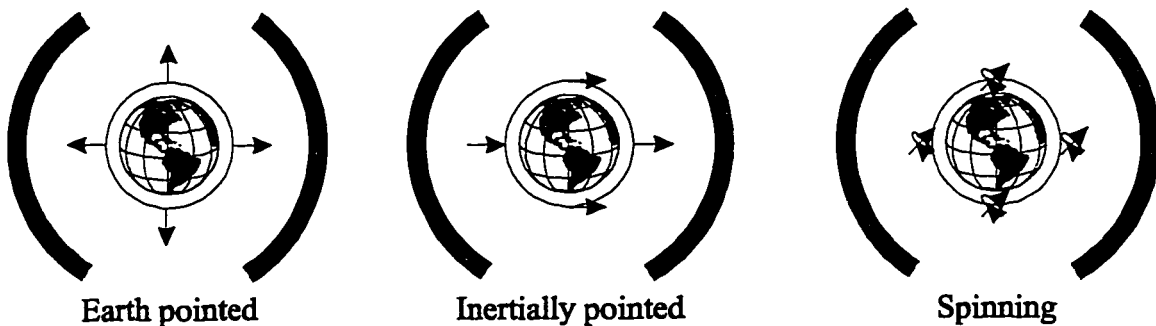
Now that the basic concepts of attitude determination have been presented, it is appropriate to consider the important differences between terrestrial and space GPS carrier phase-based attitude determination. The most common LEO spacecraft attitude determination applications are classified in terms of three types of pointing: Earth referenced, inertially referenced, and spinning. These may be contrasted with typical static terrestrial environments, such as survey applications, and dynamic terrestrial environments, such as aviation or maritime applications. The differences between the space and terrestrial cases can be separated into two important categories, shown in Table 3.1: antenna pointing and carrier phase motion (these will be explained below). A single, uniform set of attitude determination algorithms is sought that supports all of these very different applications.

Antenna pointing is easy to appreciate. In terrestrial applications, whether dynamic or static, the antenna array is generally always pointed approximately upwards. The GPS Constellation resides within the hemisphere to which the antenna array points. Even in the most demanding applications, such as aircraft attitude determination during a steep bank, the bank angle rarely exceeds 45 degrees.

For an inertially fixed or spinning spacecraft, however, there is no hemisphere on the vehicle body that points in the direction of the GPS constellation all the time. These pointing profiles are shown schematically in Figure 3.3. An inertially fixed axis that is pointed towards the zenith vector at one time will be aligned with the nadir vector a half orbit later. Even in the case of a nadir pointed spacecraft, there may be transitional or contingency pointing modes where vehicle alignment is not fixed to one hemisphere. In

**Table 3.1. Comparison of Terrestrial and Orbital
GPS Attitude Determination Environments**

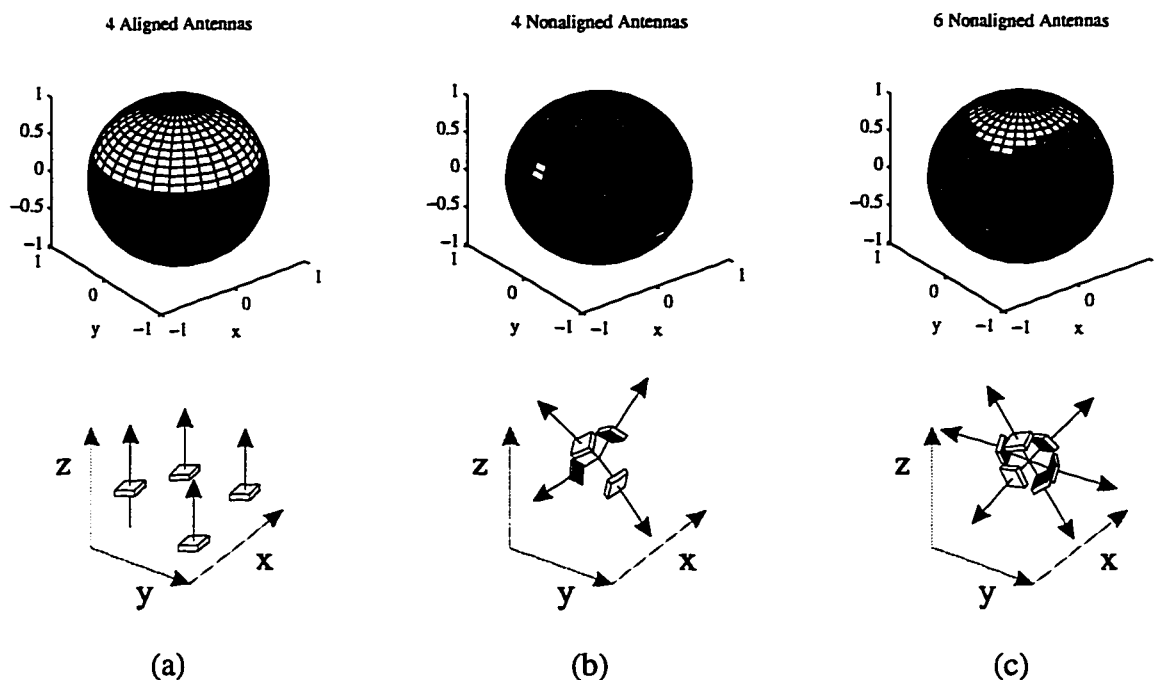
Application	Terrestrial		Orbital		
Type	Static	Dynamic	Earth Pointed	Inertially Pointed	Spinning
Antenna Pointing	Zenith		Zenith	Full Sky	
GPS Line of Sight Motion	180 degrees per 360 minutes		180 degrees per 45 minutes		
Vehicle Dynamics	None	Several deg. Per minute	< 1 rev. per orbit = < 4 deg. per minute		0.1 - 20+ rev. per min.
Carrier Phase Motion Relative to GPS Line of Sight Motion	None	More	Same		More



The arrows denote on face of the vehicle, and the gray band is the region of GPS constellation visibility

Figure 3.3. Three Different Pointing Profiles for Spacecraft

order to ensure that at least one antenna is favorably aligned with the GPS constellation, it is necessary to point the antennas in different directions, as shown in the last two examples of Figure 3.4.



(Lighter shades indicate regions with more common antenna coverage.)

Figure 3.4. Three different antenna array geometries (bottom) and their coverage patterns in body coordinates

These types of nonaligned configurations will guarantee navigation solution availability regardless of orientation; however, they will also greatly reduce the common field of view between each antenna pair. Consequently, it is of great importance to utilize every available measurement to have any chance of providing good attitude determination availability and continuity. Furthermore, the measurements must be adjusted to account for the phase contribution due to the circular polarization of the nonaligned antennas. This effect is common mode on aligned antennas and therefore has not been previously modeled. If attitude determination *can* be performed on nonaligned arrays, it can support all of these space and terrestrial pointing applications. The necessary modifications are discussed in Section 3.5.

The other substantive difference between terrestrial and LEO space applications has to do with the magnitude and the *cause* of the motion in the carrier phase measurements as recorded by the GPS receiver, and their magnitudes *relative* to GPS line of sight motion. The reasons that make the differences important are discussed in Section 3.4 on carrier integer ambiguity resolution, but the differences themselves must be first understood and these are now presented.

When carrier phase measurements change due to motion, the motion may come from two sources. The first source is the GPS signal line of sight motion. In the terrestrial case, the GPS line of sight motion is dominated by the GPS satellite motion and slowly traverses the sky: 180 degrees of motion occurs in about 6 hours, or 360 minutes. The terrestrial motion of the GPS line of sight is therefore about 0.5 degrees per minute. There is also line of sight motion due to Earth rotation, but this effect is smaller, since the Earth rotates 180 degrees in 12 hours (and this motion is common to both terrestrial and space applications). For the LEO spacecraft, the line of sight motion is dominated by the receiver motion. In this case the receiver moves 180 degrees through its orbit in 45 minutes. The LEO GPS line of sight motion is therefore approximately 4 degrees per minute, roughly an order of magnitude greater than in the terrestrial case.

The other cause of carrier phase measurement motion is vehicle (or platform) rotation. For platform dynamics on the Earth, there are generally only two cases of platform rotation. These are static platforms, where the platform is fixed to the Earth (that is, not rotating at all), and kinematic platforms, where attitude motion of at least several degrees per minute is occurs as the object moves along its path. The usually rare exception of a tightly controlled vehicle attitude (hence not changing) may be treated as a static case. In the static case, all the carrier phase measurement changes may be assumed to be due to the GPS satellites as they pass slowly overhead. All measurements may be applied to a

single platform attitude estimate. When the platform is kinematic, all the motion in the carrier phase measurements is assumed to be due to the vehicle motion itself. The vehicle motion is assumed to occur fast enough that the GPS line of sight is essentially stationary during the time interval over which the motion has occurred.

In space there are also two cases of vehicle motion. The first case, a rapidly spinning spacecraft, is the same as the terrestrial kinematic platform. As long as the spinning motion is fast enough, say more than 20 degrees per minute, all the carrier phase motion may be assumed to be due to the vehicle rotation. In the second case: a nadir pointing, inertially pointing, or slowly rotating satellite, the vehicle dynamics are much slower. These vehicles may be assumed to be rotating roughly 1 revolution (or less) per orbit. For a LEO spacecraft, 1 revolution is completed in about 90 minutes, meaning the vehicle motion is occurring at approximately 4 degrees per minute. This motion has almost exactly the *same* magnitude as the GPS line of sight motion.

The cause of *relative* motion is important to the structure of the cycle ambiguity resolution equations, as will be seen in Section 3.4. On the ground, the relative motion is due almost entirely to either GPS line of sight motion (static array), or vehicle rotation (kinematic array). Each of these cases is discussed in detail in prior work.⁴ But in space, the interesting case often occurs where the GPS line of sight motion is almost the same as the vehicle rotation motion. The key point here is that motion techniques of attitude determination used on the ground must be modified to account for the greater range of possible dynamics that are encountered in space. A new method for resolving cycle ambiguities in a way that is highly autonomous is now presented.

3.4. Cycle Ambiguity Resolution

Equation 3-5 contains a term, k_{ij} , which represents the integer number of carrier wavelengths in the range measurement of antenna baseline vector \underline{b}_j projected onto the GPS signal line of sight \underline{s}_j . This term is solved and removed from the “real-time” attitude determination algorithm of Equations 3-6 through 3-13. The method by which this term is solved and an initial attitude guess $(\underline{A}_{E \rightarrow B})_0$ is provided to the first execution of the real-time attitude determination loop is known as cycle ambiguity resolution.

3.4.1. Search and Motion Methods for Space

There are an abundance of innovative algorithms that enable cycle ambiguity resolution to occur efficiently under many different circumstances. Most of these methods fall into two classes: those that utilize a “snapshot” instant set of measurements and those that operate on a batch set of measurements taken over a specified period of time. Another interesting approach by Montgomery uses a direct nonlinear solution technique.⁷

The snapshot methods pick a solution that minimizes the error residual at that instant by *searching* through an exhaustive list of all possible integers and rejecting classes of solutions when the residual gets too large.⁸ The appeal of these methods are that they provide an “instantaneous” attitude solution, limited only by computation time, and are well suited to the short baselines that are often found on spacecraft. However, as has been noted elsewhere,⁴ the minimum residual does not guarantee a correct solution in the presence of noise. In fact, it is possible, and has been operationally observed, that the search method can report a *wrong* solution as valid, especially when some of the calibration information, such as line bias, is incorrect. This lack of integrity can be very

troubling if the sensor output is used to control a high bandwidth actuator such as gas jets.

Another consideration regarding the use of the search method is that these algorithms sometimes require that the antenna array must be within a defined angle (typically 30 degrees) of a reference attitude, which is often true on the ground but less likely to be true in space. This constraint narrows the search space of possible solutions, but candidate solutions outside of the defined angle are not considered. Also, structural flexibility is not modeled and may lead to erroneous solutions. These limitations mean that the search method, while attractive because of its fast solution, is not totally acceptable for *general* purpose spacecraft applications. Nonetheless, it has been successfully employed on-orbit in specific cases and has been found to work well in certain applications.

The other technique for resolving cycle ambiguities is to collect data for a given period of time and to attempt a large batch solution in which the integer terms remain constant over the data collection (phase wraparounds are handled by incrementing the 'fractional' carrier phase term and maintaining the constant cycle ambiguity integer). These methods rely on the fact that a certain amount of *motion* has occurred during the data collection, either from the vehicle body rotation or the GPS signal line of sight motion. The main disadvantage of this method when compared to the search technique is that it takes time for the motion to occur, and this time may be on the order of several minutes for a slowly rotating spacecraft. Another consideration is that a potentially significant amount of memory is required for the storage of the batch data collection. But motion methods also enjoy advantages over their search counterparts. Most importantly, they are inherently *high integrity* methods because there are a number of checks that can be built into the solution before it is accepted. These include the computed value for the integers, which are solved as floating point numbers but turn out to be approximately integral in value as

a check; and the integer part cannot be greater than the baseline length in carrier wavelengths. The error residual and the matrix condition number are also available to assess the adequacy of the solution. The probability of an erroneous solution being reported as valid can be made as small as desired by appropriately setting the thresholds on these many integrity checks. Motion methods also handle any vehicle attitude and any external reference frame very easily.

3.4.2. Quasi-Static Integer Resolution

Traditional matrix motion methods of cycle ambiguity resolution rely on the fact that either GPS line of sight motion or vehicle rotation dominates the changes in differential carrier phase measurements. Cohen⁴ originally proposed an algorithm known as “Quasi-Static” integer resolution to be used when the GPS line of sight motion and the vehicle rotation both account approximately evenly for the differential carrier phase measurement changes. A very interesting feature of this algorithm that will be employed in the next section is that it can be adapted to almost *any* type of vehicle motion—slow or fast—by varying the sample rate and the data collection time. This property makes Quasi-Static integer resolution a suitable algorithm for a highly autonomous means of integer resolution that does not require advance knowledge of the vehicle dynamics to be successfully employed.

Quasi-static method solves a collection of differential phase measurements for a *single* attitude estimate and then considers perturbations to the initial estimate at each measurement epoch to produce a time varying batch attitude solution to the data. Its main current limitation is that if the data collection covers too long a time span relative to the vehicle motion, then small perturbations of attitude will not allow the attitude to converge to the correct solution at every time step, and the integrity checks will reject the result.

This behavior is, of course, the purpose of the integrity checks, since any solution based only on small perturbations is, in this case, incorrect. For spacecraft, the success of the algorithm can be substantially improved by allowing for an unknown, but *constant* rate of motion to be estimated over the data set. Small perturbations may then be successfully taken about the motion profile which includes a constant rate of attitude motion.

First, an initial guess of the vehicle attitude must be obtained to which small perturbations may be made for the final solution. Begin by taking measurements for $k = 1$ to L samples ('measurement epochs') to which a single solution for vehicle attitude will be determined. Repeating the basic scalar measurement equation for $i = 1$ to M GPS signals, and $j = 1$ to N baselines:

$$\Delta\phi_{ij} = [\underline{s}_i^T]_E \underline{A}_{E \rightarrow B}^T [\underline{b}_j]_B + k_{ij} + \beta_j + v_{ij} \quad [3-5]$$

$[\underline{b}_j]_B$ is a 3-by-1 vector for each antenna baseline in the body reference frame. Therefore $[\underline{b}_j]_B$ are known. For now, assume that all MN measurements are taken each epoch. Over N baselines, a $3N$ -by-1 vector representation of all baseline vectors in the external ('E') reference frame can be constructed as follows:

$$[\underline{Ab}]_E = \begin{bmatrix} \underline{A}_{E \rightarrow B}^T [\underline{b}_1]_B \\ \underline{A}_{E \rightarrow B}^T [\underline{b}_2]_B \\ \vdots \\ \underline{A}_{E \rightarrow B}^T [\underline{b}_N]_B \end{bmatrix} \quad (3-15)$$

The notation $[\underline{Ab}]_E$ is used as a reminder that this vector contains embedded information about the vehicle attitude.

For a given measurement epoch (all measurements taken in the same sample), there are MN total measurements. Since each measurement (in the same epoch) has a unique integer, a new line of sight matrix should be constructed:

$$\underline{\underline{S}}_k = \begin{pmatrix} \begin{bmatrix} \underline{s}_i^T \end{bmatrix}_E & \begin{bmatrix} \underline{e}_1 & \underline{e}_2 & \cdots & \underline{e}_N \end{bmatrix}_1 \\ \begin{bmatrix} \underline{s}_i^T \end{bmatrix}_E & \begin{bmatrix} \underline{e}_1 & \underline{e}_2 & \cdots & \underline{e}_N \end{bmatrix}_2 \\ \vdots & \vdots \\ \begin{bmatrix} \underline{s}_i^T \end{bmatrix}_E & \begin{bmatrix} \underline{e}_1 & \underline{e}_2 & \cdots & \underline{e}_N \end{bmatrix}_{MN} \end{pmatrix} \quad (3-16)$$

$\underline{\underline{S}}_k$ is the MN -by- $3N$ line of sight matrix, for measurement epochs $k = 1$ to L . $\begin{bmatrix} \underline{s}_i^T \end{bmatrix}_E$ is the 1-by-3 line of sight row vector that corresponds to the correct measurement (the number of measurements goes from 1 to MN , and each measurement has a line of sight vector associated with the GPS signal from which the measurement was made). $\begin{bmatrix} \underline{e}_1 & \underline{e}_2 & \cdots & \underline{e}_N \end{bmatrix}$ is a 3-by- $3N$ matrix composed of N , 3-by-3 matrices \underline{e}_j , that are the Identity matrix if the measurement corresponds to the j th baseline, and the Null matrix otherwise.

The notation of Equations 3-15 and 3-16 allows a very compact and convenient representation of the measurement vector at the k th measurement epoch:

$$\underline{\underline{S}}_k [\underline{\underline{Ab}}]_E + \underline{\underline{k}} = (\underline{\Delta\phi} - \underline{\beta})_k \quad (3-17)$$

$\underline{\underline{S}}_k$ is a MN -by- $3N$ line of sight matrix, $[\underline{\underline{Ab}}]_E$ is a $3N$ -by-1 antenna baselines vector, and $\underline{\underline{k}}$, $\underline{\Delta\phi}$, and $\underline{\beta}$ are MN length column vectors. Compare this vector equation to the scalar form of Equation 3-5. The unknown quantities in Equation 3-17 are the antenna baseline vector in the external reference frame $[\underline{\underline{Ab}}]_E$ and the cycle ambiguity vector $\underline{\underline{k}}$.

If every epoch has measurements taken from the same GPS signals and antenna baselines, but less than a full set of MN measurements (if, for example, one channel is not tracking anything and therefore not taking measurements), the same measurement structure of Equation 3-17 applies with the invalid states removed.

If a channel loses signal lock before the end of the data collection process (L measurement epochs), all further measurement epochs should simply enter zero elements for both sides of the appropriate row of Equation 3-17. In this manner, useful information from earlier in the data collection is retained for the solution even if the number of available measurements changes.

If a channel acquires a signal in the midst of the data collection (between measurement epochs $k = 2$ to $L-1$), the new information may be incorporated by adding a new state (i.e., measurement row) to Equation 3-17 and padding the previous measurement epochs with zero rows prior to signal acquisition.

This active maintenance of the measurement equation may be used to obtain the maximum amount of available information as GPS satellites rise and set during the data collection, which may last several minutes.

The measurement vectors are then collected for L epochs and partitioned into the following form:

$$\begin{bmatrix} \underline{\underline{S}}_1 & \underline{\underline{I}}_1 \\ \underline{\underline{S}}_2 & \underline{\underline{I}}_2 \\ \vdots & \vdots \\ \underline{\underline{S}}_L & \underline{\underline{I}}_L \end{bmatrix} \begin{pmatrix} [\underline{\underline{Ab}}]_E \\ \underline{\underline{k}} \end{pmatrix} = \begin{bmatrix} (\underline{\Delta\phi} - \underline{\beta})_1 \\ (\underline{\Delta\phi} - \underline{\beta})_2 \\ \vdots \\ (\underline{\Delta\phi} - \underline{\beta})_L \end{bmatrix} \quad (3-18)$$

This is a set of LMN linear equations to be solved using the traditional Least Squares methods for $(3+M)N$ unknowns. The square matrices $\bar{\underline{I}}_k$ are MN quasi-identity matrices with possible zeroes along the diagonal where states have been added and removed at various measurement epochs. In the event that there are no changes in cycle ambiguity states during the data collection, the $\bar{\underline{I}}_k$ matrices are in fact identity matrices. The solution is the initial guess for the integers \underline{k} and the antenna baselines vector expressed in the external reference frame, $[\underline{Ab}]_E$. The attitude matrix $\underline{A}_{E \rightarrow B}$ may then be solved via Wahba's method for vector observations.⁴

As in Section 3.2.2 (Equations 3-6 through 3-13), linearized solutions about the initial attitude guess are sought, that will converge to the nonlinear solution for the attitude of the antenna platform. In this case, the perturbations at each measurement epoch also allow for the attitude to change slightly with time, accounting for slowly moving vehicles. Following a similar approach as before, a perturbations vector is defined at each measurement epoch:

$$\begin{aligned} [\underline{\delta\phi}_k] &= [\underline{\Delta\phi}_k - (\underline{\Delta\phi}_k)_0] = \begin{bmatrix} [\underline{s}_1^T]_E (\underline{A}_{E \rightarrow B}^T)_0 (\underline{B}_1^\times)^T \\ \vdots \\ [\underline{s}_{MN}^T]_E (\underline{A}_{E \rightarrow B}^T)_0 (\underline{B}_{MN}^\times)^T \end{bmatrix} \bar{\underline{I}}_k \begin{bmatrix} \underline{\delta\theta}_k \\ \underline{\delta k} \end{bmatrix} \\ &\equiv \begin{bmatrix} \underline{H}_k & \bar{\underline{I}}_k \end{bmatrix} \begin{bmatrix} \underline{\delta\theta}_k \\ \underline{\delta k} \end{bmatrix} \end{aligned} \quad (3-19)$$

Equation 3-19 is a set of MN equations with $(3+MN)$ states. \underline{B}_j^\times is the antenna baseline cross matrix, defined in Equation 3-11, for the corresponding measurement. Now generalize to allow perturbations at all epochs:

$$\begin{bmatrix} \underline{\delta\phi}_1 \\ \underline{\delta\phi}_2 \\ \vdots \\ \underline{\delta\phi}_L \end{bmatrix} = \begin{bmatrix} \underline{H}_1 & \underline{0} & \cdots & \underline{0} & \underline{\bar{I}}_1 \\ \underline{0} & \underline{H}_2 & \ddots & \vdots & \underline{\bar{I}}_2 \\ \vdots & \ddots & \ddots & \underline{0} & \vdots \\ \underline{0} & \cdots & \underline{0} & \underline{H}_L & \underline{\bar{I}}_L \end{bmatrix} \begin{bmatrix} \underline{\delta\theta}_1 \\ \vdots \\ \underline{\delta\theta}_L \\ \underline{\delta\mathbf{k}} \end{bmatrix} \quad (3-20)$$

This compact representation has LMN rows (potentially hundreds) and $(3L+MN)$ states. In principle, the integers and the attitude of the vehicle at each measurement epoch may be solved by applying Equation 3-20 iteratively and updating the initial guesses at each measurement epoch in Equation 3-19. In practice however, the large observation matrix in Equation 3-20 may have numerical problems, which might drop rank or be poorly conditioned. Fortunately, the method required to assess the condition of the matrix (also the observability of the system) is also the most stable method of solving Equation 3-20.

3.4.3. Singular Value Decomposition Solution

Many textbooks such as Golub⁹ discuss the properties of the Singular Value Decomposition (SVD). It is often bypassed as a method of matrix inversion for other, more computationally efficient, algorithms. In cycle ambiguity resolution, however, where large matrices are inverted once as part of a bootstrapping procedure, numerical stability can be more important than the number of processor flops. Another key property of the SVD is its utility as a real-time analytical tool for the computation of the condition number of the observation matrix. *This is the main concept that can be used to automate the integer resolution process*, independent of vehicle motion rates. This point will be explained in more detail.

In review, the SVD of the matrix \underline{A} is given by:

$$\underline{A} = \underline{U} \cdot [\text{diag}(w_j)] \cdot \underline{V}^T \quad (3-21)$$

where \underline{U} and \underline{V}^T are unitary matrices and $w_j (>0)$ are the singular values of the matrix \underline{A} .

The solution to the linear system $\underline{b} = \underline{A} \cdot \underline{x}$ (that is, Equation 3-20) :

$$\underline{x} = \underline{V} \cdot [\text{diag}(1 / w_j)] \cdot (\underline{U}^T \underline{b}) \quad (3-22)$$

minimizes:

$$r = \|\underline{A} \cdot \underline{x} - \underline{b}\|_2 \quad (3-23)$$

Published programs exist for performing these standard numerical operations.¹⁰

Equations 3-21 through 3-23 state that the SVD can be used as the solution to minimize the error residual in the Least Squares method. The usefulness of the SVD algorithm for this application, however, goes much further. Because the singular values are computed in the solution to Equation 3-21, the condition number of the matrix is readily available (as the ratio of the maximum and minimum singular values). Poorly conditioned matrices that may have numerical problems can therefore be readily identified. The minimum singular values and their associated vectors in \underline{U} and \underline{V}^T may be removed, if desired, to solve the partial system as the orthogonal projection of the remaining subspace (with the singular value removed) onto the solution space.

The condition number may also be used as a measure of the observability of this dynamic system given the available measurements. As the observability improves, the condition number lowers to a value determined by the GPS signal line of sight and measurement geometry over the complete data collection. In other words, the condition number may be

used as a *logical input* for a feedback loop to select the best sample period and collection time for the Quasi-Static integer resolution algorithm. If the condition number is high, the sample period should be increased, allowing more geometry change during the data collection. It is not necessary to specify a fixed sample time in advance, which implies assumed knowledge about the vehicle dynamics. The receiver can adjust itself to the best sample period and collection time for Quasi-Static integer resolution, regardless of the nature of the vehicle motion. If the vehicle dynamics change during the data collection, the receiver will adjust to the change. The Quasi-Static method is therefore implemented as a *highly autonomous* algorithm for spacecraft integer resolution, which does not require foreknowledge of the vehicle dynamics.

In Section 3.4.1 it was mentioned that the principal drawback for the motion algorithms was the time required for the motion to occur. In particular, if the motion is not known in advance, a conservative data collection time must be used to guarantee that the integer resolution equations are sufficiently observable. The Quasi-Static SVD algorithm cannot change the physics controlling the rate of geometry motion, but it can guarantee that integer resolution is obtained *as soon as* there is enough motion in the measurements to attempt a solution, regardless of the nature of the vehicle dynamics.

As an example, consider data which has been post-processed from the RADCAL spacecraft, which will be discussed as a flight application in Chapter 5. RADCAL is an Earth pointed, gravity gradient stabilized satellite with canted (nonaligned) antennas. The condition number of the cycle ambiguity resolution observation matrix using the Quasi-Static method (Equation 3-20) is shown in Figure 3.5. It is seen that as the sample time increases, the matrix becomes better conditioned, gradually leveling off beyond 20

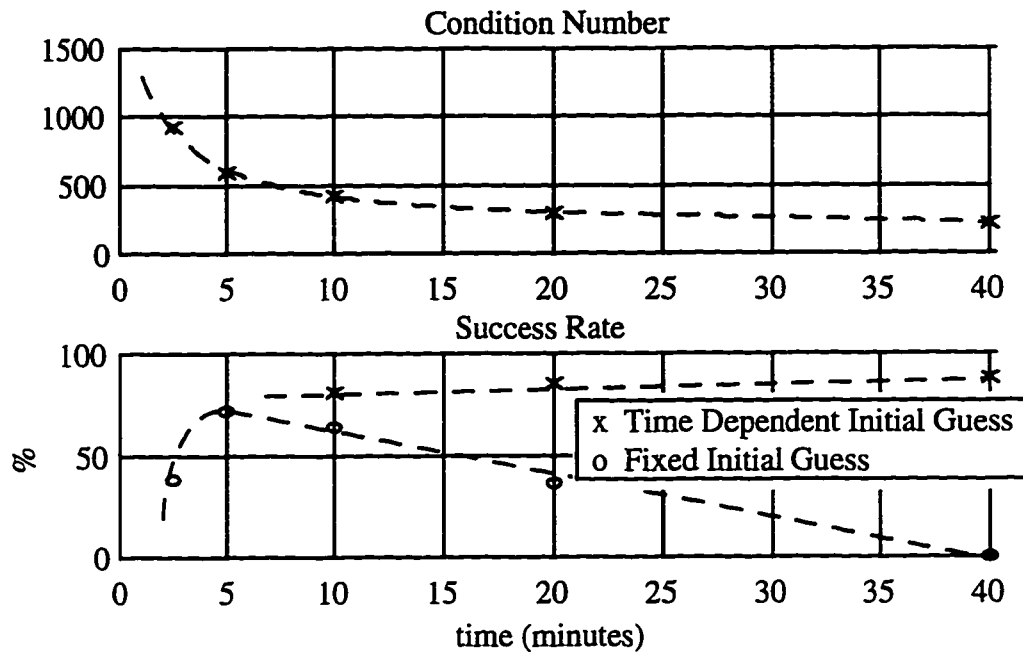


Figure 3.5. Integer Resolution Performance for Earth Pointed Platform

minutes, where more data does not significantly increase the information about the attitude of the vehicle. As the condition number drops, the probability of successful integer resolution (that is, the number of times cycle ambiguity resolution was successfully performed out of the total number of attempts) steadily increases to about 85% at 20 minutes. Interestingly, if the initial guess is fixed, the probability of success peaks at about 5 minutes and steadily decreases thereafter. The reason for this behavior is that as the time interval increases, the perturbations to the initial guess become too large for the Quasi-Static method to converge to a solution. By augmenting the state equations to include a constant, but unknown, body rate which is also estimated, the success rate continues to increase, becoming approximately constant at 20 minutes.

An autonomous integer resolution algorithm could be applied to this receiver, which would attempt a solution at a set condition number. If the condition number is too high

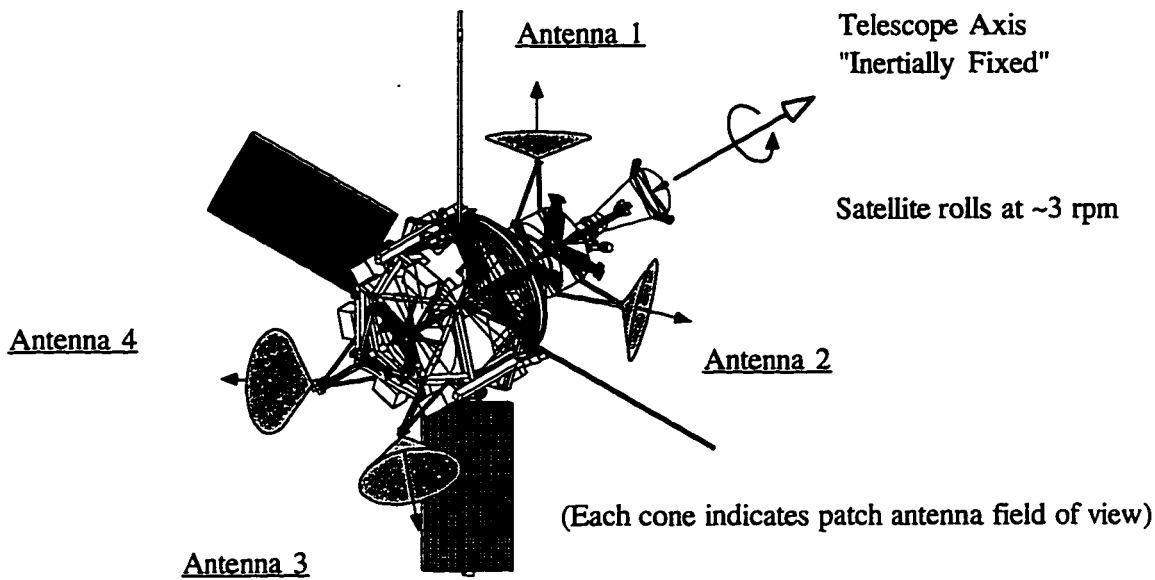


Figure 3.6. Gravity Probe B Spacecraft with 4 Nonaligned GPS Patch Antennas

initially, the sample rate and collection time would be lengthened, in such a way that would not discard previous information, until the probability of a successful resolution is reasonably high, perhaps 75% (about a 5 minute collection time in many cases).

3.5. Nonaligned Antennas

The motivation for nonaligned antenna arrays was presented in the Section 3.3. A satellite design¹¹ with nonaligned GPS antennas is shown in Figure 3.6. One effect of nonalignment is that the antenna gain pattern produces different signal strengths on each antenna, since the GPS signal line of sight occurs at different elevation angles for each antenna (in the antenna centered reference frame). Another effect is that the right hand circularly polarized (RHCP) antenna phase pattern is not common mode and must be modeled to produce correct differential carrier phase measurements. Also, common

fields of view between antennas are reduced, resulting in fewer differential carrier phase measurements. All of these effects will be discussed.

3.5.1. Roving Master Antenna

Many GPS patch antennas may be effectively modeled as having a hemispherical gain pattern. When all antennas are aligned, they have the same GPS signal visibility and gain. In this case a single master antenna may be chosen and fixed, since all GPS signals will present the same elevation angle to all antennas. For nonaligned antennas, the received signal strengths may vary considerably from antenna to antenna, and some antennas may not have visibility to a given GPS satellite. If all differential carrier phase measurements are made with respect to a common master antenna (another approach will be discussed in Section 3.5.2), it is desirable to use the antenna with the strongest received signal for each GPS satellite as the master antenna. This method will produce the most quality measurements.

Mathematically, the differential carrier phase measurements must be interpreted consistently, and the antenna baseline vectors must reflect the correct master antenna. When the master antenna changes as shown, for example, in Figure 3.7, the differential phase and antenna baseline vectors are linear combinations of the previous case as follows:

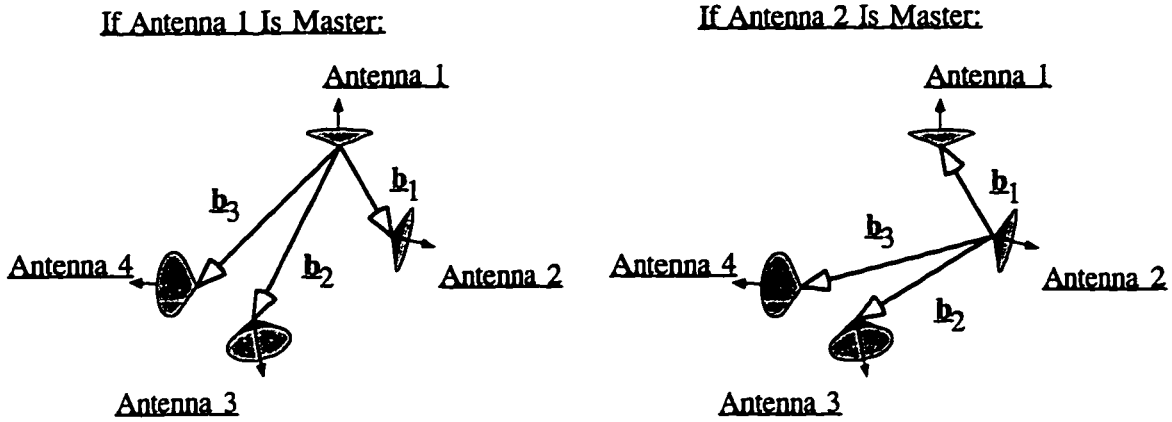


Figure 3.7. Roving Master Antenna Concept

$$\begin{bmatrix} \Delta\phi_1 \\ \Delta\phi_2 \\ \Delta\phi_3 \end{bmatrix}_{m1} = \begin{bmatrix} \phi_2 - \phi_1 \\ \phi_3 - \phi_1 \\ \phi_4 - \phi_1 \end{bmatrix} \quad (3-24)$$

$$\begin{bmatrix} \Delta\phi_1 \\ \Delta\phi_2 \\ \Delta\phi_3 \end{bmatrix}_{m2} = \begin{bmatrix} \phi_1 - \phi_2 \\ \phi_3 - \phi_2 \\ \phi_4 - \phi_2 \end{bmatrix}, \quad \begin{bmatrix} \Delta\phi_1 \\ \Delta\phi_2 \\ \Delta\phi_3 \end{bmatrix}_{m1} = \begin{bmatrix} -\Delta\phi_1 \\ \Delta\phi_2 - \Delta\phi_1 \\ \Delta\phi_3 - \Delta\phi_1 \end{bmatrix}_{m2} \quad (3-25)$$

$$[\underline{b}_1 \quad \underline{b}_2 \quad \underline{b}_3]_{m1} = [-\underline{b}_1 \quad \underline{b}_2 - \underline{b}_1 \quad \underline{b}_3 - \underline{b}_1]_{m2} \quad (3-26)$$

It should be emphasized that although Equation 3-25 demonstrates how differential carrier phase measurements are related to one another using an alternative master antenna, this extra differencing operation is not actually performed (which would increase the resultant measurement noise). Instead, the unmodified differential carrier phase measurements are interpreted separately using the antenna baseline vectors as defined in Equation 3-26. Once these changes are inserted in Equations 3-5 and 3-15, the remainder of the attitude determination logic is performed the same as presented in the previous

sections. Similar relations may be derived for the other possible master antennas combinations.

The end result is that more valid measurements are taken from each GPS signal, since each signal may have a different master antenna—the antenna that provides the strongest signal to noise ratio. A software Schmitt trigger is added to prevent noisy switching between master antennas when the signal strengths are approximately equal on two or more antennas.

3.5.2. All in View Carrier Phase Measurements

If the incoming carrier phase is measured independently at each antenna (rather than relative to a single master antenna), an “all in view” approach may be used to combine all possible permutations of differential phase measurements (Figure 3.8). For n antennas, up to $n(n-1)/2$ differential phase measurements may be taken at a each sample using this method; this provides a significant increase in measurements when the number of antennas becomes large.

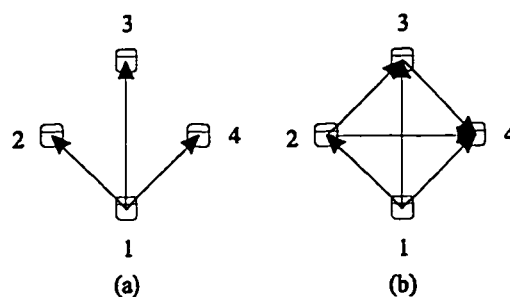


Figure 3.8. Differential Phase Measurements from 4 Antennas, using (a) Master-Slave Method, and (b) All in View Method

3.5.3. Differential Phase Angle Correction

GPS signals are right hand circular polarized (RHCP) for broadcast through the ionosphere. The fact that this is so can be seen by rotating an antenna counterclockwise about its boresight. The received signal is seen to go through a positive phase angle change equal to the angle of rotation. When the receiving antenna is perpendicular to the direction of propagation of the GPS signal (0 degrees elevation), rotation about its boresight produces no change in the received signal.

For differential carrier phase measurements, this effect cancels out when the antennas are aligned with each other. Even if the antennas are installed rotated about their boresights by a fixed angle, as long as the boresight *vectors* are aligned the resultant additional phase angle is a fixed value that may be calibrated out of the measurement with line bias.

When the antenna boresights are *not* aligned, this effect must be modeled to produce accurate differential phase measurements. The first derivation of this correction term was applied to absolute carrier phase positioning by Lawrence.¹² This correction method may also be extended to nonaligned antenna arrays for attitude determination.

Consider two antennas with boresight unit vectors, $\hat{\mathbf{z}}_1$ and $\hat{\mathbf{z}}_2$. These vectors form the z-axes of local antenna reference frames. Imagine x- and y-axis vectors attached to the in-plane components of the antennas to complete the definition of the local antenna reference frames. At the time of antenna array installation, the relationship between the two antenna reference frames is measured and stored as a known transformation matrix $\underline{\mathbf{A}}_{2>1}$, so that any vector \mathbf{r}_2 in the 2-antenna reference frame may be transformed to the 1-antenna reference frame:

$$\mathbf{r}_1 = \underline{\mathbf{A}}_{2>1} \mathbf{r}_2 \quad (3-27)$$

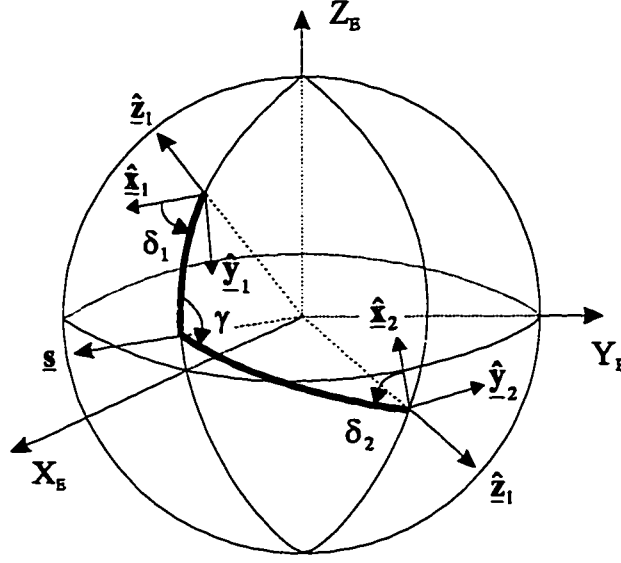


Figure 3.9. Spherical geometry accounting for RHCP phase contribution to nonaligned antennas

For an aligned array, the $\underline{A}_{2>1}$ matrix is identity. For a nonaligned antenna array, the $\underline{A}_{2>1}$ matrix defines the relationship between the master (1) and slave (2) antenna reference frames. The master antenna reference frame is then defined to be (or is transformed back to) the vehicle body reference frame.

The geometry of the RHCP contribution to differential phase measurements is shown in Figure 3.9. The nonaligned antenna boresight vectors \hat{z}_1 and \hat{z}_2 are translated to the origin and shown with the GPS signal line of sight unit vector \hat{s} as they pierce the unit sphere. The local antenna reference frames are completed with the vectors \hat{x}_1 , \hat{y}_1 , \hat{x}_2 , and \hat{y}_2 drawn tangent to the sphere. Assume that the attitude of the vehicle with respect to the external reference frame, $\underline{A}_{E>B}$, is known, so that all vectors can be represented in a single, consistent reference frame.

To calculate the magnitude of the RHCP contribution, consider that a right-handed rotation about the boresight of an antenna increases the phase measurement by the

magnitude of the rotation, whereas a rotation normal to the antenna boresight does not change the phase measurement. Begin by rotating antenna 1 about its boresight vector through the right-handed angle δ_1 so that the x-axis points along the great circle to \hat{s} . The phase angle measured at antenna 1 is increased by δ_1 radians. Rotate the antenna boresight \hat{z}_1 along the great circle so that it coincides with \hat{s} . Because the rotation is normal to antenna boresight, the phase measurement at antenna 1 is unchanged.

Now rotate antenna 2 about its boresight vector through the right-handed angle δ_2 so that the x-axis points along the great circle to \hat{s} . The phase angle measured at antenna 2 is increased by δ_2 radians. Rotate the antenna boresight \hat{z}_2 along the great circle so that it coincides with \hat{s} . Because this rotation is normal to antenna boresight, the phase measurement at antenna 2 is unchanged.

The x- and y-axes of antennas 1 and 2 are now separated by the angle γ while the boresight vectors of both antennas point along the line of sight vector \hat{s} . To complete the calculation, rotate antenna 2 about its boresight vector through the angle γ to bring the antennas to a common reference. The phase measurement at antenna 2 is increased by γ radians.

Summarizing, antenna 1 was rotated through the angle δ_1 and antenna 2 was rotated through the angle $\delta_2 + \gamma$ to be brought to a common reference:

$$(\varphi_1)_c = (\varphi_1)_u + \delta_1 \quad (3-28)$$

$$(\varphi_2)_c = (\varphi_2)_u + \delta_2 + \gamma \quad (3-29)$$

$$(\varphi_2 - \varphi_1)_c = (\varphi_2 - \varphi_1)_u + \delta_2 + \gamma - \delta_1 \quad (3-30)$$

This is a real addition to the differential carrier phase measurement due solely to the RHCP effect of the transmitted signal. To calculate the correction angles from known quantities, first specify the direction of rotation of δ_1 to be normal to $\hat{\mathbf{z}}_1$ and $\hat{\mathbf{s}}$:

$$\hat{\mathbf{r}}_1 \equiv \frac{\hat{\mathbf{z}}_1 \times \hat{\mathbf{s}}}{\|\hat{\mathbf{z}}_1 \times \hat{\mathbf{s}}\|_2} \quad (3-31)$$

Then define the pointing vector from $\hat{\mathbf{z}}_1$ to $\hat{\mathbf{s}}$ to be normal to $\hat{\mathbf{z}}_1$ and $\hat{\mathbf{r}}_1$:

$$\hat{\mathbf{p}}_1 \equiv \frac{\hat{\mathbf{r}}_1 \times \hat{\mathbf{z}}_1}{\|\hat{\mathbf{r}}_1 \times \hat{\mathbf{z}}_1\|_2} \quad (3-32)$$

The rotation angle δ_1 is then given by:

$$\delta_1 = \left[\cos^{-1}(\hat{\mathbf{x}}_1 \cdot \hat{\mathbf{p}}_1) \right] \left[\text{sgn}((\hat{\mathbf{x}}_1 \times \hat{\mathbf{p}}_1) \cdot \hat{\mathbf{z}}_1) \right] \quad (3-33)$$

which can be expressed in terms of fundamental quantities as:

$$\delta_1 = \left[\cos^{-1} \left(\frac{\hat{\mathbf{x}}_1 \cdot \hat{\mathbf{s}}}{\|\hat{\mathbf{s}} - (\hat{\mathbf{z}}_1 \cdot \hat{\mathbf{s}}) \hat{\mathbf{z}}_1\|_2} \right) \right] \left[\text{sgn}((\hat{\mathbf{x}}_1 \times \hat{\mathbf{s}}) \cdot \hat{\mathbf{z}}_1) \right] \quad (3-34)$$

Likewise:

$$\delta_2 = \left[\cos^{-1} \left(\frac{\hat{\mathbf{x}}_2 \cdot \hat{\mathbf{s}}}{\|\hat{\mathbf{s}} - (\hat{\mathbf{z}}_2 \cdot \hat{\mathbf{s}}) \hat{\mathbf{z}}_2\|_2} \right) \right] \left[\text{sgn}((\hat{\mathbf{x}}_2 \times \hat{\mathbf{s}}) \cdot \hat{\mathbf{z}}_2) \right] \quad (3-35)$$

γ is the angle between the two pointing vectors $\hat{\mathbf{p}}_1$ and $\hat{\mathbf{p}}_2$:

$$\gamma = \left[\cos^{-1}(\hat{\underline{\mathbf{p}}}_2 \cdot \hat{\underline{\mathbf{p}}}_1) \right] \left[\text{sgn}((\hat{\underline{\mathbf{p}}}_2 \times \hat{\underline{\mathbf{p}}}_1) \cdot \hat{\underline{\mathbf{s}}}) \right] \quad (3-36)$$

The form of this equation in terms of fundamental quantities is more involved, but evaluates easily:

$$\gamma = \left[\cos^{-1} \left(\frac{1 + (\hat{\underline{\mathbf{z}}}_1 \cdot \hat{\underline{\mathbf{s}}})(\hat{\underline{\mathbf{z}}}_2 \cdot \hat{\underline{\mathbf{s}}})(\hat{\underline{\mathbf{z}}}_1 \cdot \hat{\underline{\mathbf{z}}}_2) - (\hat{\underline{\mathbf{z}}}_1 \cdot \hat{\underline{\mathbf{s}}})^2 - (\hat{\underline{\mathbf{z}}}_2 \cdot \hat{\underline{\mathbf{s}}})^2}{\| \hat{\underline{\mathbf{s}}} - (\hat{\underline{\mathbf{z}}}_1 \cdot \hat{\underline{\mathbf{s}}}) \hat{\underline{\mathbf{z}}}_1 \|_2 \| \hat{\underline{\mathbf{s}}} - (\hat{\underline{\mathbf{z}}}_2 \cdot \hat{\underline{\mathbf{s}}}) \hat{\underline{\mathbf{z}}}_2 \|_2} \right) \right] \cdot \left[\text{sgn}((\hat{\underline{\mathbf{z}}}_2 \cdot \hat{\underline{\mathbf{s}}})(\hat{\underline{\mathbf{z}}}_1 \cdot \hat{\underline{\mathbf{s}}})[(\hat{\underline{\mathbf{z}}}_2 \times \hat{\underline{\mathbf{z}}}_1) \cdot \hat{\underline{\mathbf{s}}})] \right] \quad (3-37)$$

Equations 3-33 through 3-37 are well defined at all points except when any two of the three vectors $\hat{\underline{\mathbf{z}}}_1$, $\hat{\underline{\mathbf{z}}}_2$, and $\hat{\underline{\mathbf{s}}}$ are parallel, which is a condition that may be tested before attempting to apply these equations.

The primary obstacle to applying these equations directly to the carrier phase measurement in Equation 3-30 is that the attitude of the vehicle, $\underline{\mathbf{A}}_{E>B}$, is embedded in the expressions of the antenna reference frames. A circular condition arises whereby to calculate the attitude it is necessary to know the RHCP correction, but to calculate the RHCP correction the attitude must be known. If the attitude of the vehicle is already approximately known, perhaps from a prior estimate, the RHCP effect may be estimated and then iterated along with a new attitude solution to convergence. If there is no prior estimate of attitude, an estimate may be constructed from other means, such as the line of sight vector along each antenna to the strongest GPS signal received on that antenna.

The actual implementation of these equations in a GPS receiver is left as a topic for future research. With the equations established to calculate the RHCP effect on differential carrier phase measurements for nonaligned antenna arrays, it should be

possible to build a receiver that employs these corrections to perform attitude determination with nonaligned antenna arrays. As has been mentioned, this augmentation of the GPS attitude determination algorithms is critical for the generalization of this capability to all types of spacecraft pointing applications.

3.5.4. Signal Visibility Using Nonaligned Arrays

Greater sky coverage of a nonaligned antenna array comes at the expense of common field of view between antennas. Since common view to a GPS signal between two or more antennas is the basis of GPS attitude determination, the question of whether a nonaligned antenna array will have enough differential carrier phase measurements must be addressed.

The GPS signal visibility is determined by two factors: the antenna elevation mask and Earth occultation. The minimum elevation mask is determined by the antenna gain pattern and a reasonable value of 10 degrees may be used for a hemispherical patch antenna. The occultation height is set to the ionosphere shell altitude of 350 km to minimize ionospheric delay and refraction.¹³ This estimate is conservative because GPS satellites can be tracked through the Earth limb (although the signal may undergo some time delay and refraction). Figure 3.10 shows the GPS signal visibility geometry. Using the satellite position vector, \mathbf{r} , the Earth occultation threshold angle is:¹⁴

$$\theta_{th} = 90^\circ + \cos^{-1} \left(\frac{(R_e + h_e)}{|\mathbf{r}|} \right) \quad (3-38)$$

And the antenna elevation threshold is:

$$\phi_{th} = 90^\circ - \phi_e = 80^\circ \quad (3-39)$$

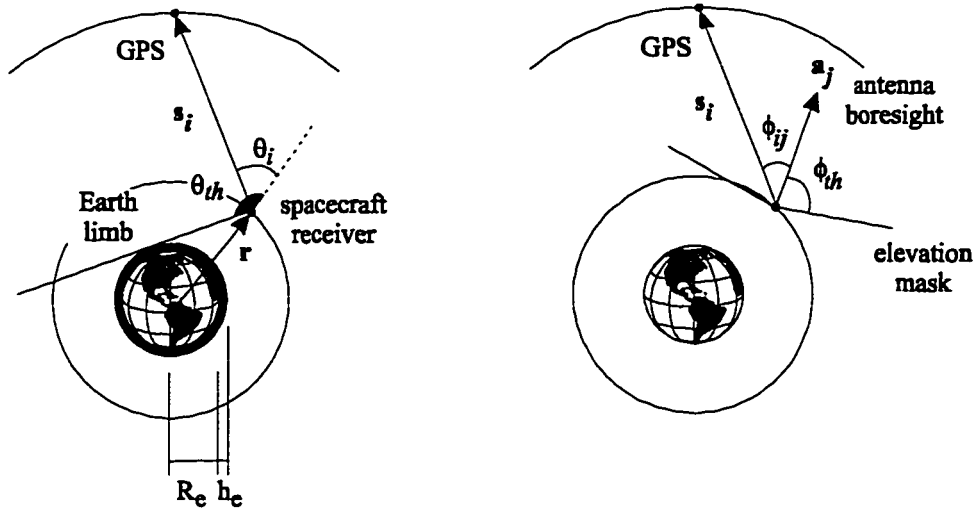


Figure 3.10. Earth occultation and elevation angle with respect to antenna boresight vector determine GPS signal visibility

where R_e is the Earth radius, h_e is the ionospheric shell height (350 km), and ϕ_e is the antenna elevation mask (10 degrees). Defining the line of sight vector to the i th GPS satellite specified in an external reference frame, $[\underline{s}_i]_E$, the j th antenna boresight vector specified in a vehicle body reference frame, $[\underline{a}_j]_B$, and the attitude of the vehicle, $\underline{A}_{E \rightarrow B}$, the antenna boresight may be transformed to the external reference frame:

$$[\underline{a}_j]_E = \underline{A}_{E \rightarrow B}^T [\underline{a}_j]_B \quad (3-40)$$

The Earth viewing angle and GPS signal elevation angle may be calculated as:

$$\theta_i = \text{acos} \left(\frac{\underline{r} \cdot \underline{s}_i}{|\underline{r}| |\underline{s}_i|} \right) \quad (3-41)$$

$$\phi_{ij} = \text{acos} \left(\frac{\underline{s}_i \cdot \underline{a}_j}{|\underline{s}_i| |\underline{a}_j|} \right) \quad (3-42)$$

where the reference frame subscripts have been removed for clarity. Using a current almanac to determine the GPS satellite positions, a GPS signal ($i=1$ to 24) is declared visible at a given antenna (j) when the following condition is satisfied for more than 30 seconds:

$$(\theta_i \leq \theta_{th}) \cap (\phi_{ij} \leq \phi_{th}) \neq 0 \quad (3-43)$$

The question of how many differential phase measurements are required at a minimum for 3-axis attitude determination must be answered somewhat heuristically. In theory, as few as 3 measurements are required to specify the orientation of a rigid body; but in the presence of measurement noise and limited observability, more measurements are usually required to obtain a solution with a sufficiently low normalized residual. On the basis of previous experience with other spacecraft experiments such as the RADCAL satellite, it is believed that approximately 8 or more valid differential phase measurements are necessary for reliable attitude determination.¹⁵

3.5.5. Orbit Visibility Study

While the results of any visibility analysis are specific to the given orbit, vehicle pointing profile, and antenna geometry, an example orbit with different pointing profiles and antenna configurations may be considered to demonstrate trends that are valid for many LEO applications.

Using the methods described in the previous section, the differential phase measurement availability was characterized for several different pointing profiles and antenna geometries using a fixed orbit. The orbit used in this study was a 650 km polar orbit, which is the planned orbit for the Gravity Probe B mission, scheduled to fly in 1999.¹¹

Visibility and measurement availability statistics were compiled for a 24 hour period using a real 24 satellite almanac. The results of the study are summarized in Table 3.2.

The nadir pointed spacecraft with aligned antennas on the zenith face (left hand side of Figure 3.3) is considered first as a benchmark. For this orbit, there are almost always greater than 4 GPS satellites in view above the 10 degree elevation mask—only 0.6% of the time are there less than 4. This means that a GPS receiver that has been designed for space should be able to maintain continuous position fixes almost all of the time (dilution of precision considerations aside). There is also an abundance of differential phase measurements in this orientation, as expected.

The next case considered is an inertially pointed spacecraft (shown in the middle of Figure 3.3). In this configuration (known as ‘vertical’), the +z face of the spacecraft points to the nadir vector at one time in the orbit and the zenith vector a half orbit later. The 3 different antenna geometries examined are shown in Figure 3.4. The first is simply the aligned array with all antennas on the +z face. The next design is a nonaligned array with 2 antennas canted at 45 degrees on the +z face and 2 on the -z face of the spacecraft. The +z pair is rotated 90 degrees with respect to the -z pair. The final antenna design considered increases the number of antennas to 6 and tilts these at 30 degrees, with 3 on the +z face and 3 on the -z face, each face forming equilateral triangles. The +z face of the antenna array is rotated 180 degrees with respect to the -z face. These nonaligned designs were chosen to provide the best total sky coverage with the given number of antennas.

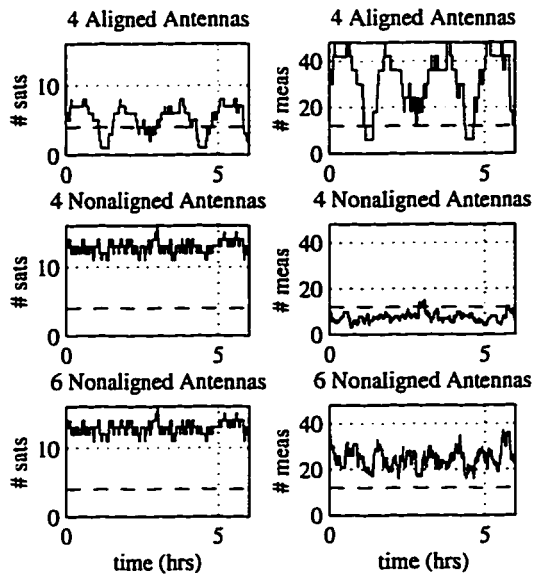


Figure 3.11. GPS satellite and differential phase measurement availability for the inertially fixed example

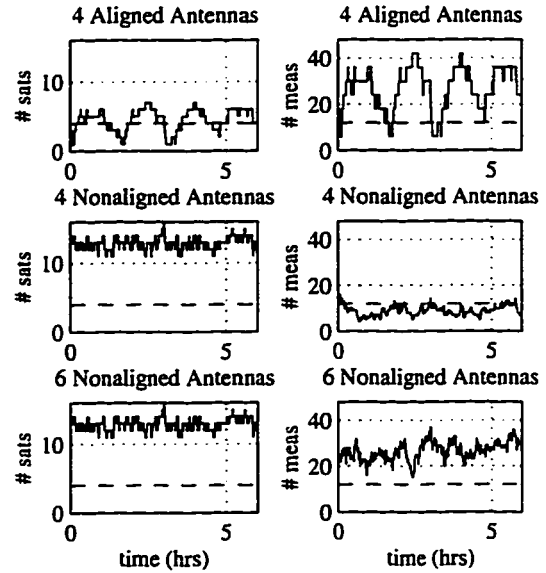


Figure 3.12. GPS signal and differential phase measurement availability for the spinning example (rate = 1/3 rpm)

Table 3.2. Navigation and attitude tracking availability versus pointing profile and antenna geometry for a polar, 650 km Circular Orbit.

Point	Antenna Geometry	GPS satellites			Roving Master $\Delta\phi$'s			All in View $\Delta\phi$'s		
		Min	Max	< 4	Mean	1- σ	< 8	Mean	1- σ	< 8
Nadir	4 on zenith face (a)	3	9	.6 %	17.6	3.3	0 %	35.2	6.7	0 %
Inertial -V	4 on +z face (a)	1	9	23.6	15.2	6.1	14.6	30.5	12.2	5.3
	4 nonaligned	10	16	0	7.1	1.8	61.3	7.6	2.2	51.2
	6 nonaligned	10	16	0	19.2	2.7	0	26.2	4.5	0
Inertial -H	4 on +y face (a)	1	8	15.0	15.3	4.5	5.7	30.6	9.0	1.7
	4 nonaligned	10	16	0	8.6	1.7	26.6	9.0	2.0	25.3
	6 nonaligned	10	16	0	19.4	2.4	0	26.7	3.9	0
Spin 1/3 rpm	4 on spin axis (a)	1	8	15.0	15.3	4.5	5.7	30.6	9.0	1.7
	4 nonaligned	7	16	0	7.3	1.7	55.5	7.6	2.0	50.2
	6 nonaligned	9	16	0	19.1	2.4	0	26.2	4.0	0
Spin 6 rpm	4 on spin axis (a)	1	8	15.0	15.3	4.5	5.7	30.6	9.0	1.7
	4 nonaligned	1	7	46.5	3.9	1.5	99.4	4.2	1.8	95.7
	6 nonaligned	3	12	3.2	13.9	2.9	3.2	19.6	4.4	1.8

The antenna geometries used in the study are the same as in Figure 3.4. The (a) subscript indicates an aligned array.

With the aligned antenna array in this inertial 'vertical' pointing configuration, there is a greater variation in the number of GPS satellites that the antenna array can see. As shown in the top plots of Figure 3.11, the orbit rate motion of the vehicle is clearly evident, with a minimum number of measurements available when the array is nadir pointed. This design achieves neither continuous position fixes (23.6% outages), nor continuous attitude determination (5.3% outages using the all in view algorithm), assuming the receiver has enough tracking loops to perform every available measurement.

Using the 4-antenna nonaligned array, it is possible to provide total sky coverage for navigation (outages drops to 0) at the expense of attitude determination (outages rises to 61.3%). The orbit rate signature of the aligned antenna array is removed from the visibility plot (middle plots of Figure 3.11), but there are not enough differential phase measurements to provide complete attitude determination. The all in view tracking algorithm provides an additional 10% of attitude determination coverage.

At the additional expense of two extra nonaligned antennas and associated receiver electronics, full attitude determination and navigation capability is possible at every point in the orbit (bottom plots of Figure 3.11). This is an important conclusion because it states that at the increase of a modest amount of hardware (from four to six antennas), complete navigation and attitude coverage can be provided by a single GPS receiver.

The next configuration examined in Table 3.2 may be visualized by taking the inertial 'vertical' case and rotating the antenna arrays 90 degrees on the vehicle body, so they now look in the direction of the orbit normal vector. The aligned array now looks at the local horizontal all the time as it proceeds through its orbit. This case is referred to as the inertial 'horizontal' orientation.

In this case, navigation and attitude outages are less than in the inertial vertical pointing mode, but the general results still hold. An aligned antenna array provides neither full navigation nor full attitude coverage. A 4-antenna nonaligned array provides full navigation coverage at the expense of attitude coverage (25.3% outages). A 6-antenna nonaligned array provides complete navigation and attitude coverage.

This inertial 'horizontal' orientation may be modified to a spinning spacecraft by rotating the +y-axis. The visibility for the aligned antenna array along the spin axis is unaffected by the spin rate, and the performance is the same as in the inertial horizontal configuration. The results of the 1/3 rpm case are shown in Figure 3.12. The 4-antenna nonaligned array once again does not provide enough differential phase measurements for continuous attitude solutions, especially when the spin rate is relatively high (6 rpm). The 6-antenna, nonaligned array generally provides the best navigation and attitude visibility, regardless of orientation or pointing profile.

The conclusion of this study is that it is possible, particularly with a receiver capable of processing 6 or greater antenna inputs and possessing 12 or more channels, to provide continuous attitude determination and navigation at all times in orbit, regardless of the pointing mode of the vehicle, and even if the vehicle is out of control and potentially tumbling. A robust system could be potentially used as a backup or safe hold sensor to provide critical spacecraft pointing and navigation functions at all times.

The study does not address changes to tracking algorithms required to provide this capability, particularly on spinning spacecraft, where GPS satellites may rotate across the field of view of any antenna in manner of several minutes or seconds. Given the pace of improvements in GPS receiver hardware and algorithms, it is believed that a designed-

for-space receiver might reach this level of performance within as short a time as perhaps two years. Some terrestrial receivers already possess these tracking capabilities.

3.6. Summary

A general set of algorithms for attitude determination on spacecraft has been presented. The sensor metrics established in Section 3.1 have guided the development of this system since its inception. The system allows for measurements on nonaligned antenna arrays, thereby providing measurement continuity and availability regardless of vehicle orientation. A highly autonomous method of quasi-static integer resolution using the Singular Value Decomposition method was presented and demonstrated with flight data from the RADCAL spacecraft. The use of motion methods for cycle ambiguity resolution along with the SVD method provides solutions that possess a high degree of integrity. The system is versatile, with the same set of algorithms being able to work on Earth pointed, inertially pointed, and spinning payloads in LEO. The performance of the attitude determination is typical of properly implemented GPS carrier phase systems; the effect of receiver calibration and miscalibration will be discussed along with the subject of accuracy in Chapter 4.

3.7. References

¹ R.L. Greenspan, A.Y. Ng, J.M. Przyjemski, J.D. Veales, "Accuracy of Relative Positioning by Interferometry with Reconstructed Carrier GPS: Experimental Results," *Proc. Of the Third Intl. Geodetic Symposium on Satellite Positioning*, Las Cruces, NM, Mar. 1982.

² L.R. Kruczynski, P.C. Li, A.G. Evans, B.R. Hermann, "Using GPS to Determine Vehicle Attitude: USS Yorktown Test Results," *Proc. Int. Tech. Mtg., Institute of Navigation (ION)*, Colorado Springs, CO, Sept. 1989.

- ³ F. van Graas, M. Braasch, "GPS Interferometric Attitude and Heading Determination: Initial Flight Test Results," *Navigation*, vol. 38, Fall, 1991.
- ⁴ C.E. Cohen, *Attitude Determination Using GPS*, Ph.D. Dissertation, Stanford University, Dec. 1992.
- ⁵ C.E. Cohen, "Attitude Determination," *Global Positioning System: Theory and Applications*, vol. II, American Institute of Aeronautics and Astronautics (AIAA), 1996.
- ⁶ R. Fuller, S. Gomez, L. Marradi, J. Rodden, "GPS Attitude Determination From Double Difference Differential Phase Measurements," *ION GPS-96*, Kansas City, MO, Sept. 1996.
- ⁷ P. Montgomery, *Carrier Differential GPS as a Sensor for Automatic Control*, Ph.D. Dissertation, Stanford University, Jan. 1996.
- ⁸ *TANS Vector GPS Attitude Determination System: Specification and User's Manual*, Trimble Navigation, Ltd., Sunnyvale, CA, 1994.
- ⁹ G.H. Golub, C.F. Van Loan, *Matrix Computations*, The Johns Hopkins University Press, 1989.
- ¹⁰ W.H. Press, S.A. Teukolsky, W.T. Vetterling, B.P. Flannery, *Numerical Methods in C: The Art of Scientific Computing*, Cambridge University Press, 1992.
- ¹¹ H.U. Uematsu, B.W. Parkinson, and E.G. Lightsey, "GPS Receiver Design and Requirement Analysis for the Stanford Gravity Probe B Relativity Mission," *ION GPS-95*, Palm Springs, CA, Sept. 1995.
- ¹² D. Lawrence, et al, "Maintaining GPS Positioning in Steep Turns Using Two Antennas," *ION GPS-95*, Palm Springs, CA, Sept. 1995.
- ¹³ J.A. Klobuchar, "Design and Characteristics of the GPS Ionospheric Time Delay Algorithm for Single Frequency Users," *IEEE PLANS*, Las Vegas, NV, November 1986.
- ¹⁴ J.R. Wertz, ed., *Spacecraft Attitude Determination and Control*, D. Reidel Co., 1978.
- ¹⁵ C.E. Cohen, E.G. Lightsey, W.A. Feess, B.W. Parkinson, "Space Flight Tests of Attitude Determination Using GPS," *Intl. Journal of Satellite Communications*, Vol. 12, 1994.

Chapter 4: Receiver Calibration

Realizing the full potential of centimeter-precision range measurements using GPS requires understanding the physical phenomena that constitute the measurement to at least the millimeter level. Details of signal reception and noise that were originally considered insignificant for basic GPS services now limit the accuracy with which the most precise measurements can be made. Characterizing, modeling, and potentially calibrating the GPS receiver for many of these error sources improves the performance of the sensor and provides a more complete understanding of the capabilities of the device.

This chapter discusses the issues affecting the accuracy of differential carrier phase measurements from a unique spacecraft perspective. An original error budget is set out and the potential attitude determination accuracy is established. Several error sources, such as patch antenna phase patterns and thermal effect on cable line length, are systematically measured for the first time. Methods of receiver calibration are examined for spacecraft, including some new techniques. A new concept for on-orbit calibration of spaceborne receivers is presented.

4.1. Error Sources

Equations 3-3 and 3-4 concisely represent differential range measurements in terms of platform attitude as follows:

$$\Delta r_0 = \left[\underline{s}_0^T \right]_E \underline{A}_{E>B}^T [\underline{b}_0]_B = \Delta\phi_0 - k - \beta_0 - v \quad (4-1)$$

where the '0' subscript has been added to denote the truth and the noise term v represents the collective effect of all noise sources. This equality holds because of the unknown noise term v ; without it, a least squares solution is sought to an overdetermined set of equations in the presence of noise (the scalar relation of Equation 4-1 represents a single measurement). The structure of the error sources in this relation may be examined by expanding the range measurement (the expanded form is defined Δr_m) to include first order perturbations, assuming the integer cycle ambiguity has been correctly resolved via the methods presented in Chapter 3:

$$\Delta r_m \approx \left[(\underline{s}_0 + \underline{\delta s})^T \right]_E \underline{A}_{E>B}^T [(\underline{b}_0 + \underline{\delta b})]_B \approx (\Delta\phi_0 + \delta\Delta\phi) - k - (\beta_0 + \delta\beta) - \delta v \quad (4-2)$$

Subtracting 4-1 from 4-2, and replacing the approximation with an equation for v (neglecting higher order terms) yields:

$$v = \Delta r_m - \Delta r_0 = \delta\Delta\phi - \left[\underline{\delta s}^T \right]_E \underline{A}_{E>B}^T [\underline{b}_0]_B - \left[\underline{s}_0^T \right]_E \underline{A}_{E>B}^T [\underline{\delta b}]_B - \delta\beta - \delta v \quad (4-3)$$

The measurement noise is composed of several distinct types of errors and physical effects. The sign of each term is dependent on the direction of perturbation; they are all

chosen here to be consistent with Equations 4-2 and 4-1. The nature and magnitude of each component will be briefly described.

4.1.1. Differential Carrier Phase Perturbation

The differential carrier phase perturbation term actually represents several additive phenomena, and may be rewritten as:

$$\delta\Delta\varphi = \delta\Delta\varphi_m + \delta\Delta\varphi_p + \delta\Delta\varphi_i \quad (4-4)$$

Each subscript refers to a different type of physical effect, as described below: *m* represents signal multipath, *p* is phase pattern variation, and *i* is antenna interaction.

4.1.1.1. Multipath

Multipath is the reception of signal reflections from objects near the antenna. The reflected signal adds an amplified or attenuated, phase-shifted component to the received signal that cannot be easily distinguished from the straight path signal (Figure 4.1). The resulting measured carrier phase is the summation of all reflections coming into the antenna.

For a complex reflective surface, it is difficult to predict theoretically what the multipath will be at any orientation, since complete knowledge of all reflections coming from the platform and the environment is required. Many objects display remarkably consistent, apparently, stochastic multipath properties. This apparently stochastic characterization

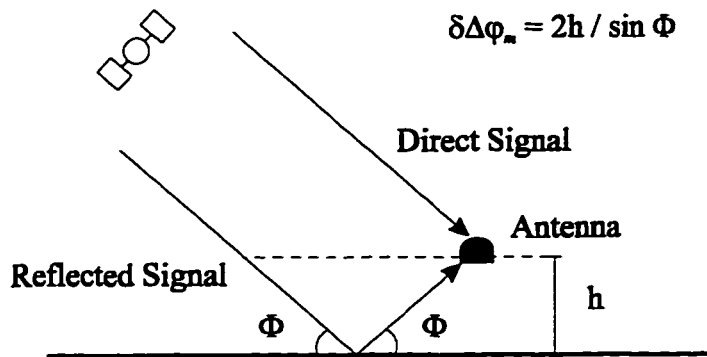


Figure 4.1. Multipath Geometry (Single Ray)

can often be represented as an autocorrelated noise source with about 5 mm RMS magnitude.

In the case of an isolated vehicle like a spacecraft, multipath is entirely due to the reflections from the vehicle itself. If there are no moving appendages on the spacecraft such as articulating solar arrays, this means that the multipath signature of the vehicle at any given time is only a function of the line of sight of the incoming GPS signal in the body reference frame. This signature is repeatable as long as the vehicle surface properties remain constant.

As will be seen, multipath dominates the differential range measurement budget, and many innovative ideas have been suggested to reduce its effects. A practical method to mitigate multipath is with the addition of ground planes or choke rings under the antenna.¹ Directional or steerable antenna gain patterns will also reduce multipath at the expense of field of view. Another idea that will be discussed shortly is the calibration of multipath using a test chamber before the flight to measure the effects as a function of

signal line of sight.² Still other ideas propose time correlated filtering or simple modeling of the vehicle surface to predict the current multipath component.³

Most of these proposals have seen only limited practical implementation. Perhaps the addition of ground planes or choke rings at the antenna base is the most common multipath reduction technique currently used. In most cases to date, the 5 mm RMS magnitude error induced by multipath is simply accepted into the error budget. It is certainly true that multipath mitigation is a promising field with many ideas for improving the differential range measurement accuracy—and hence the attitude solution accuracy—by a factor of 5 or more.

4.1.1.2. Phase Pattern Variation

Antennas are traditionally characterized by their amplification patterns in the antenna reference frame. GPS patch antennas are usually designed to have symmetric hemispherical gain patterns. Antennas have phase patterns, too, and these patterns may significantly affect the measured incoming phase signal, particularly near the edges of the antenna field of view. In the case of a differential phase measurement, it is not the absolute phase pattern, but the *variations* in phase pattern that are important. For aligned antennas, the only variations seen are those introduced by antenna placement, and manufacturing variations between the different antennas. In the case of nonaligned antennas, line of sight variations between antennas are also possible.

An experiment was conducted to determine the potential magnitude of this effect using patch antennas supplied with the Trimble TANS Vector receiver. The test setup is depicted in Figure 4.2. A GPS signal was fed along two paths to different inputs of the receiver. One path was a direct route which was unchanged, and the other path was

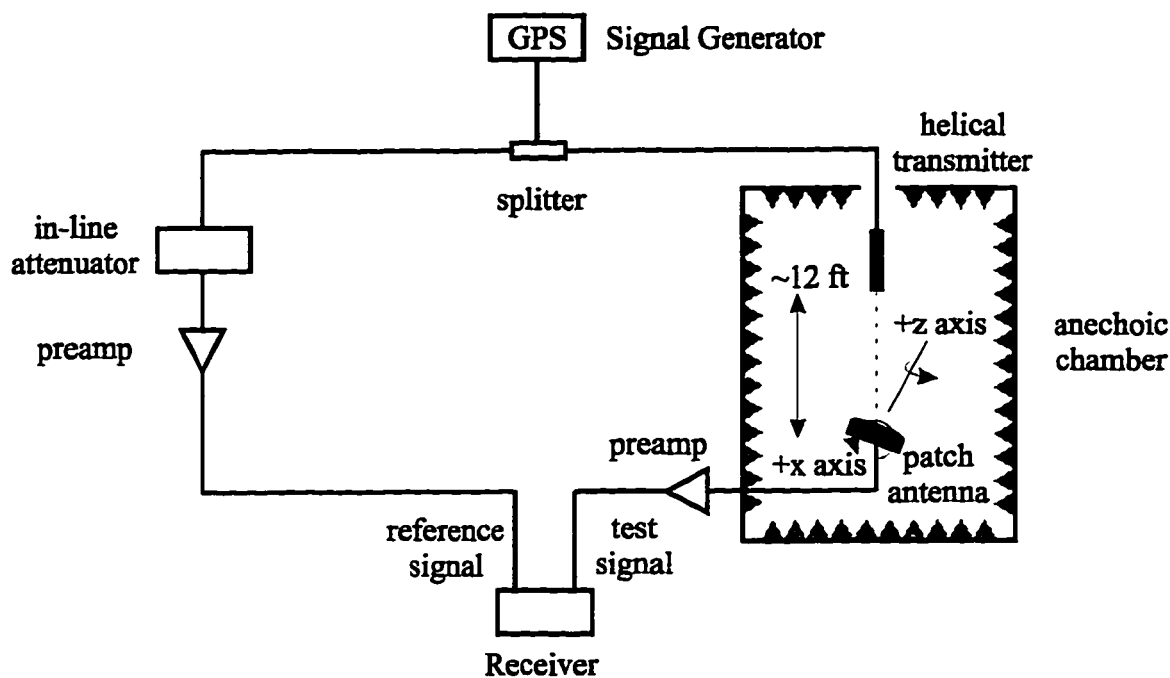


Figure 4.2. Experimental Measurement of Antenna Phase Pattern

transmitted in an anechoic test chamber (provided by Trimble Navigation, Ltd.) to the patch antenna which was mounted on a platform with two rotational degrees of freedom (shown as +x and +z axes). The rotational angles of the platform were measured from a stepper motor to about 0.1 degrees accuracy. As the antenna was rotated in roll (+z-axis) and azimuth (+x-axis) differential phase measurements were recorded and stored in the antenna body reference frame. The data was then fitted to a spherical harmonics model of increasing order. These results are shown in Figure 4.3. The “bullseye” in the horizontal plane is the phase contribution looking along the boresight of receiving antenna, and the circular edge is the antenna horizon. The bias term (the 0th order spherical harmonics model) was removed, because it depends arbitrarily on the electrical length of the reference path, and it is solved and accounted as part of the line bias calibration term explained below. The first order cosine variation of the antenna phase

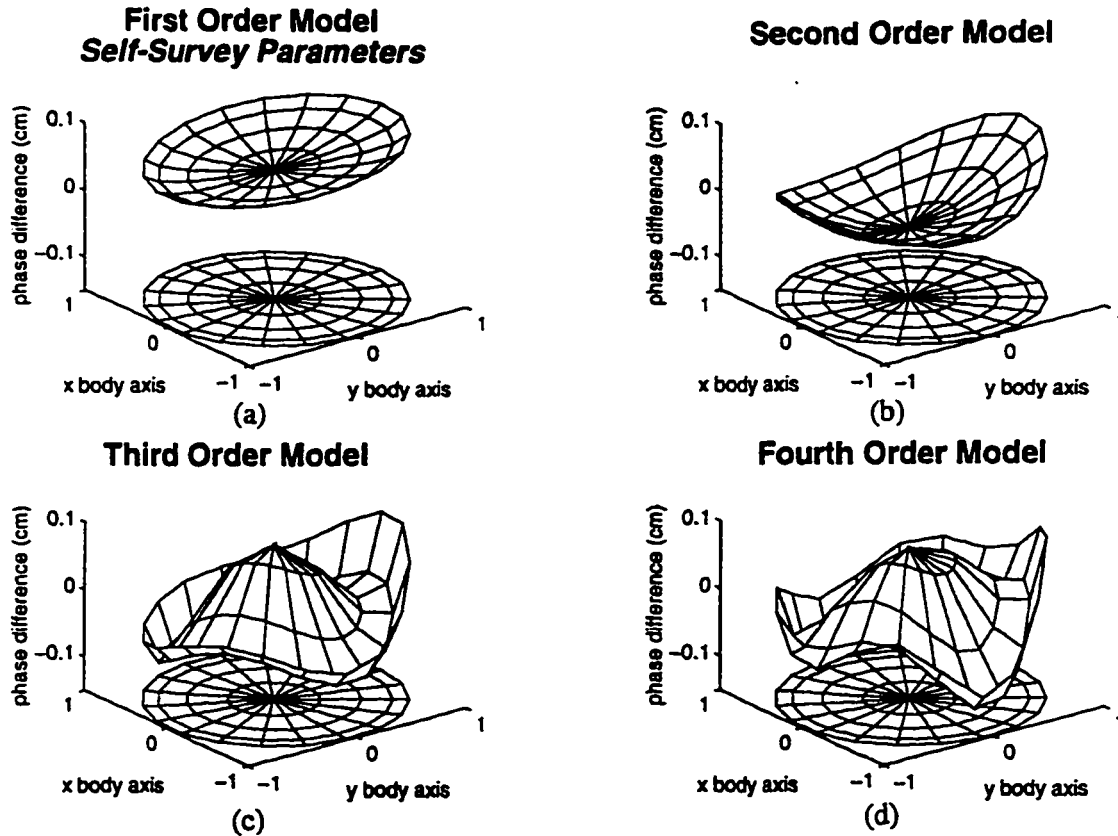


Figure 4.3. Spherical Harmonic Fit to Measured Patch Antenna Phase Pattern

pattern is shown in Figure 4.3a. It represents the offset of the axis of rotation from the antenna phase center. When the GPS signals are infinitely far away, passing above the fixed antenna, the axis of rotation is the phase center, so this term too, may be discarded.

Higher model orders improve the level of detail represented in the antenna phase pattern. These results are shown up to 4th order in Figures 4.3b through 4.3d. The important characteristics to note are that the pattern experiences its greatest variations near the horizon (as expected), and the peak-to-peak variations in the worst case are no greater than 2 mm. This bounds the error due to antenna phase pattern variations, *for this antenna*, to less than about 1 mm RMS for nonaligned antenna arrays.

This test was only performed on a single antenna and so does not address the issue of manufacturing variations between antennas. The observations that most manufacturing processes are fairly standardized for mass production, and that the peak-to-peak variations are relatively small (about 3 mm) in this case, however, suggest that the manufacturing variations should be about the same magnitude. Different antenna designs, of course, will produce different phase pattern results, with the possibility that there may be greater phase pattern variations, especially among highly directional antennas.

4.1.1.3. Antenna Interaction

Antennas may affect one another, and in fact, the entire spacecraft may be considered to be part of each individual antenna. This coupling is expected to be weak, however, presumably less than 1 mm RMS. As long as the antenna locations remain fixed, whatever contribution occurs is repeatable as a function of GPS signal line of sight geometry in the antenna body reference frame.²

4.1.1.4. Differential Phase Calibration

These effects have separate physical causes, but because they are similar in manifestation (all are functions of antenna placement and line of sight geometry), they are in fact indistinguishable in measurement. Cohen has proposed that a single calibration test could be performed on a spacecraft in an anechoic chamber to measure the term $\delta\Delta\phi$ as a function of signal line of sight and fit the results to a spherical harmonics model (similar to what was performed to produce the curves in Figure 4.3).² For spacecraft without moving appendages, this concept presents an interesting method to lower the measurement noise floor by a factor of 5-10.

Unfortunately, there are practical barriers to the implementation of this idea on many spacecraft. Obtaining a large chamber and performing the test could require several days with the fully integrated spacecraft. Many spacecraft programs run out of time and money in their development schedule by spacecraft integration. Usually the cost of the calibration does not justify the performance improvement. Also, many spacecraft with deployable mechanisms or moving parts such as solar arrays can not be tested in all flight configurations under the load of gravity.

There are spacecraft nonetheless (such as microsatellites, where the spacecraft are mechanically simpler, and testing requirements are not as difficult) for which carrier phase calibration could produce a dramatic, beneficial performance improvement. It would be a worthwhile experiment to perform the calibration test to demonstrate the potential accuracy of a fully calibrated GPS attitude determination system.

4.1.2. Line of Sight Perturbation

Returning to Equation 4-3,

$$v = \Delta r_m - \Delta r_0 = \delta \Delta \phi - \left[\underline{\delta s}^T \right]_E \underline{A}_{E \rightarrow B}^T \left[\underline{b}_0 \right]_B - \left[\underline{s}_0^T \right]_E \underline{A}_{E \rightarrow B}^T \left[\underline{\delta b} \right]_B - \delta \beta - \delta v \quad [4-3]$$

The next perturbation term is the error in the line of sight computation, $\underline{\delta s}$. The line of sight is calculated from the transmitter and observer positions as shown in Equation 2-29:

$$\underline{s} = \frac{\underline{r}_t - \underline{r}_o}{\left| \underline{r}_t - \underline{r}_o \right|} \quad [2-29]$$

This value may be in error from two sources: position errors in Equation 2-29, or ionospheric bending of the signal near the Earth limb. In the first case the perturbation is quite small, since even for position errors as large as 1 km the magnitude of this term never exceeds 1 part in 10,000. In the latter case (Earth limb deflection), the signal line of sight may be refracted from the calculated value depending on its proximity to the Earth's ionosphere. The current state of the art does not attempt to correct for this effect. Its significance is reduced, however, because predominantly higher elevation signals are used for attitude calculations (which nominally do not pass through the ionosphere). Future work could improve attitude performance by employing an ionospheric model to estimate and correct this error term.

4.1.3. Baseline Perturbation

The baseline vector is simply the difference between the location of the slave antenna and the master antenna phase centers. As shown in Figure 4.4:

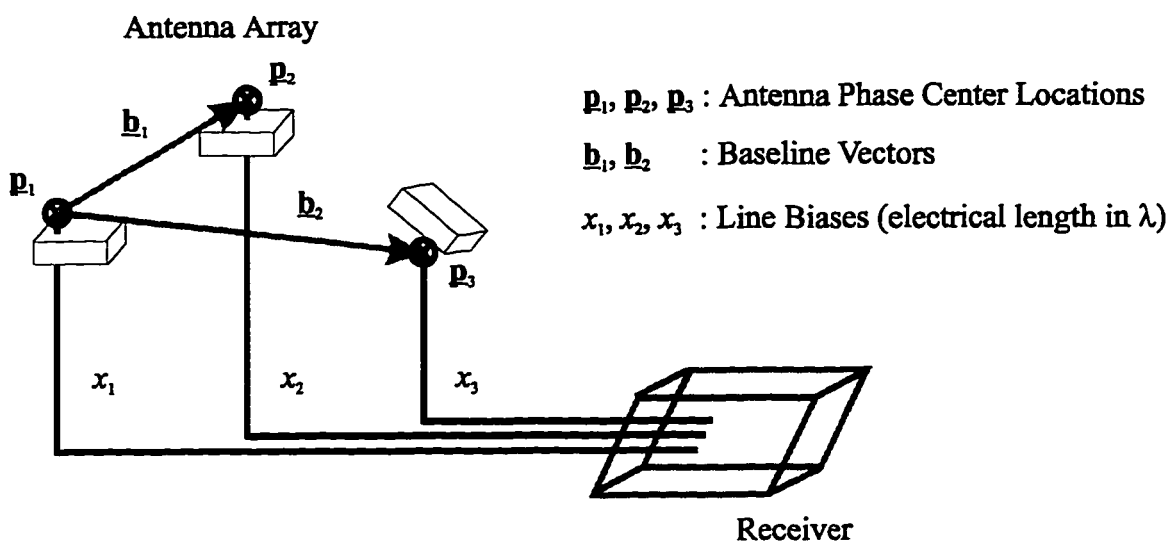


Figure 4.4. Receiver Calibration Parameters

$$\underline{b}_1 = \underline{p}_2 - \underline{p}_1, \quad \underline{b}_2 = \underline{p}_3 - \underline{p}_1 \quad (4-5)$$

The phase center is the idealized center point of reception of the antenna element. It is *not* generally the same location as the geometric center of the antenna element. When measurements of a 1 m baseline are to be resolved to within millimeters, better than 1 part in 1,000 knowledge of the phase center location is required.

4.1.3.1. Phase Center Measurement Error

Without explicitly measuring the antenna phase center location, the geometric center of each antenna element would be the best logical guess for computing the baseline vectors. This assumption might introduce perturbation errors of at least several millimeters in the baseline vector term of Equation 4-3. The error term could dominate the error budget for differential range measurements in this case.

Fortunately, it is possible to measure the baseline lengths to precision levels of about 1 mm as part of a pre-flight receiver calibration. Two different methods for performing this task will be discussed later in this Chapter.

Once established, baseline lengths are structural parameters which will remain fixed if the structure does. They may therefore be assumed as a priori information in the attitude determination calculation of Equation 4-1. Phase center motion may occur as a function of signal line of sight (the phase center is an idealization), but this type of motion is the same as antenna phase pattern variation which was previously discussed in Section 4.1.1.2.

4.1.3.2. Structural Flexibility

The structure itself may deform significantly during the receiver operation. This behavior is especially true for large space structures, such as solar arrays, long booms, or space trusses. Only a few millimeters of unmodelled motion could effect the error budget. If the mode of motion is anticipated, however, the state equations may be augmented to measure and account for this motion; in fact, the differential carrier phase measurement may be used as a vibration sensor in addition to its other functions.⁴ Significant work has also been performed to identify modes of motion on flexible space structures using GPS differential carrier phase sensors.⁵ This work gives promise that with enough sensors, structural motion may be identified and controlled.

For most LEO spacecraft—which are compact and built to withstand launch loads—structural deformation may be minimized by placing the antennas on the central body of the spacecraft. In this case, any thermal or plastic deformation of the structure that may have occurred prior to deployment may be limited to less than 1 mm. It is possible, of course, for larger deflections to occur due to thermal gradients on different surfaces of the spacecraft, so some care must be taken to minimize (or perhaps measure and calibrate) this effect.

There is a tradeoff in attitude determination accuracy between minimizing structural deflections and maximizing baseline lengths (by placing antennas on a boom or solar array, for example). It is not always true that unmodelled structural deformations between antennas are unacceptable. In fact using the differential range measurement as a deformation sensor is an interesting and useful application in its own right that might be a primary application in some cases.

4.1.4. Line Bias

The last categorized perturbation to the differential range measurement is known as line bias. The *absolute* line bias, shown in Figure 4.4, is the electrical line length from the antenna phase center, through the cable, to the measurement point inside the GPS receiver. The phrase “line bias” in the context of attitude determination refers to the *differential* line bias:

$$\beta_1 = x_2 - x_1, \quad \beta_2 = x_3 - x_1 \quad (4-6)$$

It is only the differential nature of the line bias term that is important, since any common perturbations to the absolute line biases x_1, \dots, x_n do not perturb the β quantities. For example, path lengths inside the receiver or through similar length cables, that undergo the same thermal variations, will cancel out of the differential line bias.

4.1.4.1. Measurement Error

Line bias is a quantity which may be measured but is difficult to determine theoretically, since detailed knowledge of all components, connectors, path lengths, and materials is necessary to develop a prediction. Measurement involves augmenting the attitude determination state equations and solving for a constant component over a period of carrier phase data collection. This test may be performed as part of a pre-flight calibration with the flight GPS hardware subsystem. The pre-flight calibration may then be refined using on-orbit data during integer resolution. These calibration techniques will be discussed below, but when operating properly, line bias determination is possible to within 1 mm.

4.1.4.2. Thermal Drift

Line bias is a characteristic of hardware, and providing the hardware configuration does not change, remains predominantly constant. The drifts that can occur in the “bias” are due to thermal variations between the different components in each electrical path. Because the term that appears in Equation 4-1 is *differential* line bias, common thermal variations, for example along identical path lengths inside the receiver or in the spacecraft harness, are not seen in the bias. The dominant cause of line bias variation is therefore in the antenna cables that do not share common paths, for example going to antennas on different faces of the spacecraft.

A test was undertaken to determine the carrier phase measurement dependence on thermal variations in RG-142 coaxial cable as has flown on spacecraft such as RADCAL. An HP 4396A Network Analyzer was used to measure the carrier phase of a reference L1 signal transmitted through a cable initially immersed in near-boiling water and allowed to gradually cool. The results in Figure 4.5 show a linear relation with temperature, as expected. The thermal coefficient of expansion at L1 is determined from the slope of the fitted line as:

$$\alpha = \frac{\text{GPS Phase Change}}{(\text{deg K}) (\text{m of cable})} = 112 \frac{\mu\text{m}}{\text{Km}} \quad (4-7)$$

A representative example of a 20 K temperature differential over two 1 m cables reveals a thermal bias difference of about 2 mm. This effect can be minimized by tracing as much of the antenna cabling as possible through a common spacecraft harness, so that all cables will undergo a similar temperature profile.

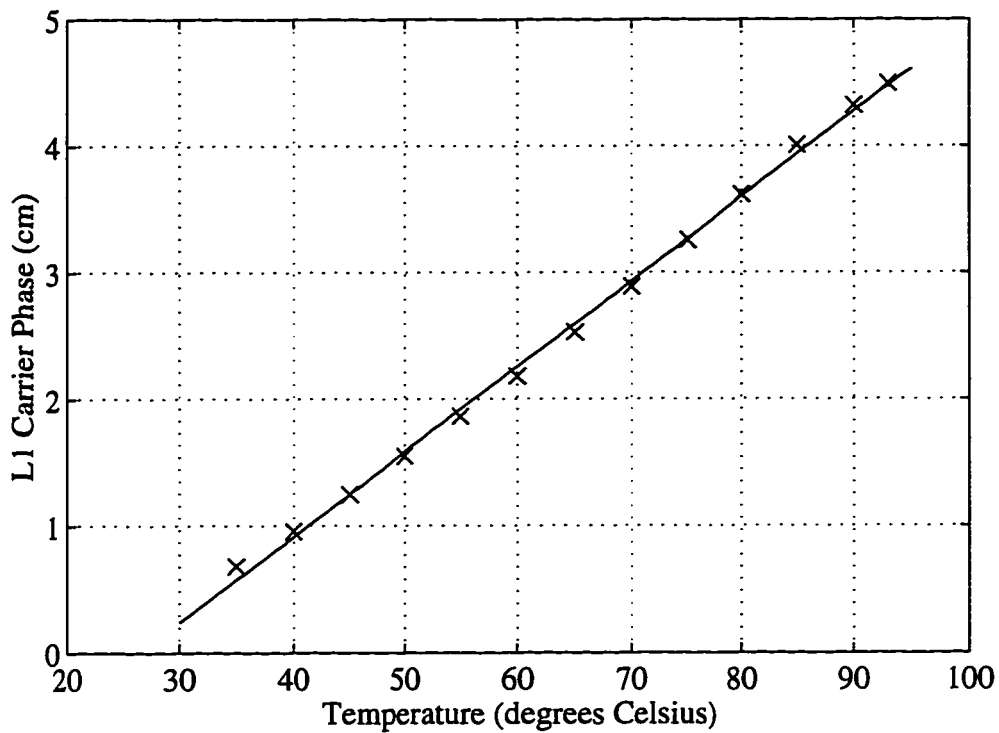


Figure 4.5. “Line Bias” Thermal Drift

4.1.5. Other Noise Sources

Any previously undescribed noise sources, such as electromagnetic interference (EMI), signal crosstalk, tracking loop noise, etc., are lumped into the final term δv . Collectively, on a properly designed receiver, these terms have been demonstrated to be less than 1mm RMS magnitude.⁶

4.2. Relative Range Error Budget

Based on the above discussion, a relative range error budget is compiled in Table 4.1. Each of the noise sources is assumed to have a Gaussian independent distribution so that

Table 4.1. Typical RMS Relative Range Error Budget

Noise Source	Effect (cm)	Total (cm)
Differential Carrier Phase, $\delta\Delta\phi$		0.5
Multipath	0.5	
Phase Pattern Variation	0.1	
Antenna Interaction	0.1	
Line of Sight, δs		0
Baseline, δb		0.1
Calibration Error	0.1	
Flexibility	0.1	
Line Bias, $\delta\beta$		0.1
Calibration Error	0.1	
Thermal Drift	0.1	
Other Noise Sources, δv		0.1
Total RMS Range Error, σ_r		~0.5

the total noise in the relative range measurement is the RSS of each of the separate components. The values selected are for a typical LEO spacecraft application where the receiver is assumed to be well calibrated and structural flexibility is small. The budget is deliberately computed to only 1 significant digit to emphasize the level of precision of the calculation.

The conclusion of the error budget is a statement that is often, but not always true: for a properly calibrated receiver, the differential range measurement accuracy (and hence the attitude accuracy) is dominated by multipath. However, it is still important to account for all other error sources and to appreciate the conditions under which they may also become significant.

4.3. Attitude Determination Accuracy

For an individual measurement on baseline 1, the attitude determination accuracy is derived from the relative range error as:

$$\sigma_{\theta} = \frac{\sigma_r}{|\underline{b}_1|} \quad (4-8)$$

Thus the main determinants of RMS attitude solution accuracy are relative range measurement error and baseline length. There are also questions of observability, since one measurement provides only two axes of information, but observability is guaranteed by taking multiple measurements on baselines that span a three dimensional space.

If there are M measurements on each of N baselines, all known highly correlated measurement terms (such as line biases) are first removed. If the residuals are *assumed* to provide approximately independent, equally weighted range measurements, then the attitude solution accuracy is given by the relation (σ_{θ} in radians):

$$\frac{1}{\sigma_{\theta}^2} = \frac{1}{\sigma_r^2} (|\underline{b}_1| + |\underline{b}_2| + \dots + |\underline{b}_N|) \quad (4-9)$$

More baselines and measurements improve the solution accuracy as well as the individual baseline length. Equation 4-10 may be used when each baseline has its own range measurement noise and number of measurements (as long as the *assumption* of measurement independence is made):

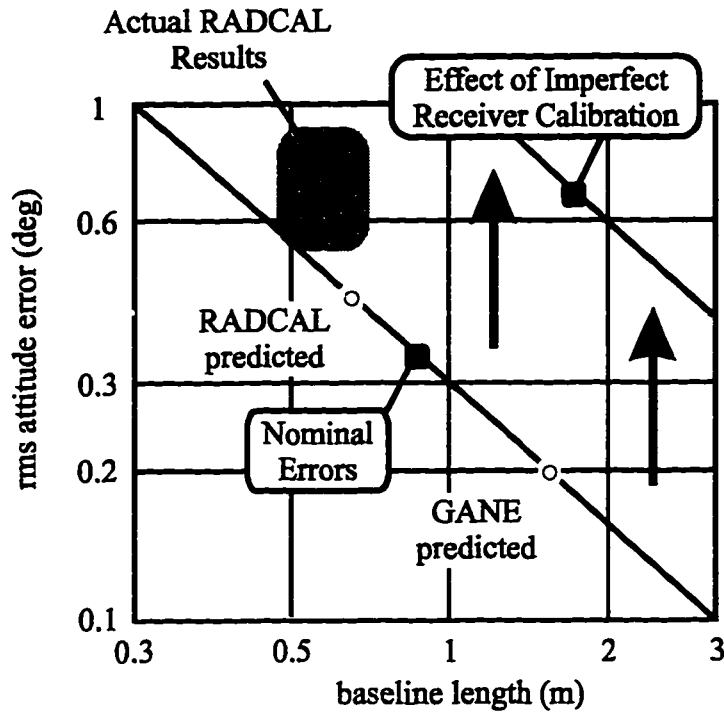


Figure 4.6. Attitude Error Budget

$$\frac{1}{\sigma_{\theta}^2} = \left(\sum_{i=1}^N \frac{|\underline{b}_i|}{\sigma_{ri}^2} \right) \quad (4-10)$$

Also, it may be advantageous in some cases to weight some baselines more than others to improve overall attitude solution performance.

Figure 4.6 shows these relationships graphically. For a given relative range RMS measurement error, the attitude determination RMS accuracy is represented by a line on a log-log plot versus baseline length. An increase in σ_r results in an upward shift of the line. A decrease in σ_r , or an increase in measurements and baselines, lowers the line. The line drawn is for a single measurement with $\sigma_r \cong 5$ mm. Data from RADCAL is estimated to be between 0.5 and 1 degree rms, slightly higher than the theoretical value of

about 0.4 degrees rms for the actual antenna separation of 0.67 m. The RADCAL receiver was not fully calibrated, however, resulting in a larger σ_r and an upward shift of the accuracy line, bringing the estimated accuracy into agreement with the theoretical prediction.

4.4. Self-Survey Calibration Methods

The importance of proper receiver calibration is now clear. Without it, errors of greater than 1 cm may be introduced into the differential range error budget, shifting the achievable attitude accuracy higher at every baseline length. In order to obtain the best possible attitude solutions, it is essential to properly determine antenna phase center locations and line biases to within 1 mm. This is commonly accomplished through a pre-flight calibration known as a receiver “self-survey,” where the antenna platform is static and several hours of carrier phase data is recorded.

4.4.1. Principles of Receiver Self-Survey

The mathematics of the self-survey procedure are described by Cohen.⁶ This is essentially a linear estimation problem to determine: the Cartesian coordinates of the antenna phase centers in a vehicle body or receiver reference frame and the differential line biases associated with each baseline. Data is usually collected over several hours to allow the principal noise source, multipath, to assume “white-like” properties of *approximately* zero-mean Gaussian distribution (although multipath is *not* a white noise source). The test should be performed using the GPS subsystem flight hardware, in the flight geometry, to produce valid results. The simplest way to achieve this configuration is to perform the test on the fully (or partially) integrated spacecraft.

This presents a difficulty for the spacecraft integration schedule. A test time of at least one day is required with contingency using the integrated spacecraft. More self-surveys may be required to repeat the survey results, or perform surveys on alternate faces of the vehicle (if the vehicle is using a nonaligned antenna array). The spacecraft integration schedule is often time-intensive, and long additional tests can impose significant hardship and cost on the integration effort. Furthermore, the required visibility of the GPS constellation during the test means that the integrated spacecraft must be either outdoors or in a properly equipped facility with a large radome. Most space flight hardware is kept in a controlled environment during integration and many have clean requirements that would make outdoor testing highly undesirable or impossible. Thus, the concept of a pre-flight self-survey on the vehicle, using the actual GPS constellation, is not practical for spacecraft in many cases.

An alternative method that has been employed on the SSTI-Lewis spacecraft is to perform the self-survey with the GPS subsystem flight hardware using only a mechanically identical mockup of the front plate with the antennas installed.⁷ The parameters are determined on the test system using the conventional self-survey, then disassembled and reassembled on the spacecraft at a later time. The spacecraft self-survey parameters (baseline vectors and line biases) are assumed to be unchanged from the subsystem test.

While this method is preferable to no self-survey at all, the ability to duplicate the antenna phase center locations and line biases to millimeter accuracy is questionable. Line biases in particular may depend on temperatures, individual connections, and cable flexure. An attitude determination system tested in this way could give self-survey errors

on the order of several millimeters, adversely affecting the attitude solution accuracy. An alternative method is sought to obtain and refine the self-survey parameters.

4.4.2. Receiver to Body-Axis Alignment

The self-survey results specify the baseline vectors in an antenna reference frame that usually defines one antenna phase center at the origin. This reference frame defines the zero attitude orientation of the vehicle with respect to the East-North-Up reference frame at the time of the self-survey. If it is desired, for example, that the attitude solution output be zero when one baseline vector is pointed along the local horizontal, then the receiver must be surveyed in this configuration (or alternatively, the rotation angles must be known so that a transformation may be applied to the receiver attitude output). This requires determining the local vertical at the survey test site and aligning the antenna array to that vector, perhaps using a theodolite and optical alignment cubes.

Once the zero attitude of the antenna platform has been defined, it must be related to the spacecraft body reference frame. This may be obtained by performing an alignment check on two optical cubes, one mounted on the spacecraft body (defining the vehicle body reference frame) and the other mounted on the GPS reference frame, perhaps on the underside of an antenna ground plane. The alignment angles should be measured while the GPS subsystem is producing attitude solutions to provide an end-to-end transformation from the GPS attitude output to the spacecraft body orientation.

4.4.3. Self-Survey Repeatability

The self-survey calibration is performed over several hours so that slowly varying biases in the data due to the multipath can be filtered out of the results. In particular, line bias

and non-zero mean multipath noise are indistinguishable in the solution. The degree to which multipath can be removed from the solution of any given self-survey is indicated by the repeatability of the test results across an ensemble of self-surveys.

Multiple self-surveys were performed on a static rooftop antenna test fixture to determine the solution repeatability. Two ensembles of 5 surveys were performed at the same time of every sidereal day for the same duration (6 hours). The local times of each ensemble, however, were different to provide a measure of the survey repeatability under similar (within each ensemble) and different (across ensembles) multipath environments. To analyze the data statistically, the mean location of each baseline vector was used as the ‘truth’ and the distance variation from the mean was considered to be the solution error. A separate mean was computed for each ensemble and also another mean for the total data set (including both ensembles). If the multipath is repeatable within each ensemble, the deviations inside the ensemble from the ensemble ‘truth’ should be measurably less than the deviations from ensemble to ensemble. Table 4.2 shows the mean error, or standard deviation from the ‘truth’ for different combinations of data sets and ‘truth’ values. E_1 refers to ensemble set 1 (5 surveys taken at the first sidereal time), E_2 is ensemble set 2 (5 surveys taken at the second sidereal time), and $E_1 \cup E_2$ is union of both E_1 and E_2 .

Table 4.2. Self-survey Repeatability Test Results

rms error (cm)	E_1 ‘truth’	E_2 ‘truth’	$E_1 \cup E_2$ ‘truth’
E_1 data	0.548	0.760	0.619
E_2 data	0.733	0.524	0.582
$E_1 \cup E_2$ data	0.641	0.642	0.600

The measured repeatability of the self-survey deviations when the same sidereal time was used was worse than expected, between 0.5 and 0.6 cm rms for this test (the diagonal terms of Table 4.2). This is at the level of the value listed in Table 4.1 for the effect of multipath, although that number applies for an isolated vehicle and a slightly higher number would be appropriate for this test array. This value is still higher than expected, however, because multipath should be common within each test ensemble; it is believed that the variability of the start time of the surveys (~1 minute) may have been large enough to cause some deviations in the multipath history even when the sidereal times were approximately matched. Nonetheless, the assertion that each ensemble has a substantially different multipath history from the other is evident in the off-diagonal terms of Table 4.2; there is about a 50% increase in rms error when the E_1 data is used with the E_2 'truth' and vice versa.

Figure 4.7a shows the variation over all surveys of the East, North, and Up components of the baseline vectors and 4.7b shows the variation in line biases. The baseline variation is significantly greater in the up coordinate (0.38 cm) than the east (0.25 cm) or north (0.15 cm); this result may be due to the greater variability of satellite positions along the East and North axes than along the Up axis (since all GPS signals come from overhead), leading to less resolution along this axis. The line bias variation, which is independent of geometry, is more uniform as expected, and shows an overall 0.25 cm standard deviation.

4.4.4. Combining Self-Survey Results

If the self-survey results are assumed to be independent (if each has a unique multipath profile) with zero mean ensemble error, then the results of multiple self-surveys can be combined into a single, more accurate set of calibration parameters. If all self-survey results are considered equally valid, the line biases may be computed trivially as the mean

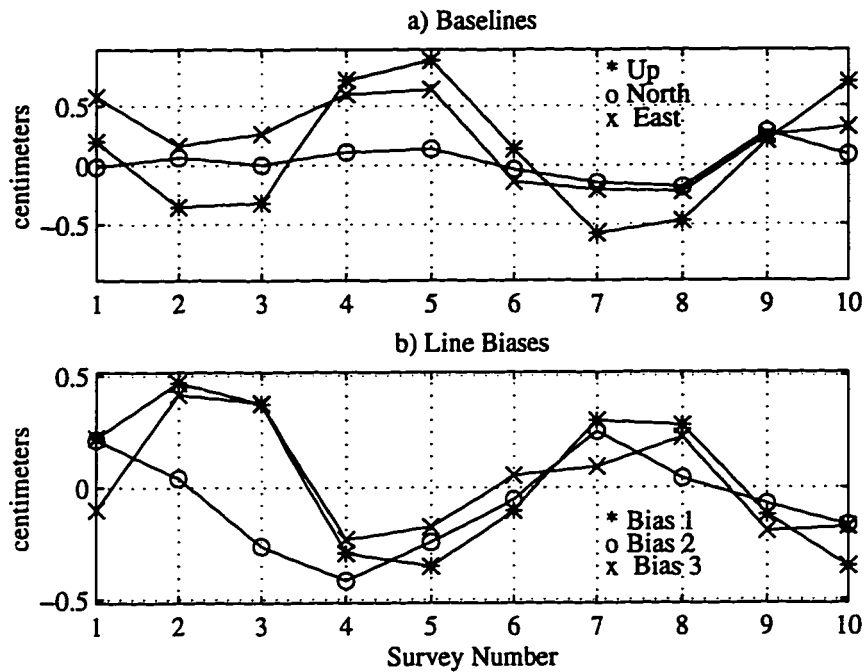


Figure 4.7. Variability of Self-Survey Parameters on Test Array

of each respective self-survey bias. Some surveys which are believed to provide better solutions may be weighted appropriately as desired.

To compute the baseline vectors, observe that the magnitude of the same baseline vector across self-surveys is slightly different. The magnitude can only be different for two reasons:

- a real deformation between antenna phase centers occurs between the time of the surveys, or
- measurement noise

Assuming that no measurable structural deformation has occurred without the knowledge of the test engineer, the appropriate course of action is to weight the results of each survey by the covariance matrix, \underline{P} , for each baseline:

$$\underline{\mathbf{b}}^* = \left(\sum_{i=1}^N \underline{\mathbf{P}}_i^{-1} \right)^{-1} \cdot \left(\sum_{j=1}^N \underline{\mathbf{P}}_j^{-1} \underline{\mathbf{b}}_j \right) \quad (4-11)$$

4.5. Other Calibration Methods

As previously mentioned, the self-survey test is a time-consuming and costly procedure to impose on an integrated spacecraft. An alternative approach is to perform the self-survey with the GPS flight hardware subsystem on either just the antenna mounting plate hardware or using a mechanically equivalent mockup of the spacecraft. These tests have their own limitations, since fabrication of extra hardware is required, and the results obtained may not be of the desired accuracy to within one millimeter. Indeed, even if the test structure is exactly mechanically correct, it may *still* not produce the correct results due to interference and other physical effects. Clearly it is desirable to develop other methods of determining and refining the receiver calibration parameters through a combination of ground and on-orbit tests that do not require the logistical constraints of a fully integrated spacecraft self-survey.

4.5.1. Baseline Measurement Using Antenna Rotation

The rotation of an antenna under repeatable multipath conditions can be used to determine the phase center location. This concept is demonstrated in Figure 4.8 and Figure 4.9. If one antenna is rotated relative to another through a known angle, the measured differential phase changes by an amount approximately equal to the angle of rotation in wavelengths due to the circular polarization of the received signal. Data from a rooftop experiment taken at the same sidereal time of the day is plotted in Figure 4.9a.

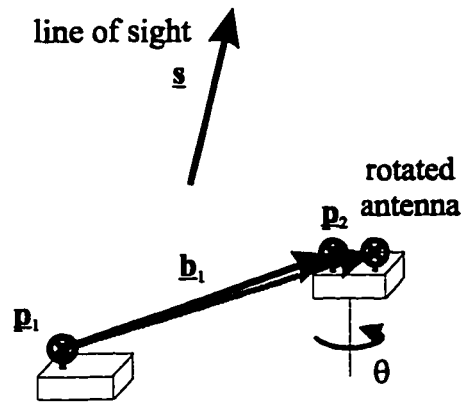


Figure 4.8. Phase Center Determination Using Antenna Rotation

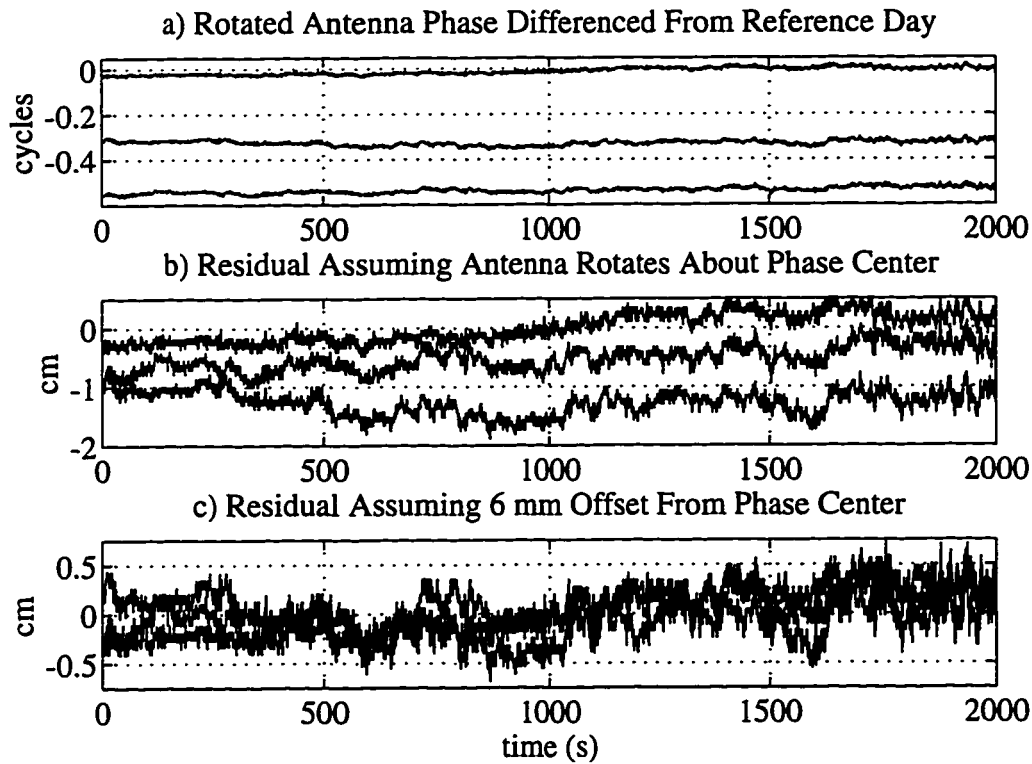


Figure 4.9. Results of Experimental Determination of Antenna Phase Center

Subtracting the angle of rotation in cycles from the measured signal yields a residual which contains a repeatable multipath signature and an offset that is a function of the rotation angle (Figure 4.9b). The offset is proportional to the motion of the phase center about the axis of rotation and may be used to solve for the location of the phase center. In this case, a 6 mm difference between the axis of rotation and the antenna phase center recovers the highly repeatable multipath signature (Figure 4.9c). This test could be performed on the GPS flight hardware using a simulated GPS signal generator (pseudolite) in a laboratory to locate the phase center of each antenna relative to its geometric center. If the phase center is repeatable once placed on the spacecraft, this test might be used as an acceptable alternative to the self-survey method of determining the baseline vector locations. More research needs to be performed to determine if this type of test can produce accurate spacecraft phase center measurements to within one millimeter.

4.5.2. On-Orbit Line Bias Estimation

Although line biases are difficult to predict theoretically, they are easier to estimate than baseline vectors in many respects. A self-survey may be performed separately using the GPS flight hardware components to generate at least a reasonable guess of on-orbit line biases. This test is significantly easier to perform than a baseline test, because the baseline vector geometry does not have to be accurately reproduced. Reassembling the hardware on the spacecraft may introduce some errors to the line bias parameters, but they are likely to be within a few millimeters of the original measurement. As long as the line bias states can be updated on-orbit, it is possible to use the initial estimate to get the iteration started.

Fortunately, it is a straightforward modification of the Quasi-Static integer resolution method to augment Equation 3-20 to include line bias perturbations. The principal issue to make this estimator work well is the selection of a suitable data collection time. As has been previously mentioned, slowly varying multipath signals will falsely register as line bias perturbations if the data collection time is not long enough.

The Quasi-Static integer resolution method in Chapter 3 was designed to provide a solution as soon as it is observable; this results in data collection times that are too short for acceptable line bias convergence. Therefore, the two problems are separated: integer resolution works as a start-up process treating line biases as known fixed quantities, and the line bias estimation works at a significantly longer collection time, as a long-term process, once the cycle ambiguities are known. As long as the original line biases are *good enough* to attain successful integer resolution, they can be refined by the line bias estimation routine to obtain more accurate solutions. In fact, since the integers are known from the integer resolution convergence, they may be removed from the line bias estimation routine:

$$\begin{bmatrix} \underline{\delta\varphi}_1 \\ \underline{\delta\varphi}_2 \\ \vdots \\ \underline{\delta\varphi}_L \end{bmatrix} = \begin{bmatrix} \underline{H}_1 & \underline{0} & \cdots & \underline{0} \\ \underline{0} & \underline{H}_2 & \ddots & \vdots \\ \vdots & \ddots & \ddots & \underline{0} \\ \underline{0} & \cdots & \underline{0} & \underline{H}_L \end{bmatrix} \begin{bmatrix} \underline{J}_1 \\ \underline{J}_2 \\ \vdots \\ \underline{J}_L \end{bmatrix} \begin{bmatrix} \underline{\delta\theta}_1 \\ \vdots \\ \underline{\delta\theta}_L \\ \underline{\delta\beta} \end{bmatrix} \quad (4-12)$$

Where the \underline{J} matrices are index matrices (like the \underline{I} matrices of Equation 3-20). This lower order matrix (than Equation 3-20) produces better convergence properties for line bias perturbations. Integrity checks are readily applied to the on-orbit line bias estimation routine in the same manner as with the motion integer resolution methods. The only

caveat to this method is that the original line bias estimates (presumably obtained from an initial self-survey) must be good enough for a successful integer resolution.

4.6. Summary

Gaining physical insight into the nature and cause of error sources in the GPS carrier phase measurement equations not only enables the prediction of GPS attitude determination accuracy, but also provides ideas to reduce the effects of the most serious sources, thereby improving solution accuracy. The groundwork for this next step has been set by establishing a detailed error budget for spacecraft in which multipath is usually the prevailing limitation to attitude determination accuracy. Under the current state of the art, it has been shown that a 1 m antenna separation leads to about 0.3 degrees rms attitude accuracy. A reduction in multipath measurement noise could improve this accuracy by as much as a factor of 5.

The outdoor calibration method for GPS receivers was examined in the context of spacecraft testing and found to be, at best, a substantial inconvenience. There is a need for a method of on-orbit self-survey calibration, and one proposed concept to accomplish that objective was presented. On-orbit self-calibration would be a great step toward fully autonomous, easily installed and maintained GPS measurement systems.

4.7. References

¹ M.S. Braasch, "Multipath Effects," *Global Positioning System: Theory and Applications*, vol. I, American Institute of Aeronautics and Astronautics (AIAA), 1996.

- ² C.E. Cohen, "Mitigating Multipath in GPS-Based Attitude Determination," *Advances in the Aeronautical Sciences*, Keystone, CO, vol. 74, Univelt, Feb. 1991.
- ³ C.J. Comp, P. Axelrad, "An Adaptive SNR-Based Carrier Phase Multipath Mitigation Technique," *Institute of Navigation (ION) GPS-96*, Kansas City, MO, Sept. 1996.
- ⁴ C.E. Cohen, B.W. Parkinson, "Aircraft Applications of GPS-Based Attitude Determination: Test Flights on a Piper Dakota," *ION GPS-92*, Albuquerque, NM, Sept. 1992.
- ⁵ E.H. Teague, J.P. How, L.G. Lawson, M. Boerjes, B.W. Parkinson, "Techniques for Real-Time Control of Flexible Structures Using GPS," *Advances in the Aeronautical Sciences*, Breckenridge, CO, vol. 79, Feb. 1996.
- ⁶ C.E. Cohen, *Attitude Determination Using GPS*, Ph.D. Dissertation, Stanford University, Dec. 1992.
- ⁷ J. O'Donnell, Jr., J. McCullough, E. Lightsey, R. Schnurr, L.A. Jackson, "Testing of a GPS-Based Attitude Control System," *ION GPS-96*, Kansas City, MO, Sept. 1996.

Chapter 5: Spaceflight Experiments

Space applications for GPS receivers have been quickly embraced by the satellite design industry, which has fortunately resulted in plentiful opportunities to fly GPS receivers as on-orbit experiments and operational platforms to demonstrate the capabilities of the receivers and their algorithms. This validation is a very important step in the development and testing of algorithms for space, since the measurement environment cannot be easily reproduced in full fidelity by simulation.

This chapter presents three case studies of on-orbit experiments that all use the GPS receiver and algorithms that were developed in this dissertation. The missions have been selected to highlight different aspects of the receiver performance and present important technical accomplishments in each case. They are presented chronologically, beginning with RADCAL (6/93) as the first application of attitude determination using GPS carrier phase measurements. For RADCAL, about 0.75 degrees rms attitude determination has been demonstrated in post-processing on a receiver with a 0.67 m antenna separation. This analysis was complicated by many factors including incomplete receiver calibration, but still validated the concept of GPS carrier phase-based attitude determination for spacecraft.

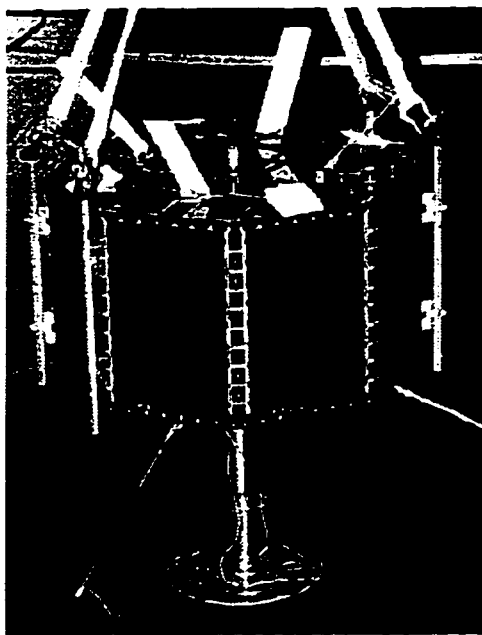
REX II (3/96) is the first application of real-time closed loop attitude control using GPS as the sole attitude sensor. The observed mean three-axis error of 2.66 degrees is well inside the 5 degree per axis pointing specification for this control system. Attitude determination of this satellite is believed to be better than 1 degrees rms with a 0.67 m antenna separation, but cannot be reliably proven since there are no other attitude sensors more accurate than GPS on this spacecraft.

GANE (6/96) is the first on-orbit demonstration of the behavior of the Quasi-static motion method for cycle ambiguity resolution presented in Chapter 3. This experiment, in addition to providing real-time GPS attitude determination in the International Space Station orbit, quantified the performance of different cycle ambiguity resolution methods (i.e., Quasi-static and search method) in flight for the first time. Real-time on-orbit attitude determination accuracy was demonstrated to be within 0.2 degrees rms for a 1.5 x 3 m antenna array using an inertial reference, after correcting for a periodic bias in the GPS receiver line of sight computation.

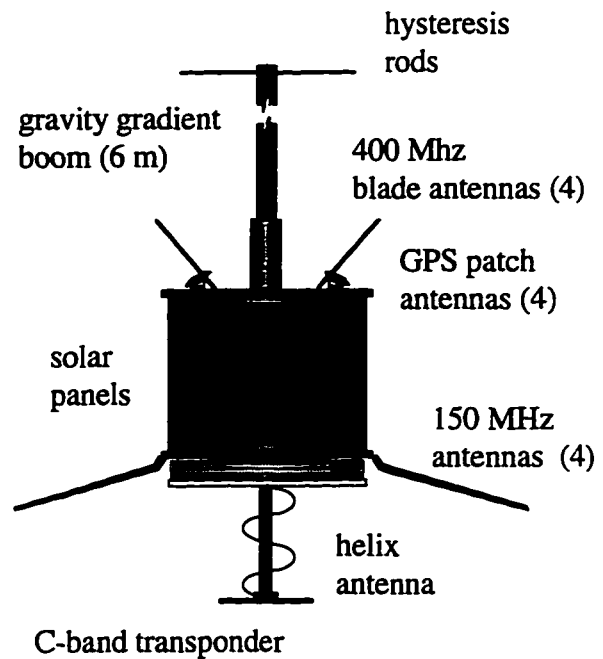
5.1. Attitude Determination: RADCAL

5.1.1. Satellite Description

The Air Force Space Test Program RADCAL (RADar CALibration) satellite was launched from the Vandenberg Air Force Base on a Scout rocket on June 25, 1993. The 89.3 kg payload was integrated by Defense Systems Incorporated, now known as CTA Space Systems. The spacecraft was placed into a circular polar orbit of 815 km altitude. The satellite is stabilized using gravity gradient torques.



(a)



(b)

Figure 5.1. RADCAL Satellite: (a) Preflight Integration, (b) Deployed Configuration

The integrated spacecraft is shown in Figure 5.1a. All appendages are deployed in the figure with the exception of the gravity gradient boom. Figure 5.1b is a conceptual diagram that labels the visible hardware in the deployed configuration. The satellite base diameter is 0.762 m (30 inches) and the boom length is 6.096 m (20 feet). The end of the boom contains magnetic hysteresis rods for attitude damping. Four GPS patch antennas are placed about the upper rim of the spacecraft bus. The satellite contains a radar transponder and a doppler ranging beacon as well as two (redundant) single frequency GPS differential phase receivers. The two GPS TANS Quadrex receivers—a previous version of the current TANS Vector shown in Figure 1.5—share the same four antennas to provide system redundancy. Four UHF blade antennas are spaced between the GPS antennas.

Each GPS patch antenna is canted away from the gravity gradient boom by 17.5 degrees. This slightly nonaligned antenna array increases the total sky visibility to larger than one hemisphere and reduces signal interference due to multipath reflection from the gravity gradient boom.

5.1.2. Signal Acquisition and Navigation Performance

Before discussing attitude determination, navigation solution performance should be briefly examined. The GPS receiver was initialized at power on (there was no battery, and therefore no memory of previous position) by the commanded orbit elements method presented in Chapter 2. The elements were provided by a ground command in this case. Due to power limitations, the receivers were generally only operated for 4 hours per day; so over the course of 18 months, more than a hundred startup sequences were performed. Once the procedure was well established, the receiver routinely acquired a position fix within 5 minutes from power on.

The receiver orbit from a typical four hour data set is shown in Figure 5.2. The spacecraft position is determined in the WGS-84 Earth Centered Earth Fixed (ECEF) Reference Frame in real-time from the on-orbit position fixes. The orbit elements for the spacecraft may be determined for the position and velocity solutions when available from the receiver. Once the orbit elements have been obtained, the orbit propagator can determine the position of the receiver even when a recent position fix is not available. This capability enables attitude solutions to be computed even if fewer than four GPS satellites are visible, once an initial position fix has been obtained.

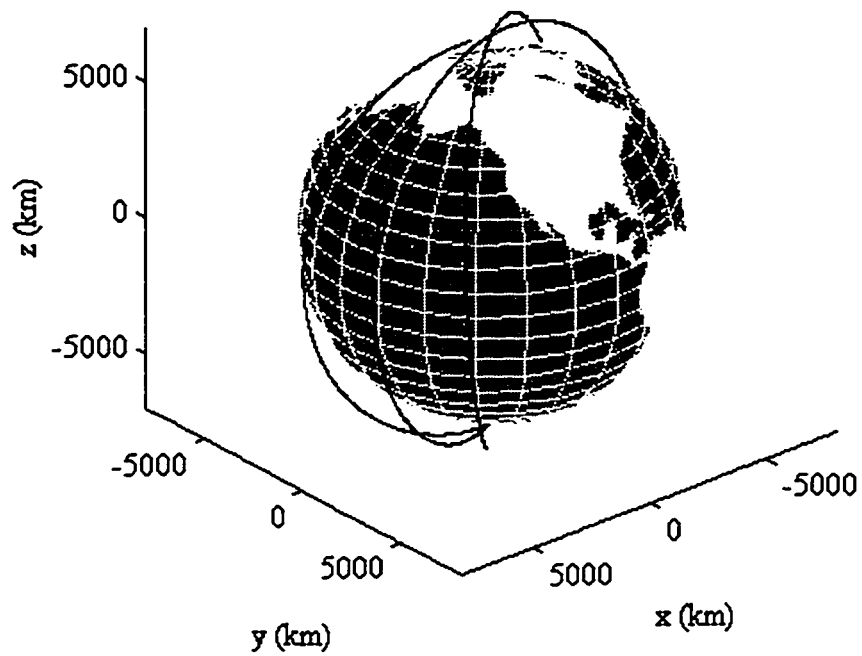


Figure 5.2. RADCAL Orbit Determined from GPS Position Fixes

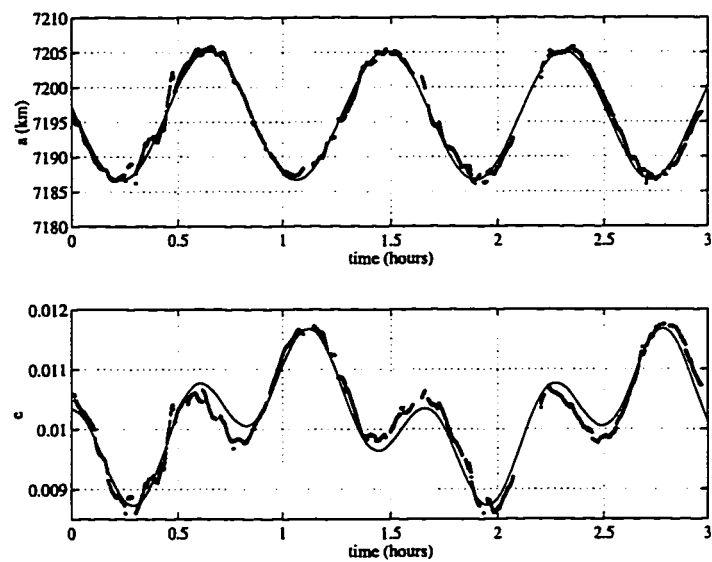


Figure 5.3. RADCAL Orbit Elements

The semimajor axis (a) and orbit eccentricity (e) are shown for the same data set in Figure 5.3. The instantaneous receiver measurements are shown as points, while the smooth line is based on calculated values from ground tracking information for the satellite at the same time. The effect of the Earth's oblateness on the osculating elements is clearly visible, accounting for almost 20 km of variation in semimajor axis.

Although the accuracy of the orbit propagator could certainly be improved with dynamic filtering, no attempt to was made here to provide better than “snapshot” solution accuracy. Even though the accuracy of the position solutions are limited by Selective Availability (SA), the instantaneous solutions are easily within the required accuracy levels for signal acquisition and line of sight determination. Langer has demonstrated a post-processed navigation accuracy of 5 m rms after the removal of SA.¹

5.1.3. Attitude Analysis

Attitude solutions were obtained in post-processing using the Quasi-static motion method presented in Chapter 3. Line of sight information was derived from orbit propagation solutions and the precise GPS broadcast ephemeris. Because of the nonaligned antenna array, the roving master antenna method was used for collecting differential phase measurements. After referencing the measurements back to a common master antenna and adjusting for cycle ambiguity, an example of the raw phase measurements for one signal (3 antenna baselines) is shown Figure 5.4. Two master antenna switches occurred during this 30 minute sample of data. The raw carrier phase measurements are seen to be well-behaved, with a standard deviation within 0.5 cm rms, as mentioned in Chapter 4. The master antenna switching does not appreciably affect the noise. Signal strength was also varying for this satellite pass, with the weaker signal at the beginning and end of the pass accounting for the slightly higher rms noise values at the edges of the plot.

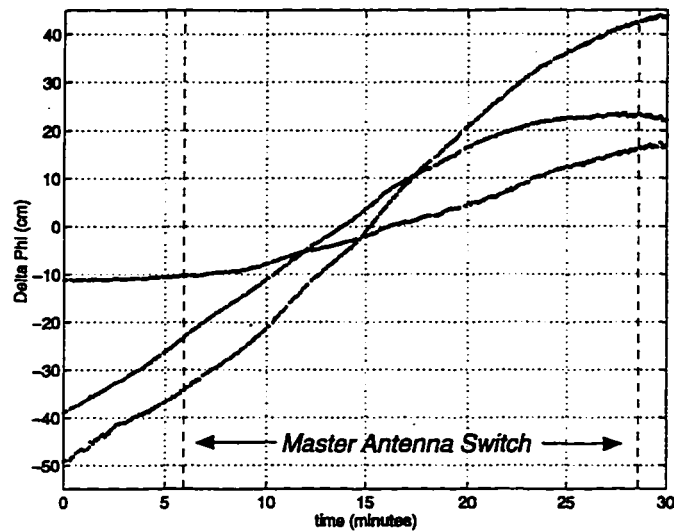


Figure 5.4. Raw Carrier Phase Measurements from One GPS Satellite

Before attitude determination can be performed, it is necessary to have a reasonable knowledge of both the relative antenna locations in the body frame of the spacecraft and the electrical line biases in the cabling and amplifiers associated with each antenna (for definitions, see Figure 4.4). Traditionally, these quantities have been measured by a static self-survey of the system. The vehicle-mounted antenna array is exposed to the sky for several hours, and differential phase measurements from the GPS satellites passing overhead are processed to solve for the antenna locations and line biases. For RADCAL, the receiver calibration was made still more difficult by the nonaligned antenna array, which reduced the amount of visible sky common to all antennas, and perturbed the uncorrected differential phase measurements due to the Right Handed Circular Polarization (RHCP) effect discussed in Section 3.4.3.

An initial sky survey test was performed prior to launch, but analysis did not yield the required accuracy in the line bias and baseline calculations. Attitude results were therefore obtained by determining the antenna spacing from mechanical drawings and

estimating the line biases from the on-orbit data as discussed in Section 4.5.2. In some cases, the line biases had to be adjusted manually to an initial value that was close enough to the estimated bias for the algorithm to converge. Other methods for on-orbit line bias estimation are discussed in detail by Ward.²

5.1.4. Dynamic Equations

In order to express the vehicle attitude, a locally level reference frame is defined as in Figure 5.5. The z-axis points along geodetic nadir, the y-axis is the cross product of this vector and the inertial velocity vector, and the x-axis completes the orthogonal set. For a circular orbit, the y-axis is the anti-orbit normal, and the x-axis points along the velocity vector. The vehicle attitude is then expressed as a 3-2-1 azimuth-pitch-roll Euler sequence. The zero azimuth condition is defined by convention when one particular antenna baseline contains a projection that points in the x-axis direction.

Because of the large angle deviations in the vehicle motion of this passively stabilized system, the full nonlinear equations of motion are derived to produce the best agreement with the measured solutions. The approach is similar to that of Kane.³

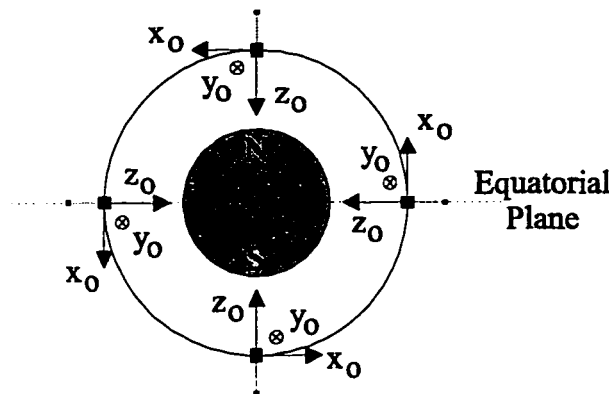


Figure 5.5. Locally Level Reference Frame

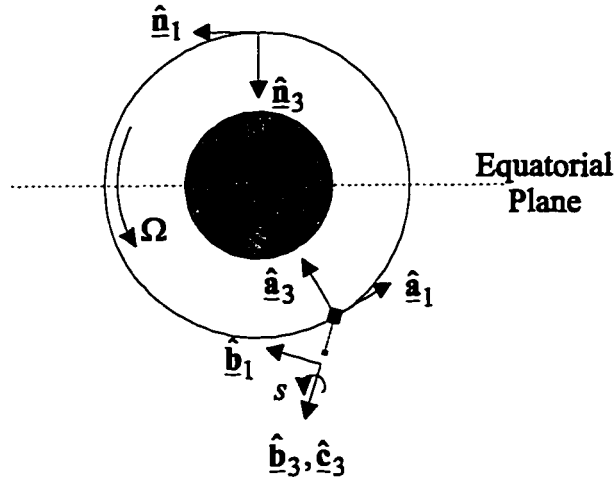


Figure 5.6. Definition of Reference Frames for Equations of Motion

Consider the axisymmetric satellite of Figure 5.6. Define 4 reference frames, as follows:

- N : an 'inertial' frame that is defined relative to, but does not rotate with,
the Earth
- A : the locally level reference frame in which the attitude is expressed, as defined
in Figure 5.5
- B : a frame with the z-axis aligned along the axis of symmetry of the body, but
does not rotate about the z-axis with the body
- C : a body fixed reference frame with the z-axis pointed along the symmetric axis

Using the notation that $\underline{\mathbf{I}}$ is the 3x3 inertia tensor (inertia cross products assumed 0), ${}^N\boldsymbol{\omega}^B$ represents the angular velocity of frame B with respect to frame N, and similarly for all other frames, the following relations may be defined:

$$I = I_x = I_y = \hat{\underline{\mathbf{c}}}_1 \cdot \underline{\mathbf{I}} \cdot \hat{\underline{\mathbf{c}}}_1 = \hat{\underline{\mathbf{c}}}_2 \cdot \underline{\mathbf{I}} \cdot \hat{\underline{\mathbf{c}}}_2 \quad (5-1)$$

$$J = I_z = \hat{\underline{\mathbf{c}}}_3 \cdot \underline{\mathbf{I}} \cdot \hat{\underline{\mathbf{c}}}_3 \quad (5-2)$$

$${}^A\boldsymbol{\omega}^C = {}^A\boldsymbol{\omega}^N + {}^N\boldsymbol{\omega}^B + {}^B\boldsymbol{\omega}^C = -{}^N\boldsymbol{\omega}^A + {}^N\boldsymbol{\omega}^B - {}^C\boldsymbol{\omega}^B \quad (5-3)$$

$${}^N\boldsymbol{\omega}^A = -\Omega \hat{\mathbf{a}}_2 \quad (5-4)$$

$${}^N\boldsymbol{\omega}^B = \omega_1 \hat{\mathbf{c}}_1 + \omega_2 \hat{\mathbf{c}}_2 + \omega_3 \hat{\mathbf{c}}_3 \quad (5-5)$$

$${}^C\boldsymbol{\omega}^B = s \hat{\mathbf{c}}_3 \quad (5-6)$$

where Ω is orbit rate and s is the axis of symmetry rotation rate. By expressing the vehicle body frame (C) with respect to the locally level reference frame (A) in quaternion format as $\mathbf{q} = [q_1 \ q_2 \ q_3 \ q_4]^T$, and with the traditional kinematic relationships, the following nonlinear equations of motion for the gravity gradient stabilized axisymmetric satellite may be derived (hysteresis torques neglected):

$$\dot{q}_1 = \frac{1}{2} [q_2(\omega_3 - s) - q_3(\omega_2 - \Omega) + q_4\omega_1] \quad (5-7)$$

$$\dot{q}_2 = \frac{1}{2} [-q_1(\omega_3 - s) + q_3\omega_1 + q_4(\omega_2 + \Omega)] \quad (5-8)$$

$$\dot{q}_3 = \frac{1}{2} [q_1(\omega_2 - \Omega) - q_2\omega_1 + q_4(\omega_3 - s)] \quad (5-9)$$

$$\dot{q}_4 = \frac{1}{2} [-q_1\omega_1 - q_2(\omega_2 + \Omega) - q_3(\omega_3 - s)] \quad (5-10)$$

$$\dot{\omega}_1 = -s\omega_2 + (1 - JI^{-1}) \left[\omega_2\omega_3 + 6\Omega^2(q_2q_3 + q_1q_4)(1 - 2q_1^2 - 2q_2^2) \right] \quad (5-11)$$

$$\dot{\omega}_2 = s\omega_1 - (1 - JI^{-1}) \left[\omega_1\omega_3 + 6\Omega^2(q_3q_1 - q_2q_4)(1 - 2q_1^2 - 2q_2^2) \right] \quad (5-12)$$

$$\dot{\omega}_3 = 0 \quad (5-13)$$

Equations (5-7) through (5-13) constitute the nonlinear dynamic model for the RADCAL satellite and may be integrated from a set of initial conditions to simulate the vehicle attitude motion. Using initial conditions from an actual GPS attitude solution (the initial

condition of Figure 5.8), the nonlinear simulation produced the plots in Figure 5.7. Equation (5-13) states that the azimuth rate of the vehicle is constant, but may in fact be nonzero, as seen in Figure 5.7a. The vehicle is seen to undergo librations up to 20 degrees in pitch and roll at about twice orbit rate. The frequencies of the librations are similar to those predicted by the mass properties of the spacecraft. Although the frequency and phase of the libration is slightly different for each axis, there appears to be a coupled exchange in amplitude motion. Note that there are no damping terms in this derivation, so this is a conservative energy simulation of the motion.

5.1.5. RADCAL Attitude Solutions

The actual GPS attitude solutions derived for an 18 hour period are presented as point solutions in Figure 5.8. The GPS carrier phase measurement sample rate was 30 seconds. The satellite is seen to undergo similar motion to that predicted by the nonlinear equations of motion, although there is more variation in the pitch and roll librations, and the azimuth rate is not completely constant. The variations between the simulation and the observed motion are believed to be due to the effects of hysteresis torques, thermal effects, flexibility, and other unmodeled details.

A extended Kalman filter (EKF) was developed using the methods of Bryson⁴ and Gelb⁵ with the dynamic equations derived above to smooth the point solutions and provide attitude estimates during times of point solution outages. The results are shown in the continuous lines in Figure 5.8. The EKF results fill the missing data very reasonably.

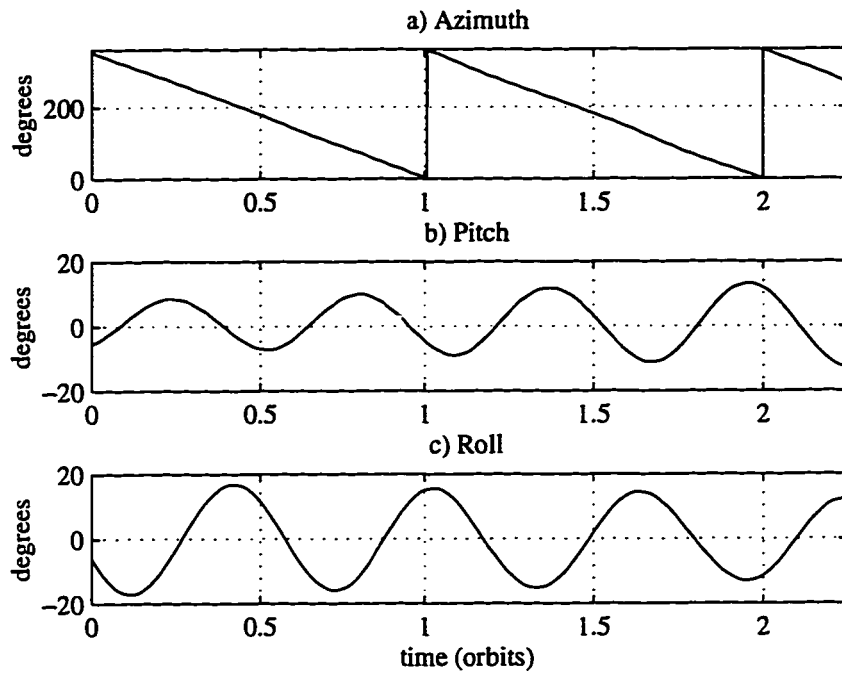


Figure 5.7. Nonlinear Simulation of RADCAL Dynamic Equations

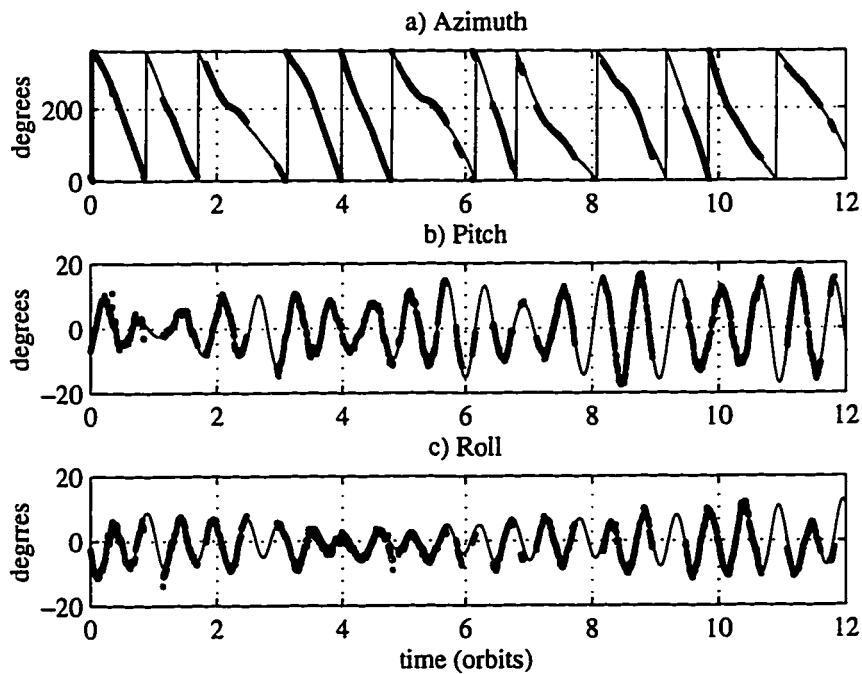


Figure 5.8. RADCAL Attitude, Point and Extended Kalman Filtered Solutions



Pitch Libration:

Theory: 1.679 rpo

Actual: 1.709 rpo

Roll Libration:

Theory: 1.930 rpo

Actual: 1.966 rpo

Yaw Rate:

-395 deg / orbit (varies)

Yaw Libration:

0.3419 rpo

Figure 5.9. RADCAL Attitude Motion

Figure 5.9 demonstrates graphically the observed RADCAL motion that is depicted in Figure 5.8. Because pitch and roll are near zero, the vehicle axis of symmetry may be thought to point nominally in the direction of the zenith vector, which is a classic gravity gradient result. The pitch and roll librations, however, which are out of phase and at slightly different frequencies, mean that the symmetry axis traces out an ellipse in a coning motion about the zenith vector. The half-cone angle varies but may be as large as 20 degrees at times, as shown in Figure 5.8. The azimuth rate superposes a rotation of the symmetry axis upon the coning motion. If the average azimuth rate is removed, a residual libration of the rate is evident, meaning that the symmetry axis rotation speeds up and slows down slightly as the vehicle goes about its polar orbit.

The pitch and roll librations are seen to agree to within a few percent of the predicted values of the nonlinear simulation. The azimuth rate is an interesting dynamic effect that was not originally expected for the vehicle motion. Although it has been observed to be

roughly constant for periods of up to a day, the rate can vary significantly over long periods of time and even change polarity. The magnitude of the rate is however never much greater than 1 revolution per orbit. The azimuth rate is believed to be related to an energy coupling with the pitch-roll libration motion. The observed changes in rate may be caused by changes in the energy state of the vehicle (assumed constant in Equations 5-7 through 5-13), due to interactions of the hysteresis rods, and thermal effects from solar heating of the gravity gradient boom. Melvin⁶ provides a more detailed dynamic analysis of the RADCAL on-orbit motion.

5.1.6. Assessment of GPS Attitude Accuracy

5.1.6.1. Magnetometer Solution Comparison

A 3-axis magnetometer was the only on-board means of independent attitude verification for RADCAL. Knowledge of the geomagnetic field and size of the data buffer (for smoothing) limit magnetometer attitude determination to approximately 3 degrees rms. Although the telemetry system for RADCAL did not originally allow data to be collected simultaneously from the magnetometer and the GPS receiver, the satellite operators were able to overcome this constraint and did in fact produce a single data collection for which both sets of measurements were available.

The magnetometer derived attitude solutions for this data set were provided by Alley.⁷ The attitude direction cosine matrix, $\underline{A}_{E \rightarrow B}$, was determined from the magnetometer data by comparing the measured values (\underline{b}_x) to the calculated geomagnetic field (\underline{b}_o) and minimizing this performance index:

$$J = \sum_i \left\| \underline{b}_x - \underline{A}_{E \rightarrow B} \cdot \underline{b}_o \right\|_2 \quad (5-14)$$

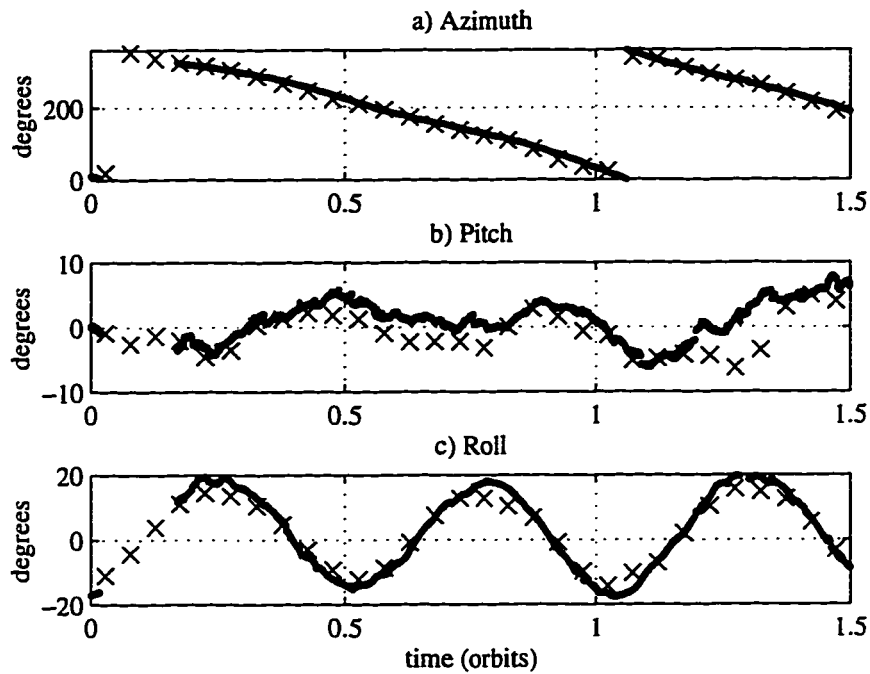


Figure 5.10. Comparison of GPS (•) and Magnetometer (×) Solutions

A dynamic model was used to obtain the third degree of freedom and the attitude solution was transformed into the locally level reference frame to produce the '×' solutions in Figure 5.10. These are compared with the GPS point attitude solutions for the same time span. The rms residual deviation between the different sensors is 4.2 degrees in azimuth, 2.0 degrees in pitch, and 2.5 degrees in roll. The GPS solutions are therefore consistent with the magnetometer derived solutions to within the bounds of the accuracy of the magnetometer attitude determination procedure.

5.1.6.2. Comparison to Theoretical Accuracy

By examining the filter solution residuals and covariances in Figure 5.10, an approximate GPS solution accuracy of about 1 deg rms is obtained per axis. Using similar RADCAL data, Melvin reports a 3- σ GPS attitude solution accuracy of about 2 degrees.⁶ Based on

a 5 mm rms measurement noise and the RADCAL antenna geometry, the attitude accuracy Equations 4-8 and 4-9 predict a theoretical value of:

$$1/\sigma_m^2 = 1/\sigma_1^2 + 1/\sigma_2^2 + 1/\sigma_3^2 = 9.1 \text{ deg}^{-2} \quad (5-15)$$

$$\sigma_m \approx 0.3 \text{ deg} \quad (5-16)$$

This value is somewhat better than the estimated $\sigma \sim 0.67 - 1$ degree that has been observed from the flight results.

There are several explanations for this deviation from the theoretically predicted accuracy. Recall that the 6 m gravity gradient boom is in the field of view of all antennas, acting as a reflection source. It is plausible that due to this mechanical design, the actual carrier phase multipath noise is substantially higher than 5 mm rms. Also, the baseline vectors were measured from mechanical drawings and the line biases were determined as a best estimate from on-orbit data. The receiver calibration parameters, which are normally assumed to perfectly known, could be in error. Finally, the canted antennas produces a RHCP carrier phase term that can be calculated from the methods of Section 3.4 but was not included in this analysis. All of these effects act to push the predicted performance line of Figure 4.6 to higher levels. The estimated solution accuracy of $\sigma \sim 0.67 - 1$ degree is therefore believable in light of these considerations.

5.1.7. Failure Description of RADCAL Receivers

As mentioned in Chapter 1, the TANS Quadrex and Vector receivers are commercial “off-the-shelf” units that are ruggedized for aviation applications, but not designed for the space environment. Vibration loads, thermal cycling, and radiation exposure in space

present extreme conditions that may cause equipment failure modes that are not encountered during terrestrial usage. These hazards are in addition to the normal lifetime failures that may occur through regular operation. Although the basic GPS hardware was sound, there was an open question regarding the survivability of these commercial receivers over long term space exposure.

The RADCAL orbit was an 815 km circular polar orbit. This orbit produces a high radiation environment due to the altitude and proximity to the Earth's magnetic poles. Nonetheless, the commercial receivers performed quite respectably well. The first receiver failed after 6 months of operation and the second receiver failed after 18 months of operation. Because of power limitations on the satellite, the receivers were cycled on and off regularly: usually once per day. The manner of failure for both receivers appeared to be related to the telemetry portion of the hardware—the ability to process commands and generate understandable messages. Investigation of the inherent radiation hardness of the device has revealed that the communications chip is probably the most radiation sensitive component, with an estimated dosage tolerance of about 5 krad Si. It is therefore hypothesized that both receivers eventually suffered from radiation-related failures in the communications portion of the unit after a reasonable amount of time in this relatively high radiation orbit. If true, this is an encouraging result for other LEO spacecraft that do not share such severe orbit conditions.

5.1.8. Summary of RADCAL Experiment

To evaluate the accomplishments of this first experiment in GPS carrier phase attitude determination, it is worth considering the many challenges that were overcome during the data processing. These are summarized in Table 5.1. The RADCAL experiment was indeed a stringent exercise of the feasibility of GPS attitude determination under adverse

Table 5.1. Challenges of the RADCAL Analysis

GPS Receiver Calibration
Antenna baselines determined from mechanical drawings Line biases estimated from on-orbit data
High Sensor Noise
Small antenna separation (0.67 m) High multipath (6 m boom) Low GPS signal strength Asynchronous data
Nonaligned Antennas
17 degree cant angle Roving master antenna
Limited Verification Capability
Magnetometer is the only independent sensor Nonlinear dynamic modeling

conditions. Perhaps this type of extreme test is the best way to demonstrate the ultimate capabilities of any new technology. In fact, this experiment and post-processing activity has served as an impetus for many of the innovations presented in this dissertation. In spite of the difficulties, it was possible to produce acceptable attitude solutions with an estimated accuracy of better than 1 degree rms per axis. The prospects for robust on-orbit GPS attitude solutions using these same algorithms under more reasonable conditions on future satellites are very good based on the performance of the RADCAL GPS attitude determination system.

5.2. Attitude Control: REX II

5.2.1. Satellite Description

On March 8, 1996, the USAF Space Test Program REX II spacecraft (Figure 5.11) was inserted into an 830 km polar orbit with two TANS Vector GPS receivers capable of performing real-time attitude determination in space. Prior to this date, experiments with GPS receivers had demonstrated the feasibility of on-orbit attitude determination on

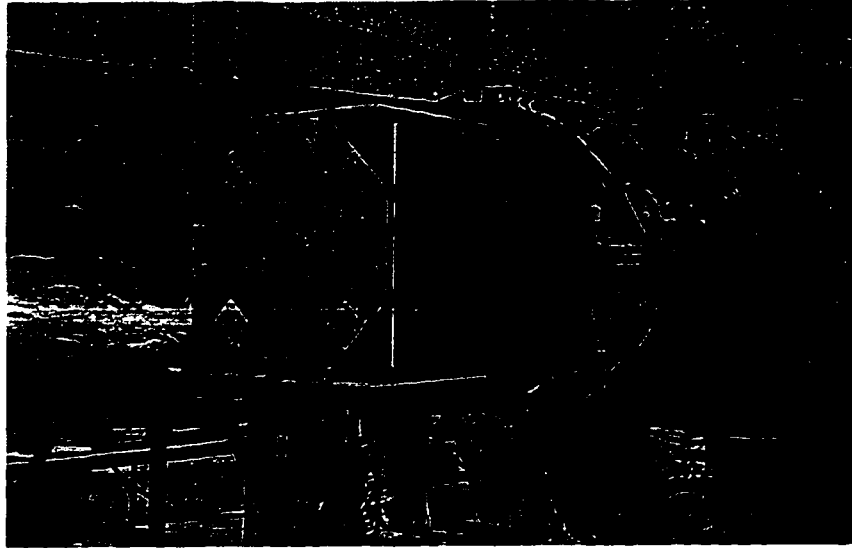


Figure 5.11. REX II Spacecraft at Integration to Launch Vehicle

The white rectangles on the near octagon are GPS patch antennas.

spacecraft in post-processing (RADCAL⁸) and real-time (Crista-SPAS⁹). These previous flights, although significant technical firsts, did not provide the practical demonstration of closed loop attitude control using GPS as the sensor for an extended real-time application. The REX II satellite marks the first known operational application of the GPS attitude sensor for closed loop control of a spacecraft.

A schematic of the REX II spacecraft is shown in Figure 5.12. It is mechanically similar to the predecessor RADCAL satellite, which was designed to be passively stabilized using a 6 m boom with gravity gradient torques and two magnetic hysteresis rods for damping. REX II is additionally actively controlled by electromagnetic coils and a pitch-axis reaction wheel which provides momentum bias. The control system requirement is to maintain a locally level orientation to within 5 degrees per axis. The vehicle attitude is expressed in the same 3-2-1 yaw-pitch-roll Euler sequence from the locally level orientation shown in Figure 5.5. The control input may be provided by the GPS attitude sensor in a 'Normal' mode or the three-axis magnetometer in a backup mode.

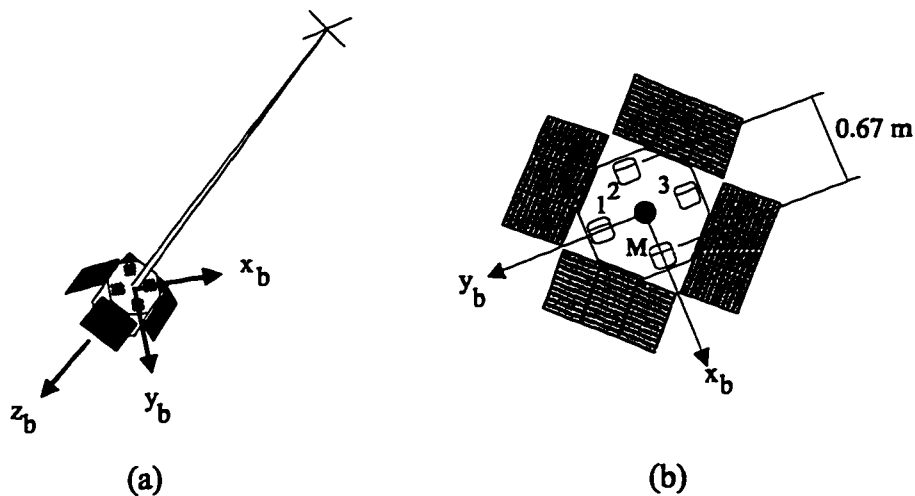


Figure 5.12. Deployed REX II Satellite: (a) Perspective, (b) Planiform

Like RADCAL, the REX II spacecraft contains a magnetometer from which milligauss-level magnetic field measurements are simultaneously available with the GPS attitude solutions. Once again, it is difficult to measure the GPS solution accuracy without a more accurate reference sensor. Additionally, the REX II telemetry system is constrained to operate with low data bandwidth over short ground passes (10 minutes), resulting in short time spans with full data or very low sampling rates that cover longer time spans. The lack of a single, long time span with full data complicates the dynamic analysis of the vehicle.

The four GPS patch antennas were mounted on the top surface of the REX II main body in a coplanar, aligned configuration, as shown in Figure 5.12b. All four antennas were keyed in the same direction to provide antenna phase center repeatability. The antenna separation was 0.67 m along the diagonal, and the gravity gradient boom extends out of the center of the main body. The GPS antenna baselines were mechanically aligned to within 0.1 degrees of the spacecraft x and y body axes.

After spacecraft integration, the GPS subsystem was placed into a self-survey mode by allowing the antenna array to collect data from the GPS constellation for several hours in a fixed position on the ground. After the self-survey test was completed, the calibration parameters were verified by witnessing that the GPS subsystem successfully computed an attitude solution.

5.2.2. Dynamic Analysis

5.2.2.1. Equations of Motion

Because REX II has an active attitude control system, with smaller perturbations than the passively stabilized RADCAL satellite, it is possible to adequately describe the vehicle attitude using a linearization of the equations of motion. The system equations of motion may be derived from the classical Euler equations:

$$\frac{d\mathbf{H}}{dt} + \underline{\omega} \times \mathbf{H} = \mathbf{T} \quad (5-17)$$

where \mathbf{H} is the angular momentum vector, $\underline{\omega}$ is the angular velocity vector and \mathbf{T} is the external torque. Let:

$$\mathbf{H} = \begin{bmatrix} I_x \omega_x \\ I_y \omega_y + h_y \\ I_z \omega_z \end{bmatrix} \quad (5-18)$$

where I_x , I_y , and I_z are system moments of inertia and h_y is the angular momentum of a constant speed pitch momentum bias wheel. Representing the spacecraft attitude by

small roll, pitch, and yaw angle (ϕ , θ , and ψ) deviations from the previously defined locally level attitude reference frame, the kinematic equations are given by:

$$\underline{\omega} \equiv \begin{bmatrix} \dot{\phi} - \omega_o \psi \\ \dot{\theta} - \omega_o \\ \dot{\psi} + \omega_o \phi \end{bmatrix} \quad (5-19)$$

where ω_o is the orbit rate.

External torques that have been taken into account include gravity gradient, controller and those due to hysteresis-rod magnetic moments. The linearized gravity gradient torque for an axially symmetric ($I_x = I_y$) satellite is given by:

$$\underline{T}_{gg} = \begin{bmatrix} 3\omega_o^2(I_z - I_y)\phi \\ 3\omega_o^2(I_z - I_x)\theta \\ 0 \end{bmatrix} \quad (5-20)$$

These equations may be combined to produce:

$$I_x \ddot{\phi} - \dot{\psi} [I_z \omega_o + h_y] + \phi [4(I_y - I_z) \omega_o^2 - h_y \omega_o] = T_x^C + T_x^H \quad (5-21)$$

$$I_y \ddot{\theta} + \theta [3(I_x - I_z) \omega_o^2] = T_y^C + T_y^H \quad (5-22)$$

$$I_z \ddot{\psi} + \dot{\phi} [I_z \omega_o + h_y] + \psi [-h_y \omega_o] = T_z^C + T_z^H \quad (5-23)$$

which represents a special case (axial symmetry and one constant wheel speed only) of those presented for an Earth-Referenced Spacecraft as shown by Wertz.¹⁰ T^C is the control torque and T^H is the hysteresis rod torque.

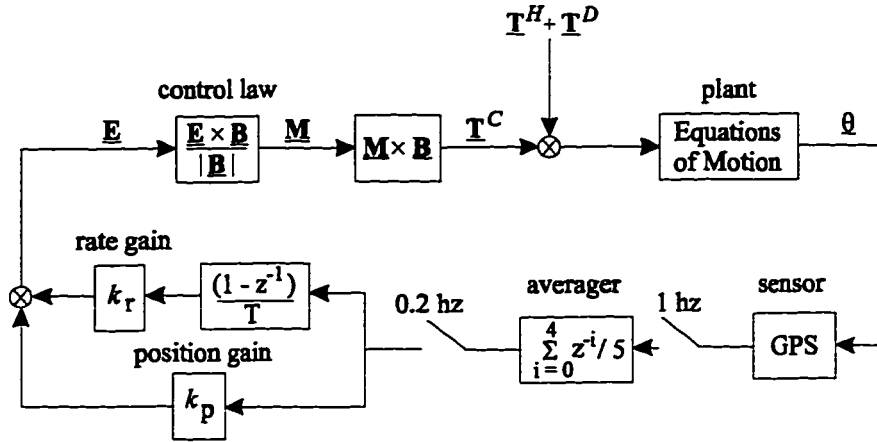


Figure 5.13. REX II 3-Axis Control Block Diagram

The control law, designed by CTA Space Systems, shown in Figure 5.13, may be computed in terms of Euler Angles as:

$$\underline{E} = \begin{bmatrix} k_{rx}(\dot{\phi} - \omega_o \psi) + k_{px}\phi \\ k_{ry}\dot{\theta} + k_{py}\theta \\ k_{rz}(\dot{\psi} + \omega_o \phi) + k_{pz}\psi \end{bmatrix} \quad (5-24)$$

where \underline{E} the control error signals, k_p and k_r are the position and rate gains, and in this case ϕ , θ , and ψ and their derivatives are the sensed Euler angles and Euler rates as provided by GPS. The Euler angles are computed as a five second time average of the 1 Hz GPS solutions to reduce sample noise, and the rates are derived rates from the last two averaged Euler angles (they are not an independent measurement).

The commanded magnetic moment is determined from the computed control error:

$$\underline{M} = \frac{\underline{E} \times \underline{B}}{|\underline{B}|} \quad (5-25)$$

And the controller torque is the cross product of the magnetic moment and the magnetic field:

$$\underline{T}^C = \underline{M} \times \underline{B} \quad (5-26)$$

5.2.2.2. Hysteresis Rods

Hysteresis rod magnetic moments are multi-valued functions of the ambient magnetic field component parallel to the axes of the rods. The moments are bounded by so-called “B/H” curve major loops which are functions of the rod material and length to diameter ratio. The magnetic moments at a particular time depend on past history and thus cannot be written as explicit functions. The mathematical model described by Flatley¹¹ was used to estimate the performance of the rods in a computer simulation of the spacecraft dynamics. Variable parameters in the model were selected to fit available tabulated empirical data for the REX II spacecraft. The model was devised during the development of the Passive, Aerodynamically-Stabilized, Magnetically-Damped Satellite (PAMS) which was released from the Orbiter Endeavour during the STS-77 Mission in May 1996. Its validity was demonstrated by observations of the on-orbit performance of that spacecraft.

5.2.2.3. Simulation Comparison to Flight Results

The closed loop GPS attitude sensor data from the spacecraft is shown in Figure 5.14. The REX II vehicle attitude was simulated for 24 hours using the closed loop dynamic equations with initial conditions provided from the GPS attitude sensor. The simulation was run with and without the effects of the hysteresis rods included in the dynamic model. The simulation results without and with hysteresis rods are shown in Figures 5.15 and 5.16, respectively.

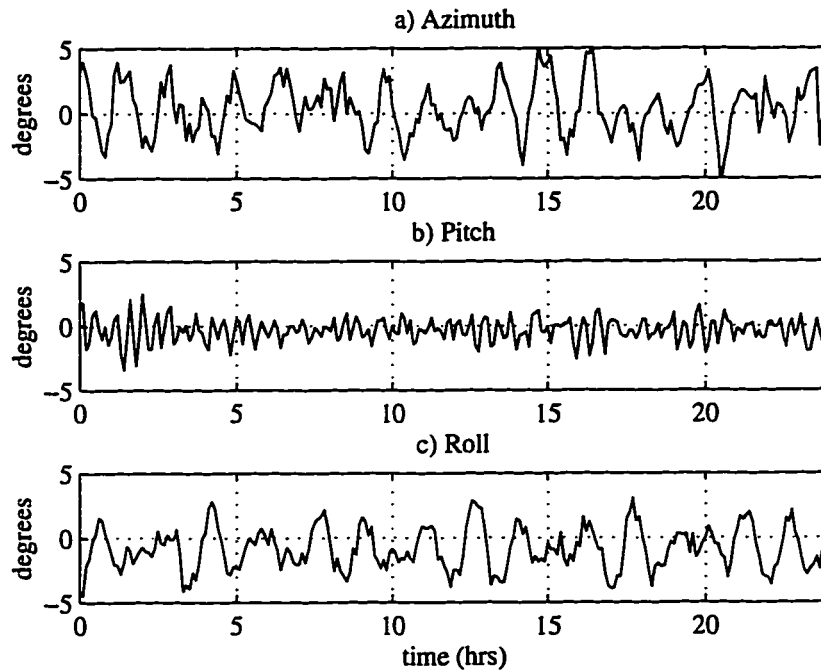


Figure 5.14. REX II Closed Loop Attitude Measurements, 24 Hours

The most interesting result from the simulation is that the fit of the simulation without the effect of the hysteresis rods included (Figure 5.15) is much better than that with the effect included (Figure 5.16). Large oscillations in all axes are observed when the hysteresis effect is included that are not observed in the GPS attitude measurements. This effect of the hysteresis rods is counterintuitive since they are usually employed on spacecraft to passively damp out oscillations.

One explanation for the large amplitude motion is an interaction of the hysteresis torques with the control system, especially in the pitch axis, which is the momentum wheel axis. When the hysteresis model is removed, the large amplitude motion is not evident in the simulation. The preliminary conclusion is that the rods are not producing the expected theoretical effect on the spacecraft, which in this case is actually better for the overall control performance.

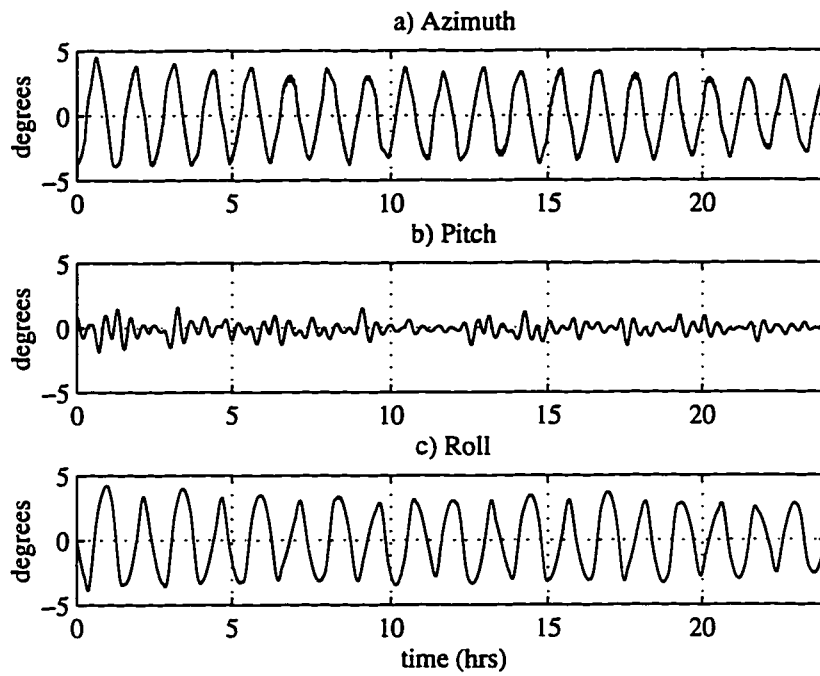


Figure 5.15. Simulated REX II Attitude Without Hysteresis Rods

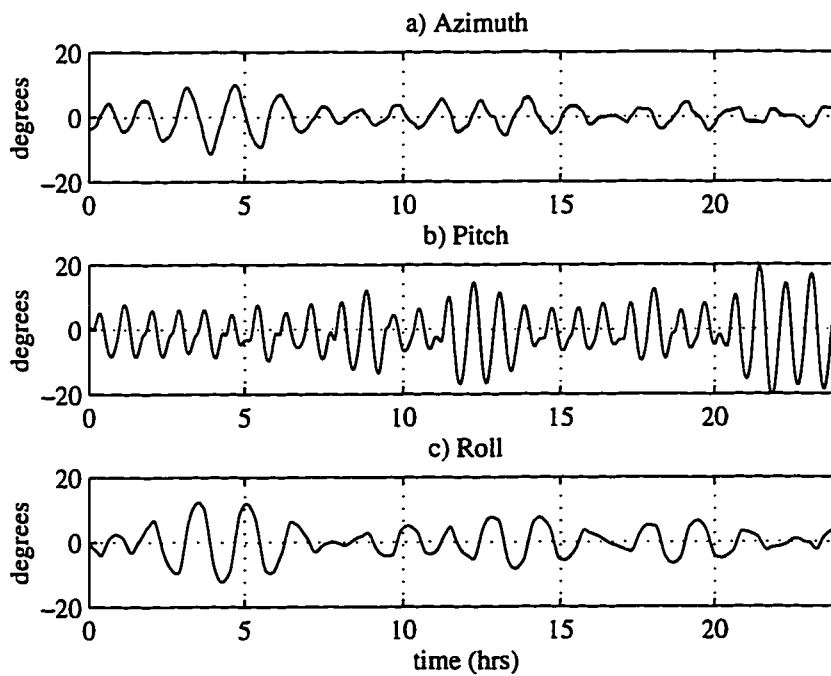


Figure 5.16. Simulated REX II Attitude With Hysteresis Rods

The residual between the simulation and the GPS attitude measurements during the 24 hour time span has a mean of 4.6 degrees without the hysteresis rods and 8.8 degrees with the hysteresis rods included. It is important to stress that the 5 degree difference does not represent a measure of sensor accuracy but instead provides general confirmation of the dynamic equations. Only a reasonable agreement between the dynamic model and the sensor results is sought to demonstrate general sensor validity. An attitude residual within 5 degrees is considered to be quite reasonable since many disturbance torques have been omitted, the dynamic model is not exact, and there are measurement errors associated with the simulation initial conditions.

5.2.3. Magnetometer Solution Comparison

As with RADCAL, REX II contained a magnetometer as the only independent sensor for attitude verification. Further, due to the data set limitations—either too short for filter convergence, or sampled very far apart—an attitude reference that may be used as ‘truth’ to benchmark GPS accuracy is all but impossible. However, at worst, using the magnetometer data and some knowledge of the kinematics and dynamic behavior, a sanity check of the GPS attitude behavior is feasible.

An estimation scheme developed by Crassidis and Markley¹¹ was adopted for the REX II data. This method involves predictive filtering specifically designed for spacecraft without gyroscopes or other rate measuring devices and has been successfully tested with flight data from the Solar Anomalous and Magnetic Particle Explorer (SAMPEX) spacecraft. The main feature that separates this filtering scheme from a traditional Kalman filter is that it does not assume that the model error, or process noise, is Gaussian and unbiased, but it instead determines the model error during the estimation process such that the model and the corrections together form an accurate representation of the

system behavior. This result is achieved by simultaneously solving system optimality conditions and an output error covariance constraint. Given the unusually awkward data characteristics caused by the low telemetry bandwidth, more reasonable attitude solutions were achieved using this approach than with a traditional Kalman filter.

Magnetometer data, along with GPS position, time, and attitude information was collected from the REX II spacecraft during a ground pass. This “short” span of data lasted 25 minutes (less than 1/3 of an orbit) at a relatively high sample period of 20 seconds. Magnetometer-only attitude solutions were derived by Ketchum¹³ using this predictive filter, with the initial attitude provided from the GPS solution. Figure 5.17 shows the three-axis difference between the GPS attitude point solutions and the magnetic field-only filter attitudes as the filter converges. The error in the reference geomagnetic field model, used in the magnetometer-only attitude computation, could be as much as 3 degrees, so that the difference in the two attitudes appears to be converging to a value within that tolerance. Further, this attitude difference is smaller than that for the previously described simulation results.

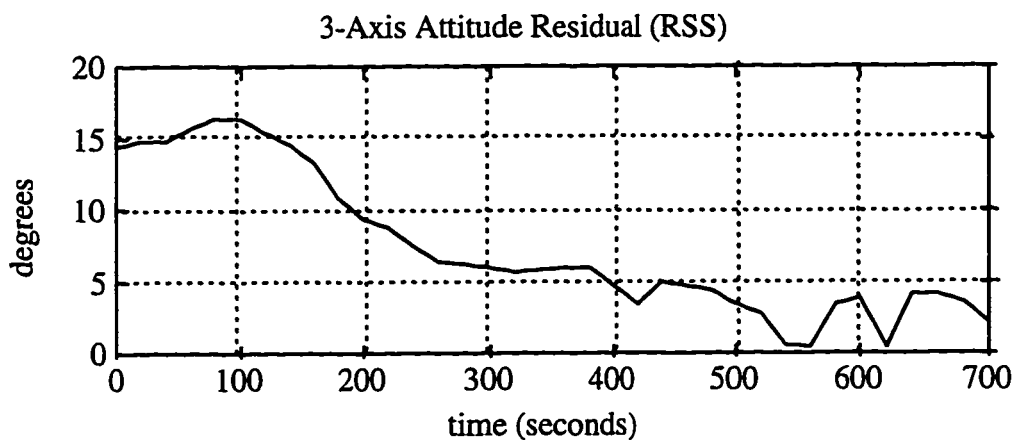


Figure 5.17. Residual of Magnetometer Derived and GPS Real-Time Solutions

5.2.4. Control Sensor Performance

Having bounded the sensor accuracy with the magnetic attitude determination accuracy of approximately 3 degrees, it remains to characterize the GPS attitude performance as a control sensor on the REX II satellite.

Figure 5.14 shows the GPS attitude measurements over a 24 hour span. *The controller performance is within the specification of 5 degrees per axis with GPS as the sole input attitude sensor.* The three-axis error during this time span has a mean value of 2.66 degrees with a standard deviation of 1.16 degrees. A simulation of the control laws given the same initial conditions of the first GPS measurement with perfect sensing afterwards (see Figure 5.15) yields a controller performance with a three-axis mean attitude error of 3.30 degrees with a standard deviation of 0.49 degrees. This result demonstrates that the controller performance is a function of the control behavior and not the sensor inputs. In other words, input sensor accuracy is not adversely affecting the controller performance.

An important topic to discuss regarding GPS sensor performance is the subject of attitude solution availability. GPS attitude outages may be caused by a number of physical effects, such as carrier phase measurement noise, solution observability, and integrity checks. With the current 6-channel TANS Vector, these outages will routinely occur during normal operations for short periods of time due to satellite selection logic. Using all available data taken to date on the REX II mission, Freesland, et al,¹⁴ have observed these brief outages at a fairly consistent rate of 1.6 times per orbit. The GPS attitude dropouts are sorted by latitude and duration in Figure 5.18. The dropouts are nearly evenly distributed at all latitudes for this polar orbit. More than 75% of all reported dropouts last between 5 and 10 minutes. This fact is consistent with the hypothesis that

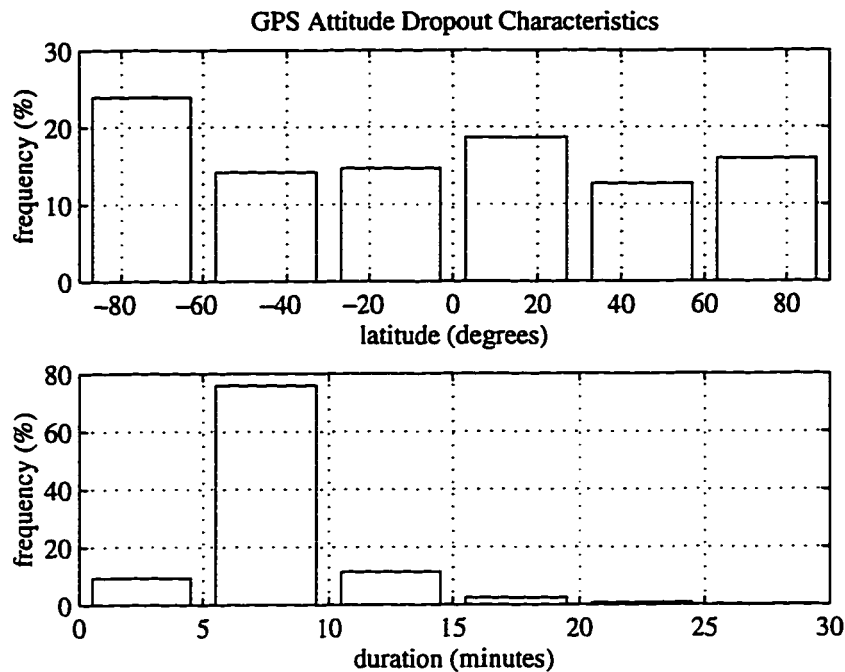


Figure 5.18. REX II Attitude Dropouts As Functions of Latitude and Duration

most outages are geometry related (although not a function of latitude), as the orbit geometry changes significantly in roughly the same time.

It is certainly true that there are many GPS signals visible for a zenith pointing spacecraft in LEO: even in the polar orbit used in the visibility study of Table 3.2, 4 or more GPS signals were visible 99.4% of the time, and 8 or more differential phase measurements were possible 100% of the time. It is therefore possible to build a GPS receiver that will provide navigation and attitude information without significant outages by taking full advantage of the available GPS signals. Four recommendations can be made to improve the solution availability on the next generation space GPS receiver:

- 1) More channels. 12 is recommended from the study in Chapter 3.
- 2) Optimal allocation of channels to satellites in view, anticipating setting and rising satellites.

- 3) Side looking antennas to increase visibility.
- 4) Tune attitude and navigation solution integrity checks to reduce the occurrence of false alarms, which cause the receiver to drop a correct solution unnecessarily, in the spacecraft measurement environment.

With these changes to the current spaceborne receiver, measurement outages should be eliminated or greatly reduced. As GPS attitude solution availability is further improved, there are many LEO applications for which the GPS receiver is completely suitable as the sole input sensor for closed loop attitude control. Dynamic filtering of the output solutions can further improve the sensor accuracy and allow continuous control in the presence of any outages that do occur.

5.2.5. Summary of REX II Experiment

REX II is the first operational application using real-time GPS carrier phase-based attitude determination as a sensor input for closed loop attitude control of a spacecraft. The controller was found to have a mean three-axis error of 2.66 degrees with a standard deviation of 1.16 degrees, which is within the controller specification of 5 degrees per axis. Launched in March 1996, the controller has operated reliably with GPS as the only attitude sensor for over 6 months, longer than the satellite mission lifetime.

The GPS attitude solutions were validated to within 5 degrees by the use of a dynamic simulation and to within 3 degrees by an independent magnetic field measurement. The dynamic model indicates better agreement with the observed GPS solutions if the hysteresis rods are not included, leading to the suggestion that the hysteresis rods simulated characterization may not match their on-orbit performance. The magnetometer validation of the GPS attitude solutions agrees to within the measurement accuracy of the

magnetic field attitude determination method (about 2 degrees). GPS accuracy of better than 1 degree is expected, but cannot be reliably proven with this sensor complement.

Although short GPS attitude sensor outages have occurred with current GPS receiver hardware during normal spacecraft operations, future improvements in GPS receivers should result in substantially less interruptions. A combined sensor output estimator with dynamic filtering may be used to reduce the effects of short duration GPS attitude outages.

5.3. Integer Resolution: GANE

5.3.1. Experiment Description

The GPS Attitude and Navigation Experiment (GANE) was designed by the NASA Johnson Space Center to test and demonstrate the suitability of a GPS attitude determination system for the International Space Station (ISS). The experiment was flown on STS-77 in May 1996 on a Hitchhiker-class truss that collected data in the Orbiter bay during the 10 day mission. The data is now being analyzed to determine the real-time and post-processed accuracy of the GPS attitude solutions.

The planar, aligned antenna array matches the geometry of the proposed ISS GPS antenna array: a 1.5 m by 3 m rectangle. The white patch antennas can be seen mounted on multipath-suppressing choke rings in the corners of Figure 5.19. The GPS receiver is the TANS Vector receiver which was modified for space during this dissertation (although, due to reliability considerations, this will not be the receiver that ultimately flies on the Space Station).

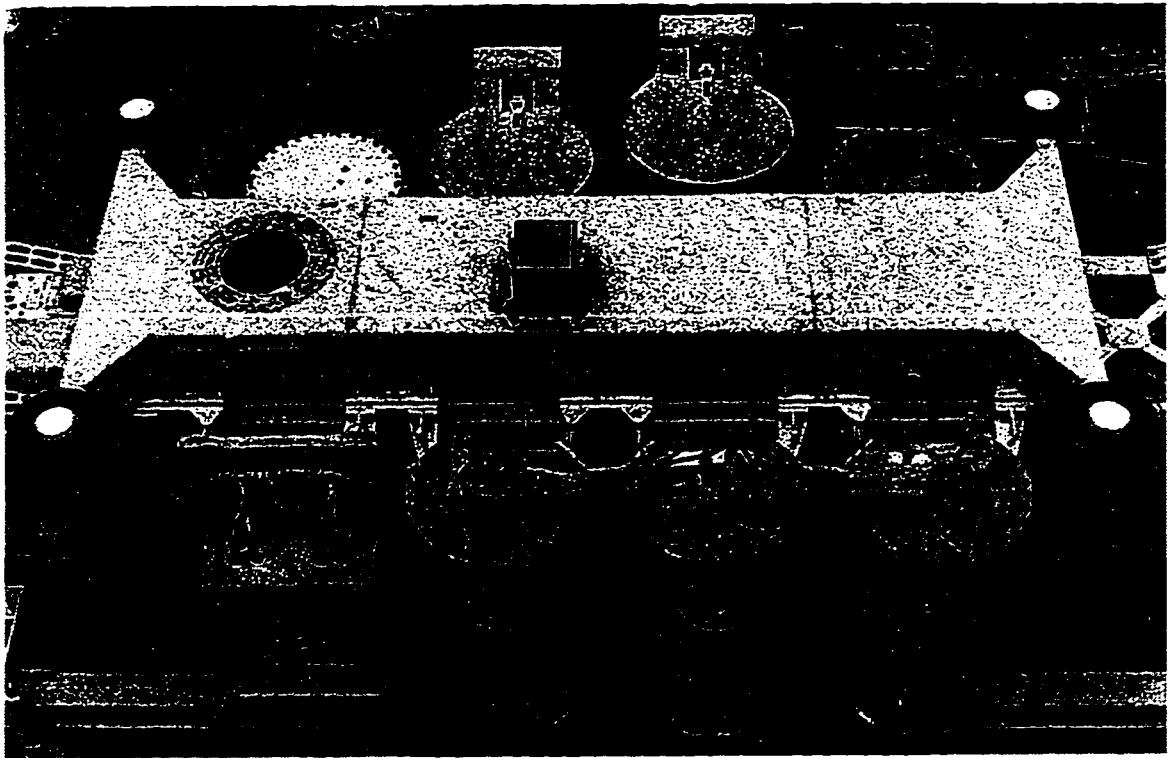


Figure 5.19. GANE Hitchhiker Payload at Integration
(carried in Orbiter Cargo Bay)

Using the error budget as outlined in Chapter 4, predicted accuracy of this design is approximately 0.1 degrees rms in pitch and azimuth and 0.2 degrees rms in roll . Unlike the earlier RADCAL and REX II satellites, GANE has other attitude references for solution comparison. The most readily available is the Orbiter attitude, which is given by an Inertial Measurement Unit (gyros) and has an estimated accuracy of 0.13 degrees rms per axis, and the "Best Estimated Attitude," which is a post-processed and filtered solution using a custom Inertial Rate Unit (gyros) payload for the GANE experiment with an estimated accuracy of 0.03 degrees rms per axis. Both inertial systems receive periodic star tracker updates. The largest error term in the latter attitude verification payload is the IRU-GANE coordinate misalignment, and achieving the 0.03 degree accuracy goal depends on how well this misalignment has been determined.

The nominal ISS attitude is such that the array will be pitched down from zenith about 41.5 degrees. This orientation reduces the total sky that is visible to the antennas, and also affects the current set of satellite selection algorithms, which use the zenith vector to determine which satellites to attempt to track (for terrestrial applications, this orientation is usually approximately true). In addition to measuring the solution accuracy, a major objective of the experiment is assessing how well the GPS system performs in the operational ISS attitude.

5.3.2. Preliminary Results

5.3.2.1. Attitude Accuracy

Although detailed reduction of the on-orbit data is now being performed to determine the “Best Estimated Attitude” results, some preliminary results of the system performance are available. Qualitatively, the mission has already been established as a success. The GANE system operated continuously for over 8 days, including 3 “Primary” data collections of 6-8 hours each, one of which was at the ISS attitude. The GPS receiver produced attitude solutions during each of the Primary data collections as well as during many of the non-critical times, when the Orbiter was performing maneuvers or during other unfavorable conditions (looking at the Earth for example). In one interesting situation it was seen that the GPS system continued to produce the correct attitude solution while tracking only 2 GPS signals (recall from Chapter 3 that attitude determination is possible with as few as 2 GPS satellites, fewer than the 4 required for a position fix if the line of sight is known). These examples demonstrate the potential ultimate robustness of the GPS attitude determination system when the technology has fully matured.

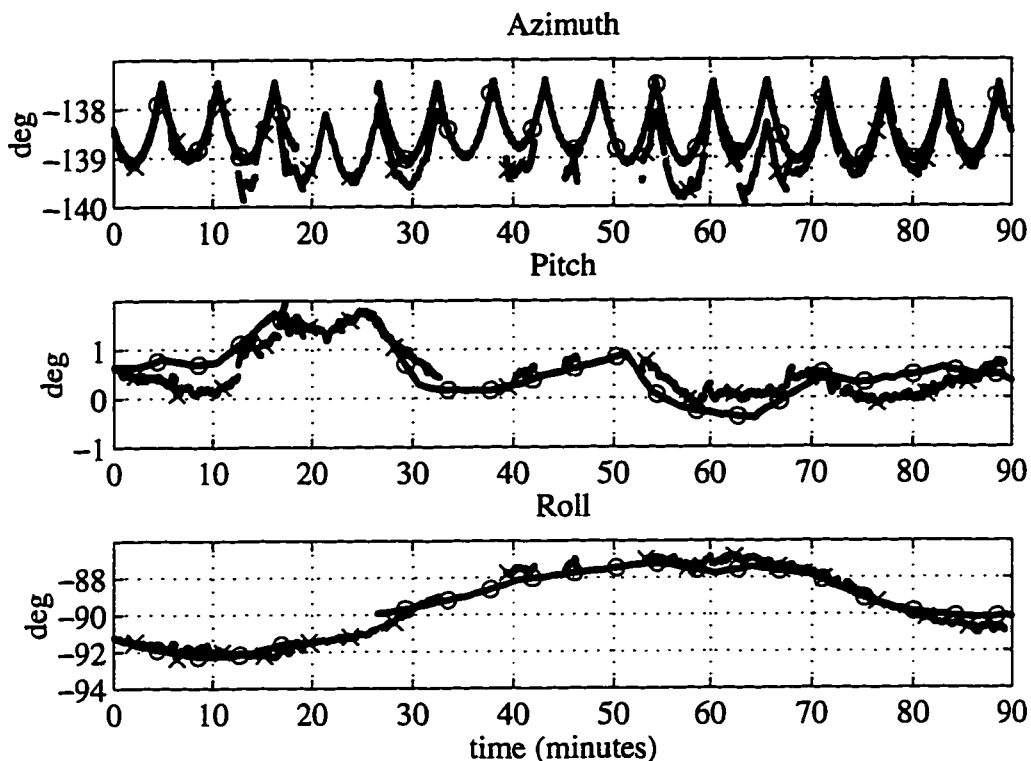


Figure 5.20. GANE Attitude Solutions at ISS Orientation, as reported by GPS (×) and Inertially-Derived (o) sensors.

A one-orbit sample of real-time GPS attitude determination is compared to the Orbiter attitude as reported by the inertial system in Figure 5.20. Because of the Orbiter was orientation (note the -90 degrees azimuth), the 41.5 degree pitched down ISS attitude appears in roll. The one-sided limit cycle of the Orbiter control system is clearly evident as it maneuvers to maintain this direction.

The Orbiter's inertially-derived attitude solution agrees with the GPS attitude to 0.2 degrees rms in azimuth and pitch and 0.4 degrees in roll. This is about twice the predicted values of 0.1 and 0.2 degrees rms, respectively, using the error budget presented in Chapter 4. However, approximately 0.13 degrees error can be attributed to the measurement accuracy of the inertially-derived attitude and any residual misalignment of

the different reference frames. In post-processing, Carpenter¹⁵ has also found what appears to be a deterministic 0.5 degree error in the GPS receiver line of sight vector calculation that occurs during approximately one half orbit (note the roll offset from 15 to 65 minutes in Figure 5.20). The cause of the line of sight calculation offset is currently under investigation. When this offset is removed, Carpenter shows that the two systems agree to within the predicted GPS accuracy of 0.2 degrees rms in roll and 0.1 degrees rms in pitch and azimuth.

5.3.2.2. Integer Resolution Method Comparison

Another very interesting aspect of this experiment was that it allowed, for the first time, an on-orbit comparison of the different integer resolution methods. In particular, the search method and the quasi-static motion method were both used during portions of the primary data collections. The results are shown in Table 5.2. Many of the comments made in Chapter 3 regarding these algorithms are validated in this experiment.

With the antenna array pointed in the zenith direction, both methods produced attitude solutions. Although the search method produced a single set of regular solutions for over an hour, the quasi-static motion method yielded more than three times as many total

Table 5.2. Solution Availability vs. Pointing and Integer Resolution Method

Algorithm	Pointing	Total Time (minutes)	Solution Time (minutes)	Solution Availability (%)
Search	Zenith	480	72	15.0
Quasi-static	Zenith	360	167	46.4
Search	Pitched down	90	0	0
Quasi-static	Pitched down	435	204	46.9

solutions than the search method over a 6 hour time span. This is perhaps a surprising result (after all, search is often a faster way to obtain a solution) that emphasizes the integrity issues that were discussed in Chapter 3.

Because the search method is an instantaneous minimization problem to determine the cycle ambiguities (that is, all data is taken from a single measurement epoch), integrity is achieved by specifying a certain separation between the minimum residual solution and the next lowest residual solution. However, because the minimum residual solution is not guaranteed to be the correct solution in the presence of noise, the separation level must be set relatively large to provide the appropriate solution integrity. This separation can then lead to most solutions being rejected due to noise, and overall less solution availability than a motion method. The motion method, in contrast, has a built in delay while data is collected, but is an inherently high integrity cycle ambiguity resolution algorithm, because it processes a batch solution (several measurement epochs), rather than an instantaneous solution (one measurement epoch) from the data.

Also, the quasi-static motion method was seen to work equally well at both the zenith attitude and at the pitched down ISS attitude. The search method did not work at the ISS attitude, due to the fact that only solutions within a certain cone angle of zenith are attempted. While the search method can be modified to use the nominal ISS attitude as an initial guess and consider a cone of solutions about that attitude, this observation emphasizes that the search method requires some *a priori* knowledge or assumptions about the vehicle orientation, while the quasi-static motion method is completely general and places no constraints on the vehicle orientation.

These points of course do not mean that the search method does not have a role for on-orbit applications. In fact there are many situations where the search method works

equally well or may be the preferred mode of cycle ambiguity resolution. It is important to stress the need for multiple algorithms, however, so that spacecraft designers have some choice to select the best solutions for each individual application. There is also potential for a combination of search and motion methods into a single set of all-encompassing algorithms that enjoy the speed of the search method with the inherent integrity and generality of the quasi-static motion method.

5.3.3. Future Research

Although much has already been learned from the GANE mission, one of the most important results that has not yet been attained is the measured attitude accuracy of the GPS system using the precise (0.03 degrees rms) attitude verification system. The less accurate Orbiter inertial attitude determination system (0.13 degrees rms) has already verified the GPS solution accuracy to within the theoretically predicted values 0.2 degrees rms when accounting for error sources. The structure of the residuals of the more precise measurements may lead to additional improvements in the algorithms for GPS attitude determination accuracy. For example, some insight into nature of the on-orbit multipath signal might be revealed by comparing the GPS solution to the high accuracy attitude determination. Other algorithm enhancements may also be suggested, as the on-orbit solutions have never before been validated to this level of precision. The misalignment of the two attitude determination systems (estimated to be about 0.025 degrees per axis) is a critical parameter in these calculations.

Other enhancements that could improve system performance are readily evident. As with REX II, there are some attitude data dropouts that occur regularly. On GANE, there are also longer attitude dropouts of up to an hour at a time, although these may be due to possible radio interference, Orbiter maneuvering, antenna visibility, and similar causes.

The integrity thresholds that define at what residual level to reject an attitude solution have not been fully tuned, and it is believed that proper selection of these thresholds using on-orbit data that is now available has the potential to significantly reduce the frequency and duration of these outages.¹⁶

One observation that should be mentioned is that the attitude solution availability was essentially unaffected by the pitched down attitude. The ability of the receiver to compute attitude solutions when it had less than 4 GPS signals in track (i.e., not computing position fixes) was a key design feature that accounted for the performance at the ISS orientation. This performance could certainly be improved by incorporating the knowledge of the vehicle orientation as provided by attitude updates into the satellite selection logic inside the GPS receiver.

5.4. Summary

The successful operation of these experiments demonstrates the capabilities and potential of the GPS receiver as a spacecraft attitude and navigation sensor. They validate many of the concepts presented in this thesis experimentally and also suggest avenues for further improvement in measurement accuracy, availability, and integrity. There is every reason to believe that the GPS attitude determination technology will continue to evolve along with GPS navigation and on-orbit experience into a highly robust and autonomous turn-key style sensor.

The very important, straightforward applications of GPS technology considered here are stepping stones to the more advanced on-orbit capabilities of the near future. These ideas will be presented in the next chapter.

5.5. References

- ¹ J.V. Langer, W.A. Feess, K.M. Harrington, M.R. Bacigalupi, M.A. Cardoza, R.G. Mach, P.A. Abusali, "RADCAL: Precision Orbit Determination with a Commercial Grade GPS Receiver," *Institute of Navigation (ION) 1994 National Technical Meeting*, San Diego, CA, Jan. 1994.
- ² L.M. Ward, P. Axelrad, "A Combined Filter for GPS-Based Attitude Determination and Baseline Estimation," *ION GPS-96*, Kansas City, MO, Sept. 1996.
- ³ T.R. Kane, P.W. Likins, D.A. Levinson, *Spacecraft Dynamics*, McGraw-Hill, Inc., 1983.
- ⁴ A.E. Bryson, *E207C: Optimal Control, Course Notes*, Stanford University, Mar. 1992.
- ⁵ A. Gelb, ed., *Applied Optimal Estimation*, M.I.T. Press, 1994.
- ⁶ P.J. Melvin, L.M. Ward, P. Axelrad, "The Analysis of GPS Attitude Data from a Slowly Rotating, Symmetrical Gravity Gradient Satellite," *AAS/AIAA Spaceflight Mechanics Meeting*, Albuquerque, NM, Feb. 1995.
- ⁷ T. Alley, private communication, Nov. 1993.
- ⁸ C.E. Cohen, E.G. Lightsey, W.A. Feess, B.W. Parkinson, "Space Flight Tests of Attitude Determination Using GPS," *Intl. Journal of Satellite Communications*, Vol. 12, 1994.
- ⁹ J.K. Brock, et al, "GPS Attitude Determination and Navigation Flight Experiment," *ION GPS-95*, Palm Springs, CA, Sept. 1995
- ¹⁰ J.R. Wertz, ed., *Spacecraft Attitude Determination and Control*, D. Reidel Co., 1978.
- ¹¹ T.W. Flatley, D.A. Henretty, "A Magnetic Hysteresis Model," *AAS/AIAA Spaceflight Mechanics Conference*, Austin, TX, Feb. 1996.
- ¹² J.L. Crassidis, F.L. Markley, "Predictive Filtering for Attitude Estimation Without Rate Sensors," *AAS/AIAA Spaceflight Mechanics Conference*, Austin, TX, Feb. 1996.
- ¹³ E.G. Lightsey, E. Ketchum, T.W. Flatley, J.L. Crassidis, D. Freesland, K. Reiss, D. Young, "Flight Results of GPS Based Attitude Control on the REX II Spacecraft," *ION GPS-96*, Kansas City, MO, Sept. 1996.

¹⁴ D. Freesland, K. Reiss, D. Young, J. Cooper, A. Adams, "GPS Based Attitude Determination: The REX II Flight Experience," *Tenth Annual AIAA/USU Small Satellite Conference*, Sept. 1996.

¹⁵ J.R. Carpenter, R.M. Hain, "Precise Evaluation of Orbital GPS Attitude Determination on the STS-77 GPS Attitude and Navigation Experiment (GANE)," *ION National Technical Meeting*, Santa Monica, CA, Jan. 1997.

¹⁶ B. Pervan, *Navigation Integrity for Aircraft Precision Approach using the Global Positioning System*, Ph.D. Dissertation, Stanford University, March 1996.

Chapter 6: Future Applications

There are many ways in which the emerging GPS space receiver technology distinguishes itself from that of previous space sensor innovations. As has been mentioned before, the GPS receiver brings an unprecedented consolidation of sensing functions into a highly compact, single device; making it a true systems sensor. Although most spacecraft sensors now contain some processing to improve their performance, few leverage the power of modern microprocessors as fully as the GPS receiver, which may employ more complex logic than the vehicle on which it is installed. And yet, from the external interface, the GPS receiver has the potential to be an extremely simple and reliable device to operate on a spacecraft, requiring only a basic familiarity of its internal workings.

The GPS receiver may be thought to represent the first of a new generation of smart sensors of the next century. These devices will localize substantial processing inside themselves and provide simple, ready-to-use interfaces that have the flexibility to provide finished solutions and/or raw measurements as outputs to an autonomous system that is highly cognizant of its surrounding environment and capable of making decisions to perform the machine function without direct human maintenance.

As much as possible (and taken with a measure of humility), this chapter looks forward to the next few years of GPS receiver developments and space applications. It discusses both planned experiments for the near future as well as the more distant ideas that will provide a sense of the currently imagined capabilities of GPS and GPS-like systems in space.

6.1. Receiver Advances

The space GPS receiver is an evolving device that is still far from technical maturity. In fact, as development continues, there will be probably not be a single all-encompassing receiver design but instead several varieties for specialized tasks. This classification of space receivers is already beginning to emerge with the latest commercially available models. Some of the most important advances that can be currently envisioned are listed below.

6.1.1. Spaceborne Integrity Monitoring

The space environment is somewhat unique from the terrestrial case as far as receiver integrity monitoring is concerned. If antenna coverage encompasses the full sky, more than 9 GPS satellites are routinely visible at one time, and up to 16 may be observed, as was shown in Table 3.2. When all these satellites can be tracked, there will be plentiful measurements to ensure solution integrity. On the other hand, the satellites are rising and setting much more quickly than observed from the ground. Terrestrial-style satellite selection and tracking loops may limit the number of satellites that can be observed at any one time. Also, in the case of an aligned array on a inertially pointed or spinning spacecraft, there may often be times when 4 or fewer GPS signals are visible due to Earth

shadowing. This dynamic environment is different enough from ground-based applications that unique satellite selection and integrity monitoring algorithms are required to achieve best performance.

As spacecraft autonomy is enhanced, so is the need for adequate GPS solution integrity. For example, if autonomous stationkeeping is desired, one must be sure that the trajectory (and the measurements on which is based) is correct before executing a maneuver.

6.1.2. Wide Area Augmentation System

The Federal Aviation Administration's Wide Area Augmentation System (WAAS), when available in a few years, will provide corrections that enable real-time solution accuracy to within 5 meters (or better) for suitably equipped ground and near-Earth space receivers.¹ Further filtering of these solutions have the potential to produce meter-level real-time navigation information. This capability will allow precision formation flight across large distances as well as proximity operations of spacecraft in the near future, in addition to the integrity functions of WAAS.

6.1.3. Multipath Suppression

As discussed in Chapter 4, carrier phase multipath is the dominant error source for GPS attitude determination, and progress is expected in the ability of the receiver and/or antenna to suppress these unwanted signal reflections. Many different approaches have been defined from purely hardware oriented (e.g., choke rings) to exclusively software oriented (spectral identification). One very promising concept that can be implemented in firmware is analysis of the correlation function of the tracked signal with an ideal equivalent. At the expense of some additional tracking hardware, the cross-correlation

function of the incoming signal may be generated, in addition to the phase offset. If the shape of the correlation function is distorted, it indicates the presence of multipath. The tracking loop may then be adjusted to mitigate the multipath error. Because this system can be implemented entirely in the receiver tracking firmware, multipath can be reduced as the measurement is made. A substantial improvement in carrier phase multipath rejection could lead to a factor of 5 improvement in real-time attitude solution accuracy.

6.1.4. On-Orbit Self-Survey

The attitude determination algorithm requires experimental measurement of certain calibration parameters to operate properly, as mentioned in Chapters 3 and 4. The procedure for calculating these parameters requires a several-hour outdoor test with the fully integrated system, or at least a realistic representation of the GPS antenna array dimensions with the flight GPS hardware. Although simple in principle, this test can be costly and time consuming when it is part of the spacecraft integration procedure. The ultimate solution to this problem is a GPS receiver that is self-calibrating on-orbit. This method has the additional advantage that the survey parameters may be periodically recalibrated over the life of the mission. There may also be some improvements in modeling these effects, which are approximated as constants but in reality depend on environmental conditions such as temperature and signal line of sight. Some preliminary work on this subject has been discussed by Ward.²

6.1.5. Integrated Transponder

A key technology for formation flight and microsatellites is receiver to receiver communications. In this case the GPS receiver can be used as a two-way communications device, receiving at L-band and transmitting at K- or L-band. Due to

interference, the transmission time might be duty cycled at 10% in between GPS measurements. The receiver could provide GPS like measurements for ranging as well as communications.³

6.2. Planned Experiments

In this section, a sample of known planned and currently funded flight experiments is discussed. Only projects that are believed to be demonstrating a new capability are listed. The activities are ordered roughly by expected chronology lasting through the year 2000. This is not meant to be an all-inclusive list, and any omissions that have been made should not be construed as a comment on the significance of the work.

6.2.1. Autonomous Orbit Determination and Spacecraft Time Distribution

The GPS Attitude Determination Flyer (GADFLY) experiment has been incorporated into the Small Satellite Technology Initiative (SSTI) Lewis spacecraft (shown in Figure 6.1) which will be launched in 1997.⁴ The primary objective of the GADFLY experiment during the 5-year operational life of the spacecraft is to demonstrate the cost-saving systems engineering features that can be exploited by using GPS receivers on space vehicles. The GPS subsystem is composed of four antennas and pre-amplifiers, cross-strapped to two Space Systems/Loral Tensor receivers. This will be the first long duration on-orbit flight of a GPS receiver capable of carrier phase-based attitude determination that has been specifically designed and environmentally qualified for space operation.

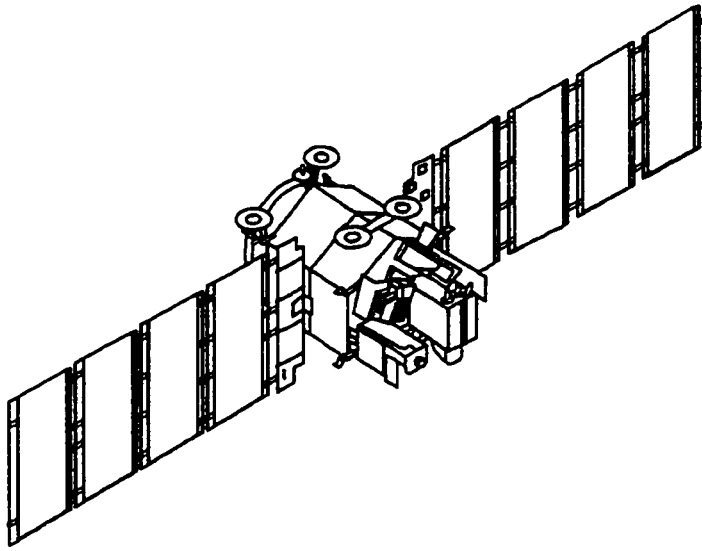


Figure 6.1. SSTI-Lewis Spacecraft

Although the Tensor receivers are being flown on GADFLY primarily as an attitude determination experiment, the SSTI-Lewis spacecraft will use the autonomous orbit determination and precision time capabilities of the GPS subsystem to improve the performance of other spacecraft experiments. The spacecraft clock will use a timing signal and a “time at the tone” message from the GPS receiver to maintain an overall spacecraft timing accuracy to better than one millisecond. This information, coupled with real-time orbit information provided by an enhanced navigation filter designed by the Goddard Space Flight Center,⁵ will be used to determine the location of objects photographed by the hyper-spectral imager experiment. The filtered real-time navigation accuracy is expected to be 20 meters rms.

6.2.2. Sounding Rocket Applications

The field of sounding rockets and sub-orbital payloads is an interesting subject for GPS receivers. These vehicles are often subjected to very high launch loads, and the entire experiment duration is usually less than 30 minutes. Speed of signal acquisition and data

continuity are essential. NASA's Wallops Island Facility has developed a special antenna that wraps around the vehicle shroud and has the gain pattern of a torus. In many cases the receiver is launched while powered on and performing position fixes. For the NASA PHAZE-2 payload, better than 1 msec timing accuracy will be available.⁶ The receiver may also assist in locating the payload after the flight and can be recovered and flown again.

Another application for sounding rockets is to measure the separation between the payload and the booster after separation (this requires two receivers, one on each vehicle). Carrier phase kinematic positioning such as has been used to land aircraft could provide centimeter level navigation accuracy in post-processing.⁷

6.2.3. Coordinated Science Platforms and Formation Flight

Using two spacecraft with GPS receivers, it is possible to look at the same object simultaneously from two platforms. The different lines of sight to the object can be used to provide sounding and three-dimensional imaging, similar to human vision. Multiple payloads on different spacecraft may measure fundamentally different quantities for the same target (e.g., water vapor, carbon dioxide, temperature, and ozone), leading to a more complete description of conditions at that point. Alternatively, one spacecraft may use autonomous stationkeeping to "shadow" another, ensuring that it follows the same ground track as the leading spacecraft.

This latter situation is the one planned for the Earth Observer-1 (EO-1) satellite which will be launched in or near 1999. The experiment will be made more complex by the fact that the leading spacecraft, Landsat-7, does not have a GPS receiver. In this case the

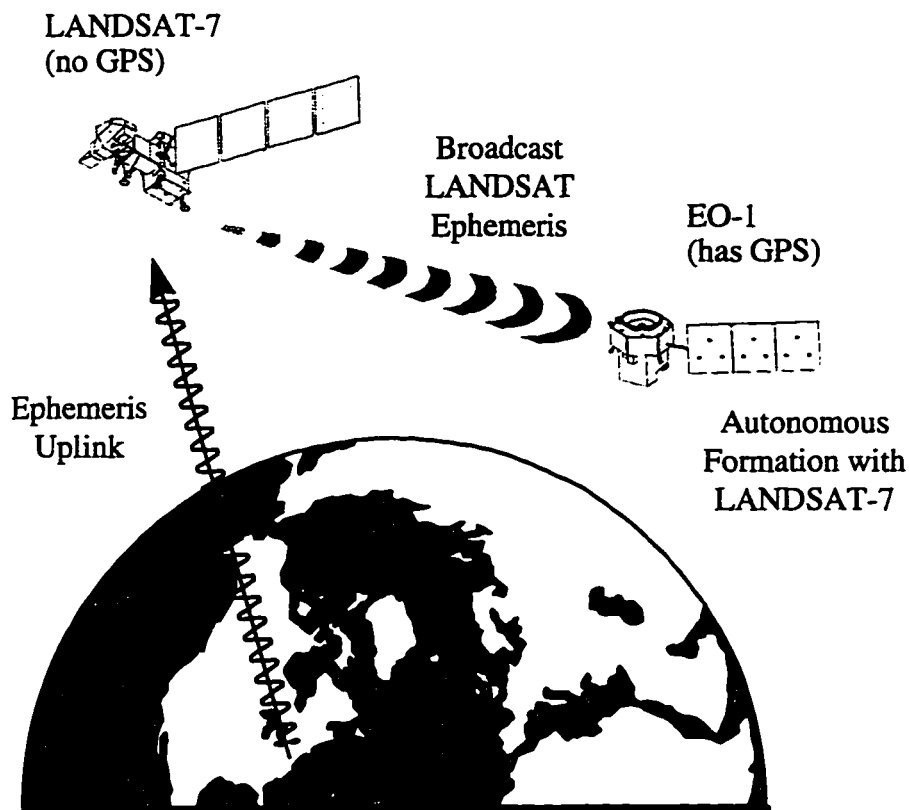


Figure 6.2. Coordinated Navigation Between Two Spacecraft

Landsat-7 spacecraft will be tracked from ground observations and the estimated position will be provided in near real-time by cross-link from Landsat-7 to EO-1 (see Figure 6.2). EO-1 will then autonomously adjust its position to maintain a fixed separation and the same ground track as Landsat-7.

The formation flight concept has tremendous commercial potential as well. At least two constellations of global coverage communications satellites may use GPS receivers to provide tracking and stationkeeping operations to maintain the proper formations (Space Systems Loral's Globalstar and Orbital Sciences' Orbcomm).

6.2.4. Integrated Navigation and Attitude Systems

As discussed in Chapter 5, the total navigation and attitude system performance for some vehicles may be enhanced by combining the GPS receiver measurements with another sensor, such as a magnetometer or an inertial navigation system (INS). The extra sensors can provide measurement updates during short GPS data outages, if they occur. The combined measurements may be used to produce a more accurate real-time estimate of position and attitude than would be possible with either sensor alone.

In the case of the GPS/INS sensor, the GPS updates perform regular calibration of the gyro drift rates, enabling the INS portion to provide highly accurate (but short duration) estimates of position and attitude. This GPS/INS concept is planned to be employed in the US Manned Space Program on the Space Shuttle, International Space Station, and Crew Return Vehicle (CRV) near the year 2000. The INS and mechanical housing will be provided by Honeywell, the prime contractor for the project. The GPS receiver will be a Rockwell Collins receiver on the Shuttle (which does not require attitude determination) and a repackaged-for-space Trimble TANS Vector on the Space Station and the CRV (both of these require attitude determination). NASA's Goddard Space Flight Center will be providing the software updates to improve the TANS Vector receiver's performance in space.

6.2.5. Attitude Determination of Spinning Spacecraft

Spinning spacecraft provide some unique challenges for GPS receivers, such as GPS signal visibility and tracking, as was described in Chapter 3. GPS receivers will almost certainly fly as experiments on spinners in the next few years. At least two proposed experiments are being considered at this time. SAC-A—an Argentine satellite that will be deployed from the Space Shuttle—will be spinning at rates up to 20 rpm. The GPS

antennas will be mounted on the face that is aligned along the spin axis, which will point in the direction of the orbit normal. In the event of GPS Attitude Determination and Control System (GADACS) reflight mission, a slowly spinning control system using GPS as the only sensor input might be attempted. In either case, there will probably be some software changes required to optimize the GPS receiver performance for spinning spacecraft, but there are no fundamental limitations to prohibit GPS from being routinely performed on spinners in the future.

6.3. Other Capabilities

The following applications are currently being planned or may come about within the next decade due to the progress of the state of the art. This list is only meant to offer the reader an idea of what is possible by using GPS in space. If the progress of the 1990's is to be used as an indicator, there will certainly be many innovative developments over the next several years that could not be presently anticipated.

6.3.1. Proximity Operations

Meter-level real-time absolute navigation as provided by real-time dynamic filtering and WAAS (Section 6.1.2), in addition to centimeter-level kinematic carrier phase relative positioning,^{7,8} allow autonomous vehicle rendezvous and proximity operations to occur under a single logistical framework. Such operations are expected to routinely occur on the International Space Station, both as part of docking and resupply operations as well as providing basic unmanned robotic maintenance vehicles. The autonomous robotic capability can reduce the cost and risk of manned operations. Intervehicle communications of navigation and attitude information, possibly provided by the

integrated transponder described in Section 6.1.5, is also essential to provide this capability.

6.3.2. GPS on High Altitude Satellites

As early as mid-1997, the Amateur Radio Organization AMSAT Phase3D satellite will fly a GPS receiver as an experiment in a highly elliptical orbit with an apogee of several Earth-radii. The objective of the experiment is to determine GPS satellite visibility and performance above the altitude of the GPS constellation. In a more long-term operational situation, the commercial and scientific value of GPS navigation solutions for satellites in geostationary and other high-altitude orbits is easily appreciated. Although the point-solution accuracy will suffer accuracy degradation from poor geometry, the disturbance forces at geostationary orbit are much smaller than LEO and a real-time filtered solution should still produce good accuracy (<100 m rms is probably achievable).

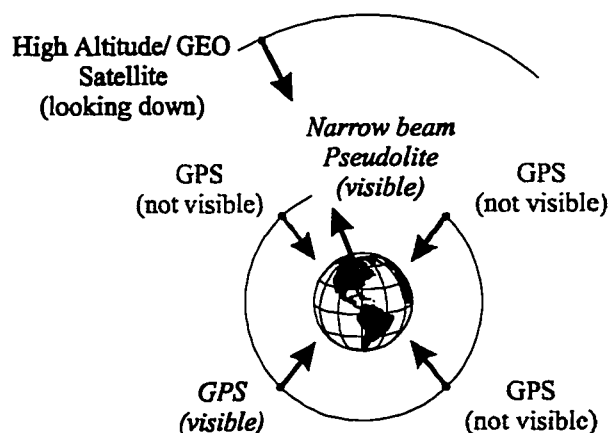


Figure 6.3. GPS Signal Visibility at High Altitude

The main challenge of GPS at high altitudes is signal visibility. Orbit studies similar to those in Chapter 3 have shown that usually only 2 GPS satellites are visible and facing the satellite in geostationary orbit (these are the ones broadcasting from the other side of the Earth, see Figure 6.3). Continuous GPS position fixes, which require 4 GPS signals to be acquired simultaneously, are not strictly needed for a real-time navigation estimator that accepts pseudorange measurements as inputs. If, however, more GPS signals are desired to improve GPS navigation integrity and availability, these could be provided from the surface of the Earth in the form of pseudolites, as shown in Figure 6.3. The signal could be tightly focused to a geostationary satellite to prevent unwanted signal interference with other GPS receivers (that might potentially have their own pseudolite applications).

6.3.3. Flexure Sensors/Control of Large Space Structures

Teague has demonstrated that, using kinematic carrier phase positioning methods and a distributed network of GPS antennas along a structure, it is possible to not only measure the structural deformation, but also to control the modes of vibration.⁹ This research has a direct application to large space structures, which are highly flexible and often lightly damped. An additional application might be measurement/control of the deformation of a tethered satellite.

6.3.4. Microsatellites

Figure 6.4 shows an advanced concept for a highly miniaturized micro-satellite (the original concept provided by Orbital Sciences Corporation), with the entire vehicle body being less than 1.5 m in diameter in the stowed configuration (in principle this could be much smaller) and 0.5 m in thickness. A miniaturized “GPS on a chip” GPS receiver

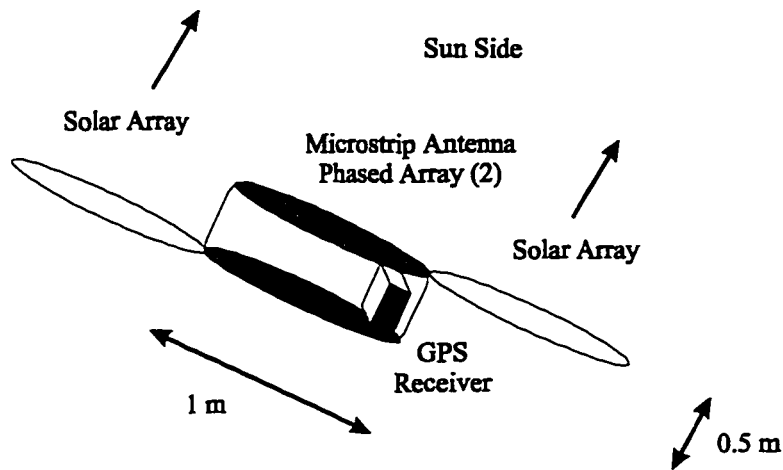


Figure 6.4. Microsatellite Concept with GPS Receiver

that is perhaps cigarette-pack sized resides inside the main body, while micro-patch phased array antennas with steerable gain patterns are used on opposite sides for both reception and transmission. The clamshell wings that rotate out are solar arrays and coupled with a highly efficient battery provide the needed power (about 2 W for the GPS receiver).

The GPS technology could be leveraged further to allow for constellations of microsatellites, each maintaining (or at least measuring) a set position and orientation relative to the others.

6.3.5. Transmit/Receive Autonomous Constellations

An interesting and challenging concept has been proposed for a constellation of satellites, not in a Earth orbit put perhaps at a Lagrange point, to maintain a fixed position and orientation with respect to each other so as to form a giant distributed interferometric telescope, as displayed in Figure 6.5.¹⁰ Such an array of satellites could be used to look at

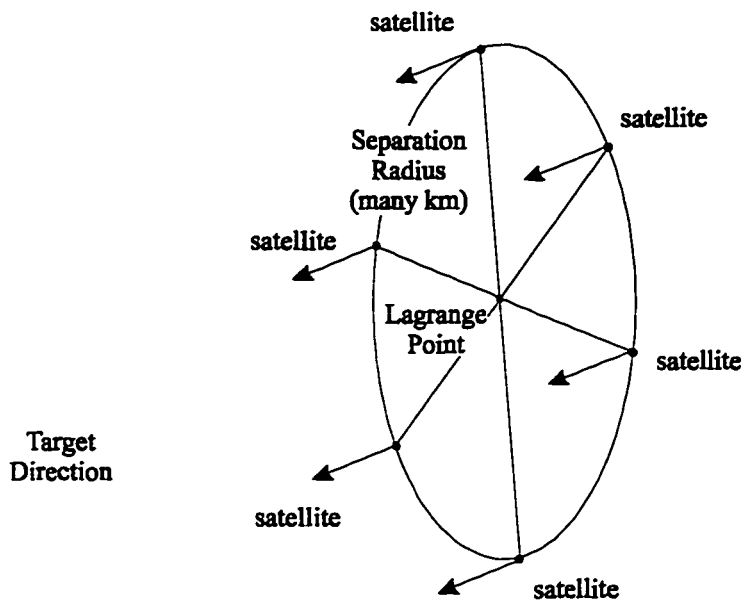


Figure 6.5. Distributed Interferometer Formation Concept

distant stellar objects with unprecedented accuracy. The constellation could redeploy itself autonomously to different separation distances by ground command.

This proposal raises many interesting ideas which are directly related to space GPS research. The constellation could control position and possibly orientation by using an integrated transmit/receive GPS or GPS-like device, as described in Section 6.1.5. The satellites would get ranging information by tracking the other GPS-like transceivers in the constellation. The commanded formation could be maintained either by a single, controlling satellite which sends commands to the other 'slave' satellites, or via a distributed method such as a neural network.

The key point is that even in an advanced application like this one, many of the fundamental required technologies are within reach by building on the basic GPS space research that has already occurred.

6.4. Summary

This chapter has provided several examples of promising avenues of research and flight demonstration for spaceborne GPS receivers in the coming decade. In the more distant future, there may be many constellations that provide GPS-equivalent services, and this particular subject of GPS receivers will merge into the more general field of ranging and control of satellites using radio frequency signals. It is certainly true that within a few years, GPS is likely to revolutionize spacecraft efficiency and performance, as the advanced concepts of today become the routine “off-the-shelf” capabilities of the next generation of satellites.

6.5. References

¹ P.K. Enge, A.J. Van Dierendonck, “Wide Area Augmentation Systems,” *Global Positioning System: Theory and Applications*, vol. II, American Institute of Aeronautics and Astronautics (AIAA), 1996.

² L.M. Ward, *Spacecraft Attitude Estimation Using GPS: Methodology and Results*, Ph.D. Dissertation, Univ. of Colorado, July 1996.

³ H.S. Cobb, C.E. Cohen, and B.W. Parkinson, “Theory and Design of Pseudolites,” *Institute of Navigation (ION) GPS-94*, Salt Lake City, UT, Sept. 1994.

⁴ F.H. Bauer, J.R. O'Donnell, Jr., “Space-Based GPS 1996 Mission Overview,” *ION GPS-96*, Kansas City, MO, September 1996.

⁵ R. Hart, *Global Positioning System Enhanced Orbit Determination Experiment: Mathematical Specifications*, NASA/GSFC, Document Number 553-FDD-95/013R0UD0, May 1996.

⁶ S. Powell, P. Kintner, "Using GPS for Telemetry System Clock Generation and Synchronization of On-Board Sounding Rockets," *ION GPS-96*, Kansas City, MO, September 1996.

⁷ C.E. Cohen, B. Pervan, H.S. Cobb, D. Lawrence, D. Powell, B.W. Parkinson, "Real-time Cycle Ambiguity Resolution using a Pseudolite for Precision Landing of Aircraft with GPS," *DSNS-93*, Amsterdam, The Netherlands, March 1993.

⁸ K.R. Zimmerman, R.H. Cannon, Jr., "GPS-Based Control for Space Vehicle Rendezvous," *ION GPS-94*, Salt Lake City, Utah, Sept. 1994

⁹ E.H. Teague, J.P. How, B.W. Parkinson, "Carrier Differential GPS For Real-Time Control of Large Flexible Structures," *ION GPS-96*, Kansas City, MO, Sept. 1996.

¹⁰ J. Adams, A. Robertson, K. Zimmerman, J. How, "Technologies for Spacecraft Formation Flying," *ION GPS-96*, Kansas City, MO, Sept. 1996.

Chapter 7: Conclusion

The most compelling proof that a capability exists is to operationally demonstrate its performance. On-orbit GPS sensors are no longer to be considered exotic devices reserved for the few spacecraft projects that have high mass, power, and cost budgets to afford them. Within 5 years, a rapid evolution in technology and capability has made these devices extremely useful and readily available to almost all Low Earth Orbit (LEO) spacecraft. Rapidly growing on-orbit flight experience and aggressive design acceptance by the spacecraft industry ensure that these trends will continue for the foreseeable future. Extensions in capability, along with reduced cost, mass, power, and size might quickly make it the exception when any Earth orbiting satellite does *not* carry a GPS receiver as part of its core sensor complement.

All on-orbit GPS functions begin with satellite selection and signal acquisition. Methods for performing rapid and efficient acquisition and reacquisition of GPS signals using orbit propagation were presented. The orbit elements are updated by ground command and each computed position fix. A bootstrap algorithm was presented which allows a first position fix within 30 minutes using limited prior information on a 6 channel GPS receiver. If an almanac is available, a first fix is possible within 10 minutes. This

capability enables quick and reliable initial acquisition even if the GPS receiver flies without a battery or a communications link.

Attitude determination based on GPS carrier phase measurements provides a substantial augmentation to the basic GPS navigation capabilities for a complex system such as a spacecraft. In order to accomplish efficient and robust attitude determination on spacecraft, however, the many differences between that exist between the ground and space-based vehicle motion must be accommodated. Spacecraft can rotate freely in all directions and with a great variety of dynamic motion, and so either a large portfolio of algorithms must be provided, or a single, very general algorithm that can accept many different operating conditions must be developed. To enhance solution integrity, generality, and on-orbit autonomy, the quasi-static motion algorithm for carrier phase cycle ambiguity resolution was created and implemented. This method may be interpreted as an extension of earlier algorithms that assumed the vehicle was in an approximately stationary or a highly dynamic environment. The quasi-static method, when implemented in such a way that the condition number of the observation matrix enhances the solution calculation, becomes an autonomous algorithm which can operate successfully in many different dynamic environments. This method was successfully demonstrated using post-processed measurements from the RADCAL spacecraft and on-orbit during the REX II and GANE experiments.

An additional complication of on-orbit attitude determination is the full freedom of motion that spacecraft commonly experience. It is no longer possible to provide full attitude determination at all orientations on some spacecraft, if all antennas are pointed in the same direction due to signal visibility limitations. To recover this capability for any-orientation attitude determination, an algorithm was developed to provide attitude determination on nonaligned antenna arrays. A differential carrier phase correction term

was derived that should be applied to the incoming measurement based on the measurement geometry to model the effect of the right-handed circular polarization of the GPS carrier signals.

Because spacecraft are almost always size limited, it is important to understand the performance that is achievable with a given antenna separation geometry. The effects of all significant error sources should also be understood so that it is possible to perceive how and to what degree each error contributes to the final solution. An error budget was therefore developed that showed, in most cases, that the dominant source of attitude error is carrier phase multipath. One case in which multipath may not be the dominant error source is when the GPS receiver is not properly calibrated for attitude determination. This problem can arise because receivers are difficult to test on a fully integrated spacecraft. Other methods for determining the calibration parameters were demonstrated, including phase center determination, and on-orbit line bias estimation. Issues concerning self-survey repeatability and combination of multiple self-surveys were addressed.

To demonstrate these algorithms in actual on-orbit conditions, several flight experiments have been performed using the TANS Vector receiver, which has been modified for space by incorporating many of the algorithms presented here into the receiver software. The spaceflight experiments that were presented were: RADCAL, a passively-stabilized gravity gradient spacecraft which was the first demonstration of spacecraft attitude determination using GPS carrier phase; REX II, an actively-stabilized nadir-pointed vehicle where the GPS attitude sensor was used to close the spacecraft control loop for the first time; and GANE, a fixed truss that was flown on the Space Shuttle Orbiter in the International Space Station attitude and compared to a precision inertial system to determine the GPS measurement accuracy. Each of these missions highlighted different

aspects of the algorithms' capabilities and presented opportunities for further research and performance improvements.

In the future, basic GPS space receiver services will continue to grow along with the sophistication of the systems onto which they are integrated. Real-time integrity and navigation accuracy of a few meters—potentially down to the centimeter level with carrier tracking—enables a host of formation flight and constellation concepts that were previously unattainable at reasonable costs. Precision control of multiple vehicles in close proximity is now possible under a single, uniform measurement architecture. Sensing and control of flexible space structures such as trusses and tethered spacecraft are possible. All these advances are in addition to the highly robust time, position, and attitude determination services that are likely to be available at low cost to almost every spacecraft in low Earth orbit and perhaps even in Geostationary orbit.